Synthesis, Characterisation, and Sorption Studies of Porous Inorganic Materials

Submitted by

Tariq M R Aqeel

To University College London
as a thesis for the degree of
Doctor of Philosophy in Chemistry

February 2008

I certify that all material in this thesis which is not my own work has been identified and that no material has previously been submitted and approved for the award of a degree by this or any other university.

ProQuest LLC
789 East Eisenhower Parkway
P.O. Box 1346
Ann Arbor, MI 48106-1346

Acknowledgements

My gratitude goes to my supervisors, Prof. Catlow, and Prof. Sankar for their guidance. My gratitude extends to all staff of the Chemistry department, the Royal Institution, and technical services, especially Dr Ian Watts for keeping the laboratories and instruments in good order, Dr Abil Aliev for providing the solid state ^{27}Al and ^{29}Si NMR spectra, Mr. Kevin Kreeves from the department of Archaeology for his help with SEM tests and Dr M. Ardakani (Imperial college) for producing the HRTEM images. I would also like to thank my wife, colleagues especially Malek, my close friends Loaay and Aiman, previous teachers at Exeter University and Kuwait University for their support, and PAAET for their trust.

Abstract

The aim of this project is to prepare various mesoporous hosts having hexagonal and cubic pore packing morphologies and improve their thermal, hydrolysis, and mechanical stabilities. Subsequently, we incorporate metal clusters and metal oxides into the pores to improve their sorption properties and to remove different types of sulphur compounds from organic liquids.

Hydrolysis, thermal and hydrothermal tests are essential to determine the stability of mesoporous materials. Mesoporous silicates produced in this project, *via* standard methods of synthesis, failed the stability tests. However, by understanding and controlling individual preparation steps, in particular the ageing time, temperature, and reaction time allowed the production of relatively stable mesoporous materials. Moreover mesoporous materials prepared by various methods behave differently under given conditions. Monitoring the structural and morphological changes of these materials upon exposing them to different conditions it was possible to correlate their behaviour, in particular the structural stability, during doping of metal ions and oxides and sorption reactions. It was found that modified true liquid crystal templating (TLCT) and precipitating methods are more suitable than materials prepared by solvothermal techniques.

We prepared micro clusters of zinc oxide, metallic gold, and silver into the pores (impregnation) of mesoporous silicate and aluminosilicate to improve the sorption ability of these hosts towards sulphur compounds. A modified method was developed by us to introduce gold and silver clusters into the mesoporous materials, which proved to be successful and more economical by decreasing the impregnation time from two weeks to only 30 minutes. This method involves two major steps; 1) solvolysis of gold or silver precursors in alcohols, 2) heat treatments using reducing gas. This new method maintains the long-range order of the mesoporous structure as confirmed by the HRTEM and XRD. We were able to produce nano scale gold and silver clusters with an average size of *ca* 1 nm.

Thiophene, Dibenzothiophene, Dimethyl-dibenzothiophene, and Dibenzosulfoxide were used in the sorption reaction. The amount of sulphur adsorption depends on the type of sulphur compound, its concentration, adsorption temperature and the type of adsorbent. In the best cases we were able to adsorb 91 % of the introduced sulphur compound.

Table of contents

Chapter 5

Table of figures

Table of Equations

Chapter 1

Introduction

This chapter highlights the scope and aims of this PhD thesis, where we have in particular viewed the synthesis, properties and classification of a range of porous materials. Furthermore, we also provide a general review on industrial desulphurisation techniques and how the materials we have examined can be used for this purpose.

Synthesis, Characterisation, and Sorption Studies of Porous Inorganic Materials

1.1 Introduction

The wide scope of applications suited for inorganic materials makes them very important in today's 'modern times'. Inorganic materials find uses in various fields, such as in medicine, equipment, industrials matters, computers, conductors, semiconductors, magnets, batteries, capacitors, and in many other applications. Therefore, there is an increasing demand to synthesize a variety of inorganic materials that possesses different properties, intrinsic and/or modified.

Many inorganic materials have been and are considered hard, impossible, and uneconomical to synthesize using traditional methods such as ceramic, sol-gel, and molten salts mixing processes. Therefore the search for milder and more economical synthesizing techniques is necessary. As a principle of rational planning, of inorganic synthesis, two important factors are promoted. First is to identify synthesizable compounds or structure, secondly, to design feasible syntheses methods for controlling and improving selective properties[1].

1.1.1 A Review of Some Methods used to Synthesize Inorganic Materials

The ceramic route is a widely used method due to its simple procedure that generally produces high yields of crystalline structures. In this method the reactants, which contain the chemical elements of interest are ground in stoichiometric quantities and heated at high temperatures (usually above1000 °C). Jansen[2] predicts that even higher temperatures could be employed to explore new thermodynamic compounds for long periods of time, to increase diffusion and to ensure that the chemical reaction of the starting components take place. However, this method has some disadvantages: (1) It is suitable for only a limited number of mixes of elements and therefore if the product contains a high number of elements, the procedure becomes uneconomical to implement; (2) the procedure contains long and repetitive processes of grinding, mixing, and heating, which could last for days; (3) controlling the size of crystals is difficult and; (4) thermodynamics is the driving force of the reaction, and there is only little kinetic influence which is a disadvantage if the kinetic product is the desired one[3].

Another common method is the Sol-Gel process. This method usually has two major steps; firstly reagents are dissolved in solvents and then mixed thoroughly until precipitation. The second step involves calcinations at high temperature (about 1000 °C) to remove the undesirable by-products, organic components of the gel, and to increase the crystallinity of the desired material. This process is lengthy, contains toxic by-products and involves high temperatures. [4]

The third method by which inorganic materials are commonly synthesised is *via* the molten salts route. This method employs a single step of mixing the reagents in a molten state to improve diffusion. Molten and sol-gel methods employ high temperature ranges but usually they are below those used in the ceramic method. The 'molten salt' method still lacks control of the crystal sizes of products and sometimes fails to produce the kinetic products. [5]

In order to overcome these limitations, new synthesizing techniques need to be explored and developed. Few of the promising methods are solvothermal routes, which is sometimes referred to as hydrothermal process, precipitating method, liquid crystal templating, and true liquid crystal templating method. In addition these methods have many applications in producing porous inorganic materials.

1.1.1.1 The Solvothermal Method

The solvothermal method has been employed to synthesize a wide range of materials such as sulphides and porous metal oxides that posses interesting properties. The properties of the inorganic materials depend on their chemical composition, and structural morphologies.[2] Solvothermal methods tend to be one of the most practical ways in tuning some of the desired properties of materials by controlling their structure and morphologies. For example, the ability to dope different compounds such as CdS-TiO or by controlling the morphologies of the products such as producing hexagonal, cubic, and lamellar mesoporous structures.

1.1.1.1.1 Definition

Solvothermal synthesis is a chemical reaction of materials in a closed vessel at a temperature above the boiling temperature of the solvent used (at or below the critical conditions). [5]

Solvothermal reaction develops an internal pressure (autogenous), which is related to various parameters such as temperature, percentage fill, and the presence of other dissolved salts. It is found that the pressure increases dramatically with the increase of heat and the percentage fill of the (sealed) container. Most of the reactions that take place *via* solvothermal synthesis techniques occur at, or close to, the critical conditions of the solvent used. This means that solvents will display different properties to that otherwise exhibited at ambient conditions. Some of these properties include changes in viscosity, density and dielectric constants [5]. It is found that as the temperature

increases, the viscosity and the dielectric constants decrease, when water is used as a solvent, that decreases the solvent resistance (*f*) to the mobility of species (see equations 1.1, 1.2, and 1.3 below). So when *f* (solution resistance) decreases and ***a*** (species radius in solution) is constant then ***D*** (diffusion coefficient of the species) increases, which means diffusion of the reactants improve compared to ambient conditions.

Einstein's law of diffusion $\quad Df = kT \quad$ ***.....(1.1)***

where ***D*** is the diffusion coefficient, *f* is the friction coefficient, ***k*** is Boltzmann constant, and ***T*** is temperature.

Stokes's law ..... $\quad f = 6\eta\pi a \quad$ ***.....(1.2)***

where η is the viscosity of the solvent, and ***a*** is Stokes' radius defined as the mean average radius of the particles in solution.

If the value of ***f*** from equation 1.2 is substituted into equation 1.1, we obtain:

$D = kT / 6\eta\pi a$ $\quad$ ***.....(1.3).***[6]

This implies that diffusion of particles improves as a function of temperature, or by decreasing friction, either by reducing the viscosity of the solvents or the density (when density is reduced Stoke's radius ***a***, shown in equation ***1.2***, also decreases as a result of the decrease of the thickness of the solvent layers covering the moving particles).

Furthermore, there are three mass transfer operations that need exploration for reactant species in solution under solvothermal conditions. These include: migration of charged species under the influence of an electrical field (this can be employed by inserting electrodes into the Teflon cup inside an autoclave to initiate migration of some of the reactants); the second is diffusion which is the movement of species under the influence of a chemical gradient (concentration) and; convection (the movement of species as a result of

solvent movement) either forced caused by heat, pressure, mechanical stirring or natural caused by the difference in densities of solvents[7]. Further experiments are required to show the effects of pressure, solvent, pH, reaction duration time, and temperature on product, produced by solvothermal synthesis.

1.1.1.2 Liquid Crystal Method

Commonly, the states of matter can be divided into three categories gas, liquid and solid, which differ in the degree of molecular ordering. Firstly, in a gas, molecules are highly disordered (in constant motion above the absolute temperature), and the volume of a gas increases inversely in proportion to the pressure applied. Secondly, in a liquid, there is a lesser degree of disorder in the long and short-range; however molecules move in relation to each other since there are significant interactions between consecutive molecules. Thirdly, in a solid, there is long-range three-dimensional ordering (especially so in crystalline forms) including the positional and orientational alignments of the molecules. There are two other states of matter however, that are not commonly referred to. These are plasma and liquid crystal states.

A plasma is a highly ionised gas, which exists under specific conditions, and can be formed by heating an inert gas in the presence of a strong magnetic field. The final state of matter, the fourth state, exists between liquid and solid states and this is known as the liquid crystal (LC) state.

Liquid crystals combine liquid-like characteristics, such as molecular mobility and fluidity, with solid-like characteristics such as orientational and/or positional ordering of the molecules. Therefore, liquid crystal are often considered as very disordered solids or rather ordered liquids.[8, 9,10]

1.1.1.2.1 Classification and Definitions of Liquid Crystal

Liquid crystals can exist in a variety of phases, known as mesophases (the word meso comes from the Greek word 'mesos' meaning 'between' and, phases, from the Greek word 'phasis' meaning 'phase'). A substance that gives rise to a mesophase is called mesomorphic and is known as a mesogen. Since mesophases are ordered liquids, it is better to distinguish between their existence states. First, a liquid with random order is called an Isotropic Liquid phase. Second, liquids that possess overall order are called Anisotropic Liquids (the change of properties of a substance depending on orientation). It is also important to note that, the temperature at which a liquid crystal is transformed from a crystal phase to a mesophase is called the 'melting point'. The temperature at which a mesophase is transformed to an isotropic liquid however, is called the 'clearing point'. Liquid crystals can be classified under two general groupings as presented in (fig.1.1). [8, 9, 10]

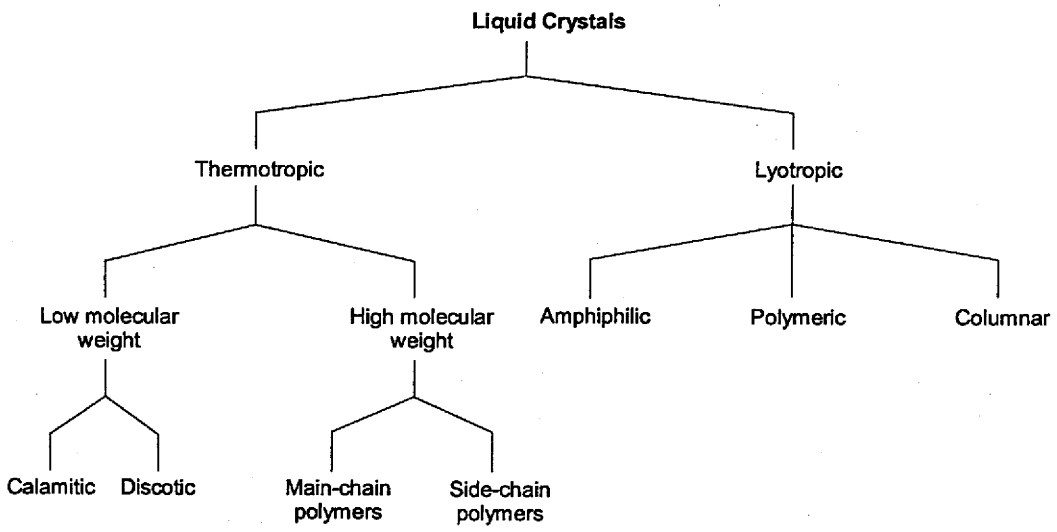

Figure 1.1. A classification of liquid crystals 10C

1.1.1.2.1.1 Thermotropic Liquid Crystal

A transition between different liquid crystal states as a result of the action of heat is called 'Thermotropic Mesomorphism'. Thermotropic liquid crystals can be further divided into high and low molecular weight categories, where distinctions are made between polymers and discrete molecules. The low

molecular weight category can also be further subdivided into calamitic (rod-like) and discotic (disk-like) divisions.

1.1.1.2.1.2 Lyotropic Liquid Crystal

The second main class, in which a mesophase is formed by the action of solvent, and which often requires a secondary action of heat, is referred to as Lyotropic. There are three subclasses of lyotropic liquid crystal: amphiphilic, polymeric and disk-like. The difference between each of these types arises from the differing chemical nature of their constitutional molecules. [8,9,10]

1.1.1.2.1.2.1 Amphiphilic Liquid Crystals

An amphiphilic liquid crystal, in which the monomer contains both hydrophilic and hydrophobic parts, is called a 'surfactant' (surface-active substance). Surfactants operate when they are placed into a solvent where by the hydrophilic ends tend to dissolve, whereas the hydrophobic ends tend to be adsorbed at the interface (air/solvent or solvent/solvent). Increasing the concentration of the surfactants to a point at which no more sites are free in the interface, leads to the effect in which further addition of surfactant forces the surfactant (monomers of amphiphiles) to aggregate and leave the interface area to the bulk of the solution in the form of micelles. Even further addition of surfactant species causes a greater increase in the numbers of micelles formed. The micelles formation in the bulk is a method to protect and cover the hydrophobic (organic) part from the molecules of the solvent, if water is used as a solvent. The concentration at which micelles are formed is called the critical micelle concentration (CMC). Further addition of surfactants will cause an increase in micelle concentration up to a point reached where the micelle concentration is too high that micelles begin to pack in an ordered form, which is defined as the liquid crystal phase. [8,9,10]

1.1.1.2.2 Shapes of Micelles and Corresponding LC Phases

The shape of micelles can be related to the cross-sectional area of the monomer head, tail length, and tail volume according to equation (1.4), see schematic representation figure 1.2. In general, surfactants with large head groups (relative to their tail volume) form spherical micelles, which leads to the formation of cubic liquid crystal mesophases such as (I_1). Surfactants with intermediate size head groups form rod-like micelles, and then hexagonal mesophases (H_1), while surfactants with small head groups form disc-like micelles that give lamellar mesophase (L_α); examples of these shapes are shown in figure 1.3.

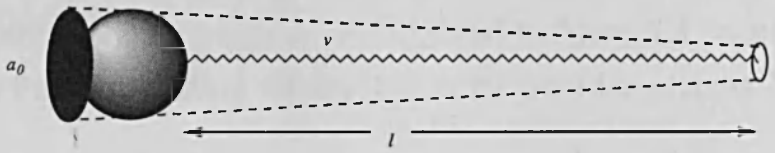

Figure 1.2 Schematic of the dimensions of a surfactant molecule[10c]

$$v/a_0 l \qquad \text{.....(1.4)}$$

v = effective volume occupied by the surfactant chain

a_0 = effective cross-sectional area occupied by the head group

l = of the 90% length of the extended tail group

Spherical micelles	$v/a_0 l \leq 0.25$
Cylindrical micelles	$0.25 \leq v/a_0 l \leq 0.33$
Disc-like micelles	$0.33 \leq v/a_0 l \leq .5$

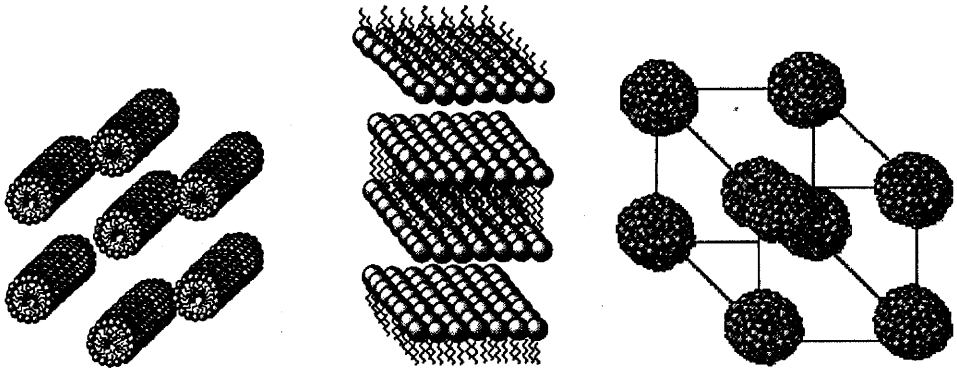

Figure 1.3 Schematic representations, from left to right, of a normal, hexagonal phase (H_1), the lamellar phase (L_α), and micellar cubic phase (I_1)[10c]

Micelle shapes do not normally change at the disorder-order transition; therefore, the micelle shape before this transition often determines mesophase structure. Generally, a surfactant will show mesophases that are always present in the same order as indicated in figure 1.4. In principle, it is very unlikely that a surfactant will show all of the possible phases[11].

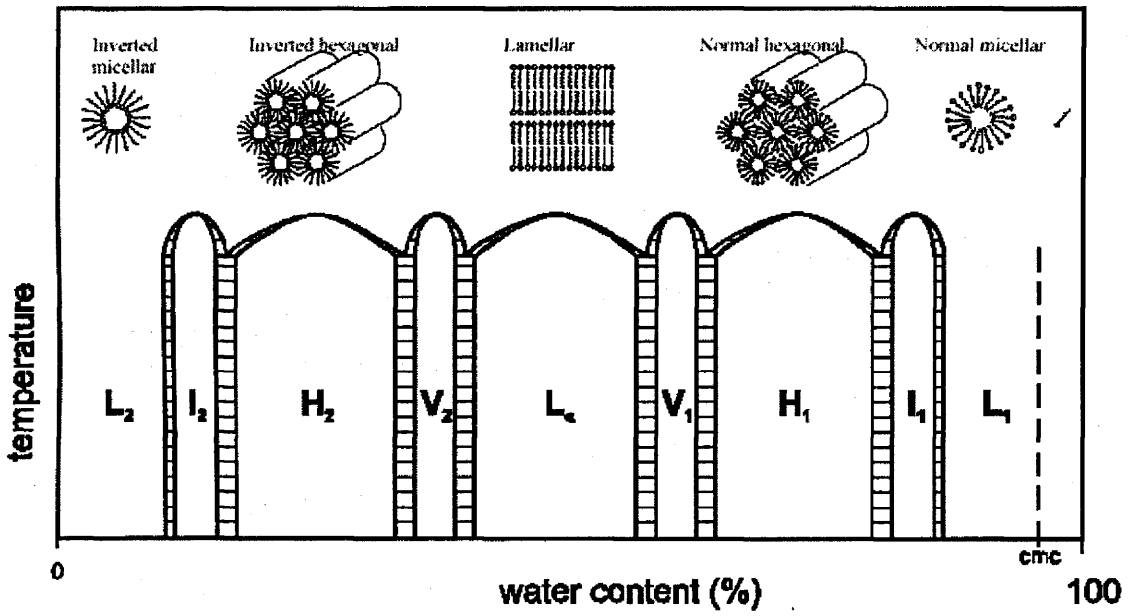

Figure 1.4. Idealised binary phase diagram for surfactant in water. (L1) normal micellar solution, (I1) normal micellar cubic, (H1) normal hexagonal, (V1) normal bicontinuous cubic, (Lα) lamellar. Subscript 2 denotes reverse phase11b

Micelles are aggregates of surfactants (figure 1.5) and have an aggregation number of 10-200 monomers; units of two or three aggregated monomers do not constitute a micelle but nevertheless are thought to be present in solution

in very small concentrations[12]. A micellar solution can be considered as a colloidal system where each micelle is a liquid droplet that is dispersed in another liquid phase. In a 'normal' micelle, head-groups act as a barrier between the water-continuous area and the hydrophobic core (figure 1.5). Conversely, in an 'inverse' micelle, the system is oil-continuous and the head-groups act as a barrier between the oil and the hydrophilic core. It follows that inverse systems are formed when water is present in small quantities. In the nomenclature, a system that is described as normal, is identified with a subscript '1', whereas an inverse system is identified with a subscript '2'. For example, normal and inverse micellar solutions are referred to as L_1 and L_2, respectively. [8,9,10]

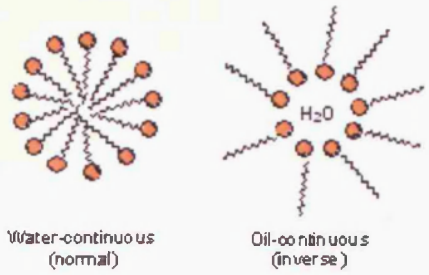

Figure 1.5. Schematic of a normal and inverse micelle[11b]

1.1.1.2.3 Mesophase Characterisation

The most common methods used to characterise mesophases are polarised optical microscopy, and low-angle X-ray Diffraction (XRD). These methods are used in a way complementary to each other to determine the phase type, the mesophase structure, and their position in the phase diagram at certain concentration and temperature. [13a, b]

1.1.1.2.3.1 Polarised Optical Microscopy

Polarised optical microscopy is the oldest and most widely used technique, usually used to make initial assignment of the mesophases exhibited by a compound by analysing its characteristic textures. Optical microscopy is useful in assigning mesophases quickly and, compared to X-ray scattering, is

relatively cheap. Optical microscopy relies on the fact that the mesophases are anistropic in nature having two refractive indices. Liquid crystals can have a variety of anistropic properties including, electronic polarisability ($\Delta\alpha$), dielectric permittivity ($\Delta\varepsilon$) and diamagnetic susceptibility ($\Delta\chi$). The anisotropy of a phase is the most important feature in optical microscopy; other types of anisotropy are inspected by other techniques. In a mesophase, there may be three different values for the polarisability along three orthogonal directions, which gives rise to three different refractive indices (see figure 1.6). [13a, b]

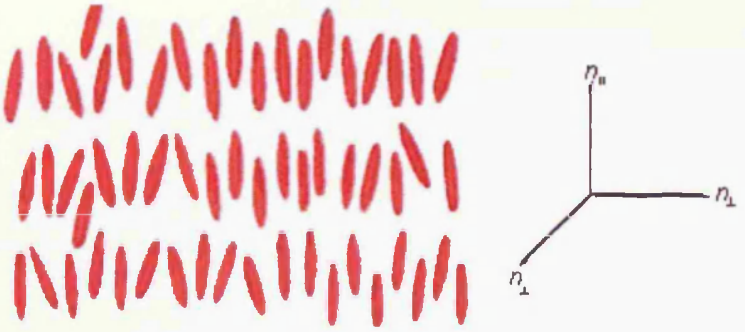

Figure 1.6 Schematic representation of a mesophase with defined refractive indices[11b]

The refractive index defined parallel to the long molecular axis of a mesophase is termed the *extraordinary* refractive index ($n_{(II)}$) and those at right angles to it are defined as the *ordinary* refractive indices ($n_{(\perp)}$). The ordinary refractive indices become equivalent if the phase has cylindrical symmetry. The difference between the extraordinary and ordinary refractive indices is the '*birefringence*', Δn (equation 1.5). It is the birefringence that is utilised in optical microscopy.

$$\Delta n = n_{(II)} - n_{(\perp)} \qquad \text{.....(1.5)}$$

When plane-polarised light is passed through a thin slice of a sample, the birefringence gives rise to interference patterns that are characteristic of the mesophase and the molecular alignment within it. When plane-polarised light is first passed through a sample, birefringence is created as a result of the interference between the two refracted rays. Light that passes through the second polariser produce an interference pattern that can be observed using

an optical microscope. In the isotropic state, such as in liquids where the molecular arrangement is random, there is only one refractive index. The birefringence for liquids is therefore zero and interference patterns cannot be observed and as a result the isotropic state appears black through the crossed polariser. Moreover, different mesophases have specific common optical textures of recognition, some of which are represented in figure 1.7.[13a,b]

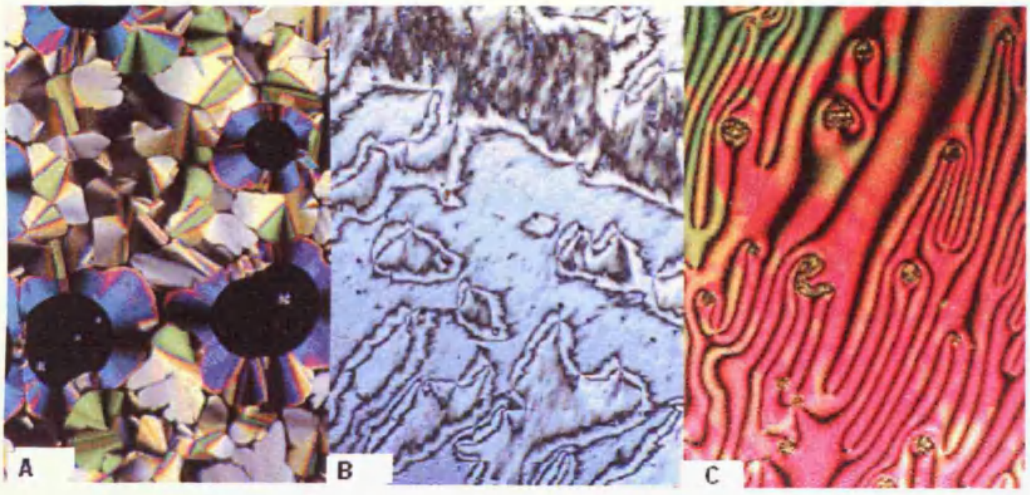

Figure 1.7 Polarised optical microscopy A) columnar mesophase of a polycatenar mesogen, B) smectic C phase of a polycatenar mesogen, C) nematic mesophase of an organomanganese complex.[13c]

1.1.1.2.3.2 Low Angle X-Ray Diffraction

Low angle X-ray diffraction is a powerful technique that can provide very detailed information about the structure of a mesophase and is often the only method of assigning structures unequivocally. The technique is represented schematically in figure 1.8a.

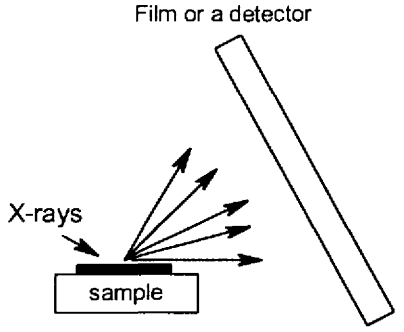

Figure 1.8a Schematic representation side view of the X-ray scattering experiment

The X-ray wavelength (usually monochromatic, produced from a specific target material and filtered by a suitable material to give X-rays of a specific wavelength) is smaller than inter-micellar distances, where there is a periodicity of aggregates. Thus, the periodic arrangement of mesophase structures acts as a diffraction grating to the incident X-rays, following Bragg's law (that will be discussed in details in chapter 2) in which only constructive interference produces a signal.

Mesophases give a number of reflections in their diffraction patterns that correspond to inter-aggregate periodic arrangements. These diffracted waves are the results of constructive interference (in-phase reflections that enhance each other and appear as distinctive peaks, usually higher than any other peaks, from which one can assign to known mesophase morphology). Conversely, out-of-phase waves either cancel each other completely, or weaken the resultant wave, and appear as low signals or might even disappear in the base line signal. Only the in-phase reflections can be indexed to a known structure. [13a, b]

1.1.1.3 Classifications of Porous Materials

Porous materials can be divided into three main categories according to IUPAC classification (see table 1.1 below). Micropores are materials that contain pores of diameter less than 20 Å, mesoporous materials contain pores

diameters between 20-500 Å and macropores are those containing internal pores of diameter larger than 500 Å.

Table 1.1 IUPAC classifications of materials according to their pore sizes

Pore-size regimes	Pores diameter ranges	Examples
Macroporous	> 500 Å	Glasses,
Mesoporous	20 – 500 Å	MCM, Pillared layered clays
Microporous	< 20 Å	Zeolites

1.1.1.3.1 Microporous Materials (Zeolites)

Porous inorganic materials, such as zeolites (figure 1.8b), have important industrial applications. Microporous materials are defined as materials that contain pore diameters that do not exceed 20 Å.

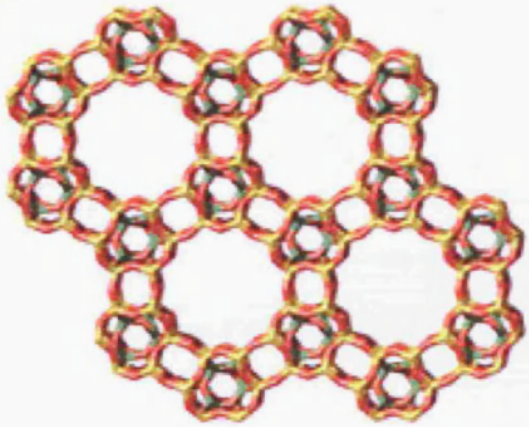

Figure 1.8b Schematic representation of zeolite's pores [14a]

Zeolites, in particular, are crystalline materials that consist of interlocking tetrahedrons of SiO_4 and/or AlO_4. The aluminosilicate structure is negatively charged and attracts positive cations that reside within the pores. It is found that aluminium and other metals ions can easily substitute the silicon atom within zeolites. Due to the differences in charges between silicon ions and other substituted metals, such as aluminium ions, the net framework charge would be more negative, see equation 1.7 below.

$$MxDy[Al(x+2y)Si(n-x+2y)\ O2n]\ (x+2y)\text{-}(H2O) \quad .....(1.7)\ ^{14b}$$

where **M** is a monovalent counter metal cation, **D** is divalent counter metal cation and there are loosely bonded H_2O molecules.

Unlike other silicates, zeolites have relatively large internal pores or cages in their structures that allow space for large cations such as sodium, potassium, barium and calcium and even relatively large molecules and cation groups such as water, ammonia, carbonate ions and nitrate ions. Of the most useful of industrial zeolites are those that contain large internal surface area and pores volume. [14b]

Zeolites are used in applications requiring ion exchange (limescale inhibitors and purification of pollutant water), filtering, odour removal, chemical sieving and gas absorption. The most well known use for zeolites is as size and shape selective catalysts where they are used on a large scale in filtration and cracking, efficiently and economically. Since zeolites have pore sizes below 20 Å, their applications are limited to small molecules and atoms. For applications involving larger molecules, researchers turn to meso and macroporous materials. [7b]

1.1.1.3.2 Ordered Mesoporous Materials

Ordered mesoporous materials consist of extended inorganic or inorganic–organic hybrid arrays with exceptional long-range ordering, highly tuneable texture, and versatile surface properties, controlled by the pore size and geometry[8, 9]. Typically, the structure of the pores in mesoporous materials are periodic and the pore sizes vary from 20 to 500 Å, which is known as the mesoporous range. Examples of mesoporous materials include M41S, aerogels, and pillared layered structures. Materials derived by means of surfactant templating are occasionally called zeolites and described as crystalline materials in reference to the long-range ordering of the pore

packing. This is not entirely correct for most of mesoporous materials since the pore walls are usually amorphous. [15, 16]

During the last decade, intensive scientific efforts have been devoted to the synthesis, characterization, and application of ordered mesoporous materials. Increasing available knowledge on mesoporous and mesostructured materials has led to a continuous development of new processes and techniques for the synthesis and modification of mesoporous structures. Ordered mesoporous materials have a wide scope of applications including in the fields of catalysis, separation, delivery and release techniques, dielectrics, sensors, and other electro-optical technologies.

Amongst milestone research findings conducted in the field of mesoporous materials, is the discovery of molecular sieves called MCMs (*M*obil *C*omposition of *M*atter, 1992). These mesoporous silicate materials, with well-defined pore sizes of 20 - 100 Å, have exceeded the pore sizes of microporous zeolites. The extremely high surface areas (>1000 m^2g^{-1}) and the precise tuning of pore sizes are among the many desirable properties that have made such materials the focus of great interest.

Figure 1.9a TEM image of hexagonal packed cylindrical mesoporous silicate

The MCM41 materials (which are hexagonally packed cylindrical mesopores, figure 1.9a) represent a new approach to materials synthesis where, instead

of the use of single molecules as templating agents (as in the production of zeolites), self-assembled molecular aggregates or supramolecular assemblies are employed as the structure-directing agents. This Inorganic self-assembly is formed around the micellar surfactant assembly, which determine the pores size of the structured solid after the removal of the surfactants (to produce a porous solid). [17–25].

1.1.1.3.2.1 Liquid Crystal Templating of Silicate and its Derivatives

The original M41S family of mesoporous molecular sieves were generally synthesized by the combination of appropriate amounts of a silica source, normally sodium silicate, an alkyltrimethylammonium halide surfactant (e.g. cetyltrimethylammonium bromide (CTAB)), a base (e.g. sodium hydroxide or tetramethylammonium hydroxide (TMAOH)), and water. For the case of aluminosilicate M41S, this was synthesized by the addition of an aluminium source to the synthesis mixture. Synthesis mixtures are generally kept at elevated temperatures (≥100 °C) for 24 - 144 hours, which results in the formation of solid precipitate. The organic-inorganic mesostructured product is then filtered, washed with water and air-dried. In the final step of the preparation, the mesoporous solids are calcined at about 500 °C under a flowing gas to burn off the surfactant resulting in opening the pores of the mesoporous material.

Uncertainty still remains regarding the mechanism involving in liquid crystal templating (LCT). A promising one was proposed by researchers at Mobil. They based their proposal on the similarity between the structure of liquid crystals of surfactant assemblies (i.e., lyotropic phases) and M41S. In particular their considerations included: 1) the mesostructure dependence on the hydrocarbon chain length of the surfactant tail group, 2) the effect of variation of the surfactant concentrations, and 3) the influence of organic swelling agents. Using MCM-41 (which has hexagonally packed cylindrical mesopores) as a representative M41S material, two mechanistic pathways are postulated by the Mobil researchers, as demonstrated in figure 1.9b. [26]

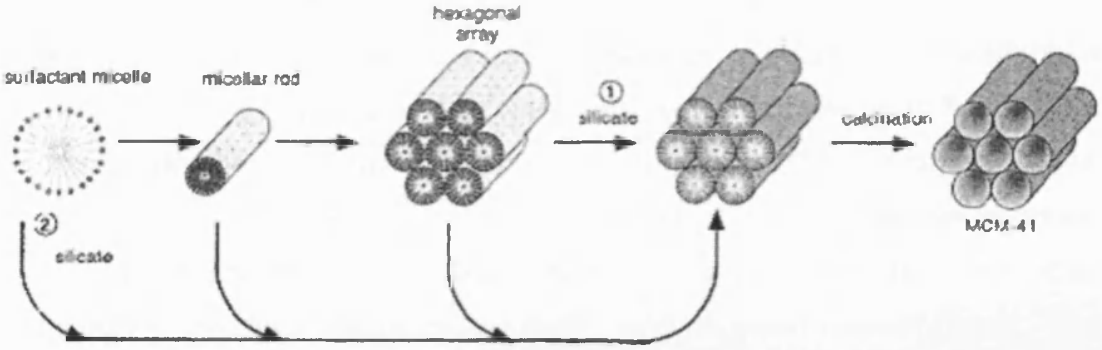

Figure 1.9b Two possible pathways for the LCT mechanism to form mesoporous structured materials.[26]

1.1.1.3.2.1.1 Liquid Crystal Templating Method

Liquid crystal templating (LCT) occurs when a surfactant is added to a hydrolysable inorganic precursor, before the formation of the mesophase, to produce a mesoporous material. This mechanistic pathway for LCT was postulated as a cooperative self-assembly of the surfactants and the inorganic precursors. The inorganic precursors mediate the ordering of the surfactants into a hexagonal packing arrangement. In the case of silicate, the inorganic components (which were negatively charged at basic pH value [20b,c]) interact preferentially with the positively charged ammonium head groups of the surfactants used (alkyl halide) and condense into a solid continuous framework, as shown by bath two in figure 9b. The resulting organic-inorganic mesostructure can be alternatively viewed as a hexagonal array of surfactant micellar rods embedded in a silica matrix; removal of the surfactants will produce 'open pores' in MCM-41 (see figure 1.9b). [20]

1.1.1.3.2.1.2 True Liquid Crystal Templating (TLCT) Method

In general, TLCT is the process that transforms surfactants into a liquid crystal phase (mesophase), at a concentration above the critical micelle concentration. Once the mesophase is established and characterized, it can

be destabilized slightly using alcohol prior to the introduction of inorganic precursors. Then it will be mixed with the inorganic precursor under a slightly reduced pressure to remove the excess alcohol to reconstruct the mesophase and to condense the inorganic precursor forming the framework of the desired inorganic material oxide surrounding the "reconstructed" liquid crystal phase (bath one, figure 9b). Removal of the liquid crystal templates will produce open pores in the framework. Attard et al.[20a] first presented this method to successfully produce hexagonal, cubic and layered mesophases and mesoporous structures. In this method of preparation, the surfactant-precursor interaction is less important than the actual presence of a liquid crystal phase. Also, there is an element of prediction of the resultant structure.

1.1.1.3.3 Removal of Templates

A templating material generally occupies about 55 % wt of the inorganic-organic product, [28, 29]. The removal procedure of the organics is of utmost importance depending on the nature of the interactions between the template employed, the surrounding matrix, and the ability of the matrix to adapt to the template morphology after this removal. [30, 31]

There are two common methods usually applied to remove templates and organic matter from the internal pores of mesoporous materials. The first method is pyrolytic elimination of the surfactant by calcination of the as-synthesized solid. The second method is by chemical extraction of the surfactant from the as-synthesized solid. [26b]

1.1.1.3.3.1 The Effect of Heat Treatments

Heat treatments are generally used to remove organic substances from mesoporous materials, enhance further condensation, and to give an indication of the stability of the prepared structure. The effects of heat on these materials leads to change in their grain (size, shape, and distribution), morphology (crystallinity, wall thickness, porosity, amount and types of

defects). In general, heat is an element that can be used to tune many properties of inorganic materials [27]. Calcination includes sintering and annealing processes. Annealing is a process in which material is heated to a certain temperature and held for specific periods of time, before which it is cooled gradually, to relieve some of the strain forces associated with its preparation. Sintering is the process in which materials are heated below their melting point and compacted either by external or internal forces to form rigid structures. It is found that the walls surrounding the internal pores in mesoporous structures usually fall under 20 Å in thickness when the structure is calcined at a temperature of 300 °C, but maintain their integrity. The effects of high temperature, above 350 °C, have a direct effect on the grain size growth and grain shape variation. Increasing the calcination temperature for some mesoporous materials increases its grain size. In the case of SnO_2, increasing the temperature increases the grain sizes and alters the grain shapes. For example, a change in grain shape from semi spherical to elongated occurs. As a result of both effects, the wall thickness around the pores increases due to the grain size effect, and due to deformations that are resultant of grain shape changes, and loss of structural directors (organic templates) that create more stress forces and pressure around the pores. It is for this reason pores are considered to be the weakest part of mesoporous structures and generally, structural collapse can be attributed to the failure of the channel walls. We note here that this problem is not encountered in porous silicate preparation because the annealing temperature tends to release and decrease some of the stresses exerted on the structure.[27]

1.1.1.3.3.2 Calcination Methods

Here we will discuss further the process involved in and the effect of calcination, which is the most common method used in laboratories to remove templates. In this method, the as-synthesized materials are alternatively heated in nitrogen, oxygen or air, burning away the organics. Any necessary charge compensating counter ions are supplied from the decomposition of organics. Usually, the heating rates required are slow with heating ramps

such as 1 °C min^{-1} up to 550 °C, followed by an extended period of heating at a temperature plateau 4 – 8 hrs. Generally, when a template is removed by calcination, the low angle reflection intensities increase, the structure may shrink, and the mesoscopically ordered structure could be dramatically affected [32, 33]. MCM-41 for example, was originally calcined at 540 °C in N_2 for 1 h and then in O_2 or air for 6 hrs. The reported framework condensation increased from Q^3/Q^4 of about 0.67 in the as-synthesized MCM-41 precursor (^{29}Si NMR data) to about 0.25 after calcination. Chen et al.[34] calcined MCM-41 samples at 540 °C in air for 10 hrs with a slow heating rate of 1 °C min^{-1}. They observed up to 25% decrease in the unit cell parameters depending on the synthesis conditions. The reported conditions for calcination of MCMs varied widely by different groups, however, a common procedure is used to calcine mesoporous structured silicate under air at 550 °C for 5 h with a heating rate of 1 °C min^{-1}.

Table 1.2 Mass losses recorded by thermogravimetry for MCM-41 samples synthesized with surfactants having different chain lengths (mass losses below 110 °C of physisorbed water) [35a]

Samples	25–110 °C (%)	110–265 °C (%)	265–305 °C (%)	305–395 °C (%) (μV/mg)*	395–1000 °C (%)	Total mass loss (%)
C12-MCM-41	3	24	5	3 (0.5)	4	39
C14-MCM-41	3	24	6	5 (0.6)	5	43
C16-MCM-41	2	21	9	8 (0.8)	6	46
C18-MCM-41	3	19	10	9 (1.10)	7	48
C14-MCM-41 aged	4	21	6	4 (0.7)	4	39
C16-MCM-41 aged	2	19	7	7 (0.9)	5	40
C18-MCM-41 aged	3	17	10	9 (1.2)	6	45

Calcination passes through different stages (table 1.2). The first stage is the removal of the physisorbed water. This is followed by the main conversion of the template species, between 180 and 450 °C, in a two-step process (200–300 and 300–450 °C) by oxidative decomposition and combustion of the organic species leaving approximately 15 % wt of carbonaceous residues. This carbonaceous species are converted to CO_2 at temperatures between 450 and 550 °C, which causes additional shrinkage to the mesoporous structure, and increases X-ray scattering intensity as a result of complete template removal (morphology dependent). [35a]

For the acidic synthesis of SBA, the template decomposition occurred in a three-step process. The desorption of water (1%), a large weight loss (25%) between 180 and 260 °C by elimination of the surfactant head group and some carbon chains resulting in an increase in X-ray scattering and no d-spacing shift. This step was followed by an exothermic process (at 260 °C – 300 °C), associated with 10 % in weight loss, which is attributed to surfactant decomposition. It was found that even though the mass loss reached 35 %, these combined processes did not show change in the scattering contrasts or d spacing values. The main exothermic process, where detected between 300 °C and 400 °C, where the weight loss was recorded to be approximately 11 %. Above 400 °C, the weight loss of 9 % correspond to the removal of carbonaceous species at 450 °C– 550 °C, and water losses *via* condensation of silanol groups at 600 °C. The total weight loss measured for SBA-3 was approximately 55 %. Furthermore, it was found that (1) thicker silica walls were found in SBA-3 materials, compared to those in MCM-41, and (2) the possible presence of disordered micropores in the inorganic framework walls. Similarly, Albouy et al. [35b] reported the presence of microporosity inside the walls of mesoporous hexagonal phase silica synthesized under acidic conditions, with CTAB as the template. [35a]

1.1.1.3.3.3 Chemical Method

The removal of templates from within the internal channels of mesoporous materials depends on the nature of the interaction between the templating materials with the framework precursors. For cases in which there are strong electrostatic interactions, it is for example advisable to add a strong acid to the solvent used, such as an HCl/ethanol solution (ca. 1 g of powder, 8.5 ml of HCl 37% and 100 ml of ethanol 99 %; for 12 – 24 hrs at 60 °C). Following this the (porous) material should be separated by filtration, washed with ethanol, and air-dried[36]. In other cases in which neutral surfactants are used, removing these surfactants from the as-synthesized material by washing with alcohol such as, ethanol under, reflux for 24 - 40 hrs. [37]

There are two practices usually employed to chemically remove templates from mesoporous materials. These are soxhlet extraction [27], or by stirring the material directly in the solvent under reflux. The advantages of using soxhlet extraction include, conservation in solvents (it is found that one portion of solvent is needed to remove templates because the nature of the soxhlet extraction procedure provides a pure solvent to wash off the surfactant each time it condenses during the reflux cycle), increasing the d spacing and the total surface area, greater control of the sample's temperature (by lowering the temperature of the solvent, way below its boiling point, which considerably effects the morphology of the product). The soxhlet extraction method also does not affect the morphology of the porous material since it prevents elongated soaking, and the temperature rise of the boiling solvent that is associated with the direct soaking method.

1.1.2 Background on Fuel Desulphurisation

The oil industry is facing increasing pressure to remove organic sulphur containing compounds from transportation fuels. The sulphur content in fuels is of an environmental concern because, upon combustion, sulphur is converted into SOx, which not only contributes to acid rain, but also poisons catalytic converters that are used to treat exhaust emissions, and is directly related to the corrosion of pipelines and vessels in refineries. The sulphur level in diesel fuels was limited to 500 ppm in both Japan and the USA and, 350 ppm in Europe. However, new regulations will cut diesel sulphur from current levels to very low ones: The US Environmental Protection Agency (EPA) value was reduced to 11 to 15 ppm in June 2006,[39] and EU value was reduced to 50 ppm at the beginning of 2005 and this will be reduced further to10 ppm by January 2009.[40] These specifications represent new and challenging tasks for both scientists and refineries, especially since remaining sulphur is likely to be contained in heavier parts of the oil fractions, which are difficult to desulphurise[38]. In addition, in attempts to meet the growing demand for clean fuels, the implications are complex, not only in regard to the need for a highly active desulphurisation catalyst, but a refinery must meet unique criteria, such as diesel blend components and hydrogen availability. In

processing heavier hydrocarbons such as military logistic fuels (JP-4, JP-5, JP-8, and JP-100), kerosene, gasoline, and diesel and to produce hydrogen for fuel cell use, several issues arise. First, these fuels have a high sulphur content, which can poison and deactivate components of the reforming process, and the fuel cell stack; second, these fuels may contain non-volatile residues (NVRs) up to 1.5 vol.%, which can potentially accumulate in a fuel processor; and finally heavy hydrocarbons have a high coking potential. Cracking using an appropriate catalyst can convert various heavy organo-sulphur species, found in fuels, into lighter sulphur species such as hydrogen sulphide (H_2S), facilitating subsequent sulphur adsorption on metals and metal oxides such as zinc oxide. [38]

1.1.2.1 Removal of Organic Sulphur Compounds

Hydrodesulphurisation technology (HDS) is able to desulphurise aliphatic and cyclic sulphur-containing compounds quite efficiently when adopted at the industrial scale. However, is limited when treating dibenzothiophene (DBT). [41] DBT is an organic compound containing sulphur; its line formula is shown in figure 1.10.

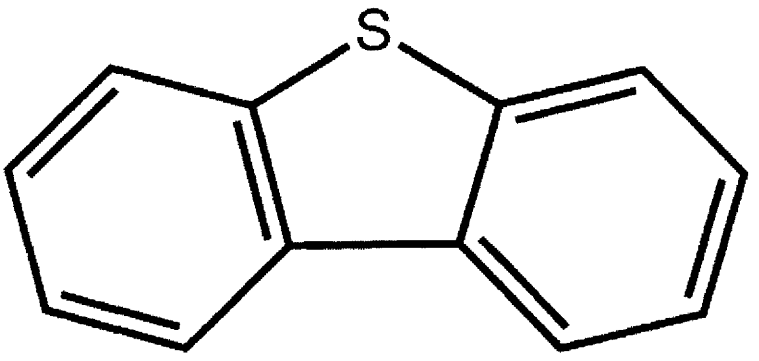

Figure 1.10 Dibenzothiophene molecule

The production of clean light oils requires extreme operating conditions and also highly active catalysts. To eliminate undesirable sulphur-containing compounds, or to convert them into more innocuous forms, several processes have been employed. Such processes include oxidative microbial transformations, physical extraction with a liquid, selective adsorption on

suitable materials, and catalytic oxidation. These techniques involve the removal of sulphur-containing hydrocarbon compounds from distillates or naphtha streams using bacteria. The greatest advantage of oxidative desulphurisation (ODS) as compared with the conventional HDS processes is that it can be performed in the liquid phase under very mild conditions at, or near, room temperature and at atmospheric pressure. In ODS reactions, the divalent sulphur can be oxidized by the electrophilic addition reaction of oxygen atoms to form hexavalent sulphur sulfones. [42-51]

The chemical and physical properties of sulfones are significantly different from those of hydrocarbons in fuel oil. Sulfones can, in general, be easily removed by separation operations such as distillation, solvent extraction, adsorption, and decomposition. Many types of oxidants have been used in ODS methods with variable outcome.[42-51] Such oxidants include nitrogen oxides, nitric acid, hydrogen peroxide, ozone, ^{t}BuOOH, oxygen and air to name a few. The oxidation of thiophene derivatives with H_2O_2 is, for example, known to take place in the presence of HCOOH, CCl_xCOOH (x=1–3), CF_3COOH, ethyltrioxorhenium(VII), vanadium acetylacetonate, phosphotungstic acid, titanium molecular sieves[52] and vanadium silicates.[53] It has been reported that tungsten catalysts are very effective for the oxidation of thioethers (R-S-R) into sulfoxides, sulfoxides into sulfones (see figure 1.11); sulfones contain SO_2 groups bonded directly to two C atoms. They are solid and stable.

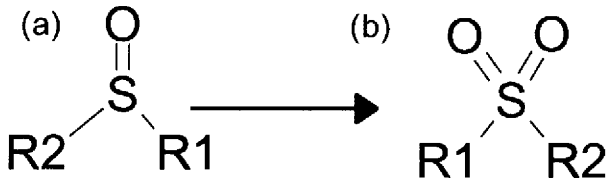

Figure 1.11 a) Sulfoxides oxidized to (b) sulfones

Using H_2O_2 as an oxidant in a two liquid–liquid (L–L) phase system, sulfones can then be regenerated at the L–L interfaces with H_2O_2 and then transferred to the polar phase where it reacts with hydrogen peroxide. Then the obtained sulfones are transferred to the polar phase due to the solubility of sulfones in

a polar solution, giving the production (organic non-polar phase) of a sulphur free phase. However, there is insufficient data available on the applicability of this oxidation method with hydrogen peroxide in the selective transformation of organic sulphur compounds contained in kerosene and light oils. The desulfurization results were highly dependent on the temperature, the nature of the solvent and the molar ratios of the reagents. [41]

The interaction of thiophene, (see figure 1.12) with metallic surfaces is of considerable practical importance. In industrial hydro-desulphurisation (HDS) processes, thiophene is found to be particularly difficult to desulphurise [54,55]. Most industrially used HDS catalysts are based on sulphated Mo supported on alumina (often promoted with Co or Ni). The surface chemistry of thiophene has been investigated on several transition metal surfaces [56, 77].

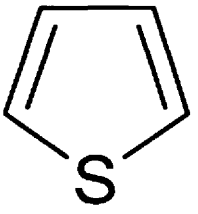

Figure 1.12.Thiophene

Early studies performed on the Pt(111) surface suggested that thiophene decomposes below room temperature to form a metallocycle intermediate. Formation of a metallocycle with C_4H_4 stoichiometry was also proposed for the adsorption of thiophene on a Ni(100) surface. The C_4H_4 metallocycle was found to be stable up to about 227 °C after which it decomposes *via* a C_4H_2 intermediate [56,57]. A similar metallocycle was also proposed for thiophene on the Ru (001) surface. On the Rh (111) surface it was recorded that elimination of sulphur begins at –223 °C, which was followed by a complex reaction sequence involving hydrogenation and dehydrogenation of hydrocarbon residues [58, 59]. Studies of thiophene adsorption on the Pt(111), Pt(100), and Pt(211) surfaces demonstrated that the elimination of sulphur begins at 77 °C. Reaction kinetics were found to be quite independent of the surface orientation and it was concluded that the reaction intermediate was not a

metallic-cycle surface. Dehydrogenation of thiophene occurred at the α-positions, resulting in the formation of a carbon-bonded surface species[60, 61]. Since C_5 species were detected among the desorption products, surface-polymerisation was suggested to occur on the Ni(111) surface. In contrast, studies of low-temperature HDS of thiophene on Ni/Pt(111) bimetallic surfaces showed a pronounced selectivity to produce C_4 hydrocarbon molecules; a Pt(111) surface covered by a monolayer of Ni and a Ni(111) surface produced butene, while the bimetallic Ni/Pt(111) and Pt(111) surfaces produced butadiene. Thiophene dehydrogenation in an α; β; β; α sequence was reported to occur on the Mo(100) surface. Selective dehydrogenation in an α; β; β; α sequence was also reported for thiophene on Fe(100), followed by surface polymerisation through an α-α, β-β coupling. This suggests that thiophene undergoes C-H scission at both α positions on the Fe(100) surface, at temperatures as low as -173 °C [62, 63]; it is known that the α positions are far more reactive than β positions in electrophilic substitution and radical reactions[64,65]. The atomistic model for dehydrogenation and surface-polymerisation is based on an adsorption geometry in which the aromatic cycle is oriented perpendicular to the surface. Previous work using near-edge extended X-ray adsorption fine-structure (NEXAFS) investigations to study thiophene adsorbed on Ni(100) and Cu(100) surfaces, has suggested that thiophene adsorbed on the surface with its molecular plane parallel to the surface and that the S atom binds to a bridge site on both surfaces[66, 67]. Thermal desorption spectra (TDS) investigations[68] of thiophene on the Al(111) surface also suggest a planar adsorption geometry, but associated with much weaker adsorbate substrate interactions compared with those found on transition metal surfaces. Moreover, X-ray photoelectron spectroscopy (XPS) and high resolution electron energy loss spectroscopy (HREELS) studies of the adsorption of thiophene on Ni(111) have shown that a cleavage of the C–S bond at –123 °C, occurs whilst NEXAFS and HREELS experiments studying thiophene adsorption on Ni(100) surface also showed a scission of the C–S bond at temperatures below –183 °C [69]. However, other studies of thiophene adsorption on Ni(111), Ni(100) surfaces and of bithiophene on Ni(110) surface[70], suggested that the molecule would decompose at high rate, even at low temperature. Therefore, no clear picture of the adsorption of

thiophene on metal surfaces has emerged from the experimental investigations[70-72].

Theoretical studies of thiophene adsorption on metallic surfaces are still very scarce.[73] Mittendorfer and Hafner[74, 75] have studied the adsorption of thiophene on Ni(100) surfaces. Two stable adsorption geometries have been identified: the highest adsorption energy (E_{ads} = 2.57 eV) is found for a configuration where one of the C–S bonds has already been broken and all four C atoms form strong bonds with Ni atoms on the surface. In this configuration, all C–H bonds are strongly tilted with respect to the surface plane indicating according to Mittendorfer and Hafner, a substantial activation for dehydrogenation existed. In the second calculated configuration, which is less stable by 0.3 eV, the thiophene molecule remains intact and both C–S bonds are stretched to 1.81 Å (compared to 1.72 Å in the gas phase). Direct desulphurisation is found to be an activated exothermic process, with a reaction barrier of 0.71 eV and an associated energy gain of 0.62 eV for the co-adsorbed S atom and C_4H_4 fragment, compared to the adsorbed linear SC_4H_4 species. Hydrogenolysis of the adsorbed molecule is found to lower the barrier for the C–S bond cleavage to 0.14 eV, but the initial steps of the formation of 2-monohydro- and 2,5-dihydrothiophene are also calculated to have activation energies of 0.98 and 0.58 eV, respectively; these values are even higher than those calculated for direct desulphurisation. The Ni(110) surface is relatively open and absorption occurs here as a result of lower symmetry, which allows for the formation of a larger variety of adsorbate geometries. There have been extended studies on the adsorption of bi- and polythiophenes on clean and sulphide Ni(110) surfaces and these have suggested that if only one molecule arrives onto the surface, it is immediately adsorbed in the flat-4 mode (more stable configuration), On the Ni(100) surface, complete dissociation into S and C_4H_4 is always an activated process, even if it occurs through a stable thiol precursor. The more complex scenario found on the Ni(110) surface is a consequence of the open and corrugated structure of the substrate which enables a variety of locally stable adsorption configurations to exist. [70, 76, 77]

The potential of supercritical water (SCW) was investigated in another study conducted by Vogelaar et al [78], to remove sulphur and metals from gas oil, either separately, or simultaneously. These experiments were carried out in a stirred batch autoclave at 400 °C and 25 MPa, using standard hydrotreated gas oil samples with different sulphur, nickel and vanadium containing model compounds. Results indicated that only non-aromatic sulphur compound react in SCW and the observed degree of desulphurisation is marginal. Aromatic sulphur compounds are too stable to react. The demetallisation of selected metal complexes was not observed but they did undergo some rearrangements in SCW; but their basic structures remained intact. Desulphurisation and demetallisation were only observed in the presence of a conventional hydrotreating catalyst. It was found that SCW alone is not a suitable reaction medium for desulphurisation and/or demetallisation of gas oil. Most of the sulphur-containing rings were found to be stable under the conditions used [78]. Other compounds have been converted by SCW. Those include thiophenols and both alkyl and aryl sulphides [79]. However, Skaugset et al.[80] successfully showed the hydrolytic cleavage of the C–S bond of thiophene complexes upon treatment with aqueous KOH. It was also found that an aqueous solution of nickel- and vanadyl-sulphates promotes desulphurisation. In addition, Sc^{3+}, VO^{2+}, Cr^{3+}, Ni^{2+}, and Cu^{2+} ions promote the decomposition of sulphur compounds.[81]

1.1.2.2 H_2S removal

The removal of contaminants in coal, such as particulates, sulphur and nitrogen oxides, has remained a key problem to be solved. Among the contaminants, sulphur has received more attention than any other because it is a main precursor to acid rain and causes severe corrosion problems in most systems using coal gasification, such as power plants and synthesis gas conversion plants. High temperature desulphurisation of coal derived fuel gas from coal gasification units is considered to be one of the most promising advanced technologies to remove sulphur components from coal and is aimed so that environmental considerations are eliminated from the choice of using coal versus oil or natural gas as fuel feedstock. In addition, this method offers

potential improvements on the thermal efficiency of the systems using coal gasification. The development of these systems depends on the ability to remove sulphur compounds, mainly H_2S, from the coal gas in the temperature range of 500–650 °C. However, the search for sorbents with high H_2S removal efficiency, good sulphur loading capacity, high regenerability and sufficient strength is still under development. [82]

Previous work has shown that the developments of supported mixed metal oxide sorbents for hot-gas desulphurisation are capable of withstanding multiple sulphurisation/regeneration cycles at 871 °C [83]. These sorbents consist of various combinations of copper, molybdenum, and/or manganese oxides supported on a high silica-containing zeolite [83]. Swisher and Schwerdtfeger[84] have previously reviewed the development of mixed-metal oxide sorbents for high-temperature H_2S removal. In their view, binary oxides of Ca, Fe, Zn, Cu, Ni, and Mn were evaluated to be possible candidate substrates for H_2S removal [84]. These experimental studies, along with the thermodynamic predictions of Westmoreland and Harrison[85], identified six metal oxides that have the potential to be desulphurisation sorbents. These include oxides of iron, vanadium, zinc, copper, manganese and molybdenum. Iron oxide, which yields equilibrium H_2S concentrations in the 100 ppm range, was researched intensively in the 1970s. Although iron oxide has a high sulphur capture capacity, and possesses high reactivity for H_2S, its applicability is limited to a moderate coal gas temperatures of up to 500 °C. Higher temperatures (>550 °C) lead to severe sorbent decrepitation due to excessive reduction and iron carbide formation [86]. Furthermore, at 700 °C, in the presence of coal gases, Fe_3O_4 is reduced to FeO; the reduction to FeO has been shown to have a detrimental effect on sulfidation reactivity [87]. However, at low temperatures, iron oxide sorbents can be safely used for H_2S removal. Furthermore, Lee et al.[83] demonstrated that iron oxide sorbents supported on silica could provide enhanced stability for desulphurisation over that of unsupported iron oxide at 400 °C. Comparative thermogravimetric testing of the oxides of Mn, Ca, Zn, and V by Westmoreland et al. [88] showed that the reaction rates of V_2O_3 with H_2S were approximately 1 order of magnitude less than those of CaO and ZnO, and 2 orders of magnitude less

than that of MnO. In addition, in relation to the problem of the slow reaction kinetics of V_2O_3, because of its toxicity, vanadium couldn't be considered for end use applications.

Relatively low cost ZnO was one of the first substrates selected as potential sorbents. However, the ease by which it can be reduced, in reducing atmosphere, and its volatilisation ability limits its applicability up to a temperature of 600 °C[89]. TiO_2 doping through the formation of potentially different titanates[90], can modify the stability of ZnO against reducing agents, but, under the usual operation conditions of calcination, only the spinal structure, Zn_2TiO_4, has been found.[91] By the formation of this compound, the applicability of zinc titanium mixed oxides can be extended up to 670 °C. The TiO_2 excess, with reference to its stoichiometry, is segregated as anatase or rutile, depending on the calcination temperature, which also affects the textural properties of the sorbent. Thermo-balance tests have shown that the overall sulfidation reactivity of these sorbents is dependent on the TiO_2 content, with this effect being derived from the intrinsic reactivity and/or modification of the structural properties that depend on the rate-determining step of the sulfidation reaction[92]. Kinetic experiments in thermo-balance, carried out with ZnO as the sorbent, have shown that the overall reaction rate at 600 °C depends on the particle size, which was in the range 50-350 μm, and on the pore structure of the sorbent. Intraparticle diffusional limitations were found to be the factor most influencing the sorbent reactivity.[93],[94] The reactivity and performance of different zinc-titanium-based sorbent extrudates for desulphurisation of coal gas at high temperature, in successive sulfidation-regeneration cycles were studied using both a thermo-balance and a fixed-bed reactor.[95] The study showed that the graphite was found to increase substantially the porosity of the fresh sorbent extrudates and, because it is eliminated at high temperature, this effect prevailed during calcination treatment and successive sulfidation-regeneration cycles. Graphite notably improved the performance of zinc titanate extrudates as hot temperature sorbents, which under the operation conditions used, was clearly evidenced by an increase of the sorbent efficiency as a result of increasing the exposed surface area by retaining its porosity. [89]

Zinc ferrite and zinc titanate sorbents, prepared by mixing iron oxide and titanium dioxide respectively, in combination with zinc oxide, exhibited better resistance to reduction and vaporization than pure zinc oxide[96]. Difficulties with zinc titanate have included extensive spalling and cracking of fixed-bed pellets, progressive loss of reactivity during multiple sulphidation/regeneration cycles and significant zinc losses at temperatures above 650 °C.[86] While ZnO-based sorbents may be applicable for temperatures as high as 650 °C, it may be desirable to develop suitable sorbents that can operate at temperatures up to 900 °C without undergoing any loss in physical integrity or reactivity. Other potentially applicable oxides include Cu, Mn, and Mo. Atimtay et al. [97] discussed the thermodynamics of copper oxide-H_2S and manganese oxide-H_2S reactions. Copper oxide showed a favourable thermodynamic equilibrium with H_2S. In a reducing atmosphere, e.g., coal gas, the dominant species is favoured to be Cu metal due to the ease by which Cu oxides are reduced to metallic Cu or Cu_2O at elevated temperatures. The sulfidation equilibria of CuO and Cu_2O are vastly superior to that of Cu metal. In a gas fire atmosphere, Mn_3O_4 was readily reduced to MnO, which means that MnO is the species that reacts with H_2S. MnO can withstand high temperatures and has a melting point of 1650 °C. Mn metal was also not found to be formed in a reducing atmosphere, indicated by the equilibrium constant for the reduction reaction being small. Molybdenum however exhibited more typical behaviour in that its higher oxidation state sulphide, MoS_2, was more stable at high temperatures than its lower oxidation state sulphide, Mo_2S_3. In the presence of a gas-fire atmosphere, the dominant Mo-containing sorbent species is therefore MoO_2, not Mo metal [83]. Kyotani et al.[98] found that the reactivity of pure CuO was lower than that of supported CuO, which was attributed to the formation of a dense sulphide layer during sulfidation. It was found that a low initial specific surface area of unsupported Cu oxide led to a low sulphur capacity. Furthermore, the reactivity of pure CuO declined greatly on the second and third cycles of sulfidation, due to loss in surface area: a surface area declined from 8 to <1 $m^2\ g^{-1}$ after both sulfidation at 600 °C and regeneration at 700 °C. Scanning electron micrographs have shown that there is a drastic change between the fine-structured fresh sorbent and the sintered

sulphided/regenerated sorbents. It has also been observed that the sulphur pickup of pure CuO sulphided at 650 °C until 10 ppm H_2S breakthrough, was only 0.19 wt % and declined to 0.13 wt % during the second and third sulfidation (in a typical sulfidation experiment, the concentration of hydrogen sulphide in the product gas rises very slowly, at first, until a certain time after which it rises rapidly to the inlet value). The time of this abrupt change in slope is called the 'breakthrough' time, and the concentration of H_2S verses normalized absorption time t/t^*, is sometimes called the 'breakthrough curve'. t^* is the theoretical breakthrough time, i.e. the time required for complete sulfidation of the sorbent, were t is the experimental time. The fractional conversion at the actual breakthrough time provides a measure of sorbent utilization efficiency, while the level of H_2S before breakthrough is also an important measure of sorbent performance. [98] Other factors explaining the poor performance of pure CuO sorbents include rapid reduction of CuO and Cu_2O to Cu metal (resulting in relatively high pre-breakthrough H_2S concentrations) and improper regeneration (particularly at high pressures, leading to sulphate formation). Two approaches have generally been used to ameliorate the problems associated with the desulphurisation performance of pure CuO. These approaches are preparation of Cu-based sorbents as mixed-metal oxides and as supported metal oxides.

Mixed-metal oxides can sometimes stabilize Cu^{2+} or Cu^{+} ions against reduction to Cu metal. Furthermore, new compounds may be formed that have more favourable thermodynamic properties with respect to sulphur removal efficiency. Mixed-metal oxides containing CuO, that have been previously studied, were prepared by a complexation method where a complexing agent such as citric acid was added to an aqueous solution of metal nitrates and then evaporated, dried, and calcined. The CuO-MnO_2 compound was prepared by co-precipitation from an aqueous metal nitrate solution by the addition of NaOH, and then filtered, washed, and dried.[99] Desai et al.[100] noted that: (1) Cu in a mixed oxide state can reduce sulphur levels below 1 ppm at 650 °C and (2) the reaction of H_2S is about 4 times faster with MnO than with ZnO. Desai argued that a sorbent containing both Mn and Cu oxides might combine the desirable properties of each metal

oxide. Experimental results[83] showed that the inclusion of manganese oxide with copper oxide greatly increases the sulphur loading capacity compared to that of pure copper oxide. During the first sulfidation cycles, a sorbent with a molar Cu: Mn ratio of 1:1 was loaded to 19 wt % at 20 ppm breakthrough at 650 °C. A $CuMnO_2$ sorbent was loaded to 28 wt % at 20 ppm breakthrough at 550 °C. Of the two, the $CuMnO_2$ sorbent appeared to regenerate well with an air/nitrogen mixture at 650-750 °C since the breakthrough performance did not show any trend of deterioration during five cycles. However, the prebreakthrough H_2S level of 30 ppm, was above the desired level of <1 ppm.[83]

A similar study of CuO and Al_2O_3 (20 wt % Cu) with sulfidation at 750 °C and regeneration in air at 900 °C, showed no deactivation of the sorbent for 10 cycles [101]. However, sulphur removal efficiency was poor, reducing the 3000 ppm inlet to a prebreakthrough H_2S concentration of 300 ppm. Another approach that tackled this issue to alumina-supported sorbents (patented by Flytzani-Stephanopoulos et al.[102]) used binary oxides that have relatively low-melting eutectics to coat the pores of the alumina with a thin film of liquid at the reaction temperature. The superior dispersion of active metal oxides in these sorbents enhanced their performance. For example, CuO and MoO_3, which form a eutectic at 560 °C, yielded prebreakthrough outlet H_2S concentrations of <0.1 ppm at both 538 °C and 650 °C.

An interesting result was observed when CuO and ZnO were supported on a zeolite. Three sorbents were prepared in three different ways: sorbent A, Zn was exchanged onto the zeolite first and then Cu; sorbent B, Cu exchanged first and then Zn; and sorbent C, Cu and Zn exchanged together, at a Cu:Zn molar ratio of 1:2. The three sorbents differed greatly in their initial sulphur capacity at 650 °C and then decreased markedly in capacity within <10 cycles. Sorbent C showed the lowest initial sulphur capacity, which dropped to 12.5% of its first cycle capacity during the second cycle. Sorbent B had the greatest sulphur capacity, which was more than 3 times that of sorbent C. These decreases in capacity were attributed to crystallite growth or sintering and, in the case of Zn, to volatilisation. Jalan et al.[83] indicated that it was not

possible to offer an explanation for the superior initial desulphurisation capacity of sorbent B, but felt that it might be related to Zn occupying more favourable cation-exchange sites.

Kyotani et al.[98] compared sorbent A, pure CuO; sorbent B, CuO/SiO_2 containing 20 wt % Cu (prepared by mixing a solution of $CuCl_2$ in ethylene glycol with ethyl silicate); and sorbent C, 15 wt % Cu on zeolite and found that the combination of Cu oxides with acidic supports such as SiO_2 resulted in superior sorption abilities compared to pure Cu oxide. At 600 °C, a first sulfidation of sorbent A, i.e. pure CuO, yielded <30% utilization of Cu, while sorbent B showed almost 100% utilization and sorbent C somewhat less than sorbent B. Although sorbent B had a Cu content approximately one-fifth of that of sorbent A, breakthrough times were similar or better than those for sorbent A. For sorbent C, some of the Cu may have been inaccessible to H_2S, due to an overlying sulphide layer and blockage of the internal pores. This problem can potentially be overcome with somewhat different preparation techniques, different zeolites, or decreased Cu loadings. Jalan [83] conducted comparative studies of unsupported CuO and CuO supported on various catalyst carriers. He found that the sulphur capacities increased in the following order: unsupported CuO < SiO_2 < Al_2O_3 < zeolite. The increase in capacity among unsupported CuO, SiO_2, and Al_2O_3 was approximately 1 order of magnitude each for certain temperatures within the range of 500-650 °C, and the zeolite capacity was approximately double that of alumina.

Voecks and Sharma [103] showed that a combination of Cu and Mo oxides on a sodium-deficient 4A type zeolite, yielded a superior sorbent. This Cu-Mo/zeolite sorbent showed optimal capacity at 400 °C, as compared to those tested at 300 °C and 538 °C. During a 14-cycle test, no significant change in capacity or reactivity was detected and at 400 °C, the prebreakthrough H_2S concentration was below 0.5 ppm.

Desai et al.[100] suggested that the combination of Cu-Mo-Mn oxides are potentially superior candidates for hot gas desulphurisation sorbent. A cmbination of Cu, Mn, and Mo oxides were selected and prepared as sorbent

pellets using a porous high-silica containing zeolite support. The purpose of using the high-silica-containing zeolite support was to minimize metal migration and volatilisation *via* support-metal oxide interactions. The operating temperature selected for both sulfidation and regeneration in the study was 871 °C. The sorbents investigated in that study were prepared by wet impregnation. SP-115 zeolite (1.59-mm) extrudates were used as the support media and had the following characteristics: SiO_2 > 99 wt %, surface area 482 m^2g^{-1}, crush strength 6.6 kg/cm (1.5 lb/mm), zeolite pore diameter 5.4 Å. The wet impregnation procedure included: (1) impregnation of the zeolite with a solution of cupric acetate, ammonium molybdate and/or manganese acetate; (2) dehydration of the sorbent in a vacuum oven at 70 °C and 2.5 mm of Hg and; (3) calcination of the sorbent in a Lindberg muffle furnace at 900 °C for 7 h. Steps 1-3 were repeated three times during the preparation of each sorbent. These sorbents were tested in a fixed-bed reactor with simulated coal gas at 1537.6 mm Hg pressure. The combination of all three metal oxides displayed synergism in their enhanced efficiency for H_2S removal and also improved crush strength on the pellets. Copper oxide was the most active component in the reaction with H_2S, while molybdenum and manganese oxides appeared to act as catalysts/promoters. During multicycle testing, this ternary metal oxide sorbent retained its reactivity and mechanical strength but lost approximately 25% of its total surface area after 5 cycles. [83]

The effect of the molar ratio of Mn:Fe on Mn–Fe/γ-Al_2O_3 sorbent performance, for hot gas desulphurisation, was examined in other work [82]. Results showed that the ideal composition for the Mn–Fe–Zn/ γ-Al_2O_3 sorbent was 2:1:0.2 molar ratios (AMFZ0.2). The regenerated AMFZ0.2 sorbent breakthrough sulphur capacity exhibited a similar value compared to the fresh sorbent, when the reaction–regeneration cycles were over 15. This shows that the AMFZ0.2 sorbent can be an ideal sorbent for removal of H_2S at high temperature for a hot gas desulphurisation process. [82]

1.1.3 Proposed project

Oil products contain a variety of sulphuric compounds, some of which are more stable than others, and therefore some harder to extract from their environment than others. It is common practice in refineries to determine the total volume or weight percent of sulphur, rather than determining the type of sulphur compound individually. Therefore, the existing type, and the percentage of each individual sulphur compound is not really determined for all oil product. In addition, different sulphur compounds have different degree of affinity towards various metals and metal oxides.

The aim of this project will focus on the preparation of various hosts that contains metals and metal oxides, which are predicted to possess a high affinity for a few selected sulphur compounds such as thiophene, dibenzosulfoxide, dibenzothiophene, and dimethyl-dibenzothiophene. The project has been conducted in a step-wise manner. The first stage was to establish a relatively stable host that contains mesopores using different synthesizing methods, determine their surface area, pore percentage volume and diameters, and analyze the effect of each step of the preparation on the overall structure and stability of the host. The second stage was to dope each host structure with one metal or metal oxide. The third step included a study of the effect that incorporation has on the total host properties, before which, completing a thorough analysis on the sorption properties of individual sorbents at low temperatures (below 100 °C).

1.1.4 References

1. J. D. Mackenzie, E. P. Bescher, *Acc. Chem. Res.*, 2007, **40**, 810–818.
2. V. Lansmann, M. Jansen, *Journal of Material Scince*, 2001, **36**, 1531– 1538.
3. R. Roy, *Journal of Solid State Chemistry*, 1994, **111**, 11-17.
4. J. Brinker, G. W. Scherer, *Sol–Gel Science; The Physics and Chemistry of Sol–Gel Processing*, Academic Press: London, 1990.
5. R. I. Walton, *Chem. Soc. Rev.*, 2002, **31**, 230–238.
6. D. J. Shaw, *Introduction to Colloid & Surface Chemistry*, forth edition 2000, Antony Rowe Ltd., Elsevier Science Ltd.1992, Chapter one.
7. a) A. J. Bard and L. R. Faulkner 2001, *Electrochemical Methods Fundamentals and Applications*, Second edition, John Wiley and sons. 2001, 137-155, b) D. F. Shriver, P. W. Atkins, *Inorganic chem.*, third edition, Oxford Univ. Press, 1999, 366-369.
8. G.W. Gray, F.R.S., *Phil.Trans.R.Soc.Lond.* 1990, **A330**, 73-94.
9. G.W. Gray, *Phil.Trans.R.Soc.Lond.* 1983, **A309**, 77-92.
10. a) E. Fairhurst, S. Fuller, J. Gray, M. C. Holmes, and G. J. T. Tiddy *Lyotropic Surfactant Liquid Crystals* in *Handbook of Liquid Crystals*, D. Demus, J. W. Goodby, b) G. W. Gray, H. W. Spiess, and V. Vill vol. 3, *High Molecular Mass Liquid Crystals*, 341 Wiley-VCH 1998,c) M. J. Danks, *PhD. Thesis Exeter U.*, Chap.1, 2,3, 2002.
11. a) S. R. Collinson and D. W. Bruce, in *Transition Metals in Supramolecular Chemistry*, ed. J. P. Sauvage, Wiley, Chichester, 1999, p. 285, b) T. Hirai, K. Suzuki and I. Komasawa, *J.Colloid Interface. Sci.*, 2001, **244**, 262.
12. D. J. Mitchell and B. W. Ninham, *J. Chem. Soc. Farad. Trans.* 2, 1981, **77**, 601.
13. a) C. N. R. Rao, FRS, J. Gopalakrishnan, *New direction in solid state chemistry*, 1st edition Cambridge Univ. Press, 1986, 66-70, b) D. W. Bruce, and D. O'Hare, in *Inorganic Materials*, 2nd Edn., Wiley, Chichester, 1996., c) fig. 7 is from professor's D. W. Bruce's web site (http://www.york.ac.uk/depts/chem/staff/dwb.html).)
14. a) Figure 8b is taken from Dr. R. Bell's web site: (http://www.chem.ucl.ac.uk/people/bell/index.html), b) P. A. Jacobs, *Carboniogenic Activity Zeolites*, Volume 7 Elsevier Scientific, New York, 1977.
15. C. Boissiere, M. A. U. Martines, P. J. Kooyman, T. R. de Kruijff, A. Larbot, and E. Prouzet, *Chem. Mater.* 2003, **15**, 460-463.
16. J.Y. Ying, C. P. Mehnert, and M. S. Wong, *Angew. Chem.* Int. Ed. 1999, **38**, 56 –77.
17. A. R. West, *Basic Solid State*, 1988, 120-182.
18. M. T. Weller, *Inorganic Materials Chemistry*, OCP, **23**,1994, 1-25.
19. L. Smart and E. Moore, second edition,1995, 79-107.
20. a) G. S. Attard, J. C. Glyde, C. G. Goltner, *Nature* 1995, **378**, 366 – 368, b) M. Chen, L. Wu, S. Zhou, and B. You, *Macromolecules* 2004, **37**, 9613-9619.
21. P. Siciliano, *Sensors and Actuators B*, 2000, **70**,153–164.
22. T. Hyodo, S. Abe, Y. Shimizu, M. Egashira, *sensors and Actuators B*, 2003, **93**, 590–600.
23. S.-S. Park, J.D. Mackenzie, *Thin Solid Films*, 1996, **274**,154-159.
24. A. Dieguez, J.R Romano-Rodriguez, U. Morante, M. Weimar, B. Schweizer, W. Gopel, *Sensors and Actuators B*, 1996, **31**, 1—8.
25. A. Teramongkonrasmee, M. Sriyudthsakr, *Sensors and Actuators B*, 2000, **66**, 256–259.
26. a) J. S. Beck, J. C. Vartuli, W. J. Roth, M. E. Leonowicz, C. T. Kresge, K. D. Schmitt, C. T. W. Chu, D. H. Olsen, E. W. Sheppard, S. B. McCullen, J. B. Higgins, J. L. Schlenker, *J. Am. Chem. Soc.* 1992, **114**, 10 834 – 10843, b) A. Stein, M. Fendorf, T. P. Jarvie, K. T. Mueller, A. J. Benesi, and T. E. Mallouk, *Chem. Mater.* 1995, **7**, 304-313.
27. T. M. R. Aqeel, *Msc thesis*, Exeter University 2003-2004.
28. Q. Huo, D.I. Margolese, U. Ciesla, D.G. Demuth, P. Feng, T.E. Gier, P. Sieger, A. Firouzi, B.F. Chmelka, F. Schuth, G.D. Stucky, *Chem. Mater.* , 1994, **6**,1176.
29. D. Zhao, J. Feng, Q. Huo, N. Melosh, G.H. Frederickson, B.F. Chmelka, G.D. Stucky, *Science*, 1998, **279**, 548.
30. J.C. Vartuli, K.D. Schmitt, C.T. Kresge, W.J. Roth, M.E. Leonowicz, S.B. McCullen, S.D. Hellring, J.S. Beck, J.L. Schlenker, D.H. Olson, E.W. Sheppard, *Chem. Mater.* 1994, **6**, 2317.

31. N.K. Raman, M.T. Anderson, C.J. Brinker, *Chem. Mater*, 1996, **8**, 1682.
32. F. Kleitz, W. Schmidt, F. Schuth, Micropor. *Mesopor. Mater.* **44–45** (2001) 95.
33. J. Blanchard, P. Trens, M. Hudson, F. Schuth, *Micropor. Mesopor. Mater.* **39** (2000) 163.
34. C.Y. Chen, H.X. Li, M.E. Davis, *Micropor. Mater.* **2** (1993) 17.
35. a) F. Kleitz, W. Schmidt, F. Schuth, *Microporous and Mesoporous Materials*, 2003, **65**, 1–29, b) P.-A. Albouy, A. Ayral, *Chem. Mater.*2002, **14**, 3391.
36. J. M. Morales, J. Latorre, C. Guillem, A. Beltrán-Porter, D. Beltrán-Porter, *J.M. Morales et al. Solid State Sciences*, 2005, **7**, 415–421.
37. X. Liu, B. Tian, C. Yu, F. Gao, S. Xie, B. Tu, R. Che, L. Peng, and D. Zhao, *Angew. Chem. Int. Ed.*, 2002, **41**, **No. 20**, 3876-3878.
38. T. J. Campbell, A. H. Shaaban, F. H. Holcombb, R. Salavani, M. J. Binder. *Journal of Power Sources*, 2004, **129**, 81–89.
39. C. Song, *Catal. Today*,2002, **77**, 17–49.
40. A.H. Shaaban, T. Anderl, *document ML-02-03*, June 2002, p. 31, also available at http://www.afrlhorizons.com/Briefs/Jun02/ML0203.html.
41. J. M. Campos-Martin, M. C. Capel-Sanchez and J. L. G. Fierro, *Green Chem.* 2004, **6**, 557-562.
42. T. Aida and D. Yamamoto, Prepr. *Am. Chem. Soc., Div. Pet. Chem.*, 1994, **39**, 623.
43. F. M. Collins, A. R. Lucy and C. Sharp, *J. Mol. Catal. A*, 1997, **117**, 397.
44. F. Zannikos, E. Lois and S. Stournas, *Fuel Process. Technol.*, 1995, **42**, 35.
45. P. S. Tam, J. R. Kittrell and J. W. Eldridge, *Ind. Eng. Chem. Res.*, 1990, **29**, 321.
46. J. F. Ford and V. O. Young, Prepr. *Am. Chem. Soc., Div. Pet. Chem.*, 1965, **10**, C-111.
47. B. N. Heimlich and T. J. Wallace, *Tetrahedron*, 1966, **22**, 3571.
48. A. Attar and W. H. Corcoran, *Ind. Eng. Chem. Prod. Res. Dev.*, 1978, **17**, 102.
49. A. Paybarah, R. L. Bone and W. H. Corcoran, *Ind. Eng. Chem. Process Des. Dev.*, 1982, **21**, 426.
50. M. Houalla; D. H. Broderick, A. V. Sapre, N. K. Nag, V. H. J. De Beer, B. C. Gates and H. Kwart, *J. Catal.*, 1980, **61**, 523.
51. Ch. Song and X. Ma, *Appl. Catal. B*, 2003, **41**, 207.
52. V. Hulea, F. Fajula and J. Bousquets, *J. Catal.*, 2001, **198**, 179.
53. Y. Shiriraishi, T. Naito and T. Hirai, Ind. Eng. *Chem. Res.*, 2003, **42**(24), 6034.
54. B. J. Wiegand, C. M. Friend, *Chem. Rev.*, 1992, **92**, 491.
55. H. Topsoe, B.S. Clausen, F.E. Massoth, in: *Catalysis Science and Technology*, vol. 11, Springer, New York, 1996.
56. J. Stohr, E.B. Kollin, D.A. Fischer, J.A. Hastings, F. Zaera, F. Sette, *Phys. Rev. Lett.*, 1985, **55**, 1468.
57. F. Zaera, E.B. Collin, J.L. Gland, *Langmuir* , 1987, **3**, 555.
58. W.H. Heise, B.J. Tatarchuk, *Surf. Sci.*, 1989, **207**, 297.
59. F.P. Netzer, E. Bertel, A. Goldmann, *Surf. Sci.*, 1988, **201**, 257.
60. J.T. Roberts, C.M. Friend, *Surf. Sci.*,1987, **186**, 201.
61. N.A. Khan, H.H. Hwu, J.G. Chen, *J. Catal.*, 2002, **205**, 259.
62. F. Zaera, E.B. Kollin, J.L. Gland, *Surf. Sci.*, 1987, **184**, 75.
63. L. Cheng, A.B. Bocarsly, S.L. Bernasek, T.A. Ramanarayanan, *Surf. Sci.*, 1997, **374**, 357.
64. I. Kardinal, G. Koller, F.P. Netzer, M.G. Ramsey, *Thin Solid Films*, 1998, **327**, 204.
65. I. Kardinal, F.P. Netzer, M.G. Ramsey, Surf. Sci. Lett., 1998, **405**, L520.
66. T. Ohta, *Physica B*, 1995, **208–209**, 427.
67. A. Imanishi, S. Yagi, T. Yokoyama, T. Ohta, *J. Electron Spectrosc. Relat. Phenom.*, 1996, **80**, 151.
68. R.I. Blyth, F. Mittendorfer, J. Hafner, S.A. Sardar, R. Duschek, F.P. Netzer, M.G. Ramsey, *J. Chem. Phys.*, 2001, **114**, 935.
69. D.R. Huntley, D.R. Mullins, M.P. Wingeier, *J. Chem. Phys.*, 1996, **100**, 19620.
70. C. Morin, A. Eichler, R. Hirschl, P. Sautet, J. Hafner, *Surface Science*, 2003, **540**, 474–490.
71. H.P. Steinruck, *J. Phys.: Condens. Matter*, 1996, **8**, 6465, and further references cited therein.
72. G. Held, M.P. Bessent, S. Titmuss, D.A. King, *J. Chem. Phys.*, 1996, **105**, 11305.
73. C. Morin, D. Simon, P. Sautet, *J. Phys. Chem. B*, 2003, **107**, 2995.

74. F. Mittendorfer, J. Hafner, *Surf. Sci.*, 2001, **492**, 27.
75. F. Mittendorfer, J. Hafner, *J. Catal.*, 2003, **214**, 234.
76. M.G. Ramsey, G. Koller, I. Kardinal, F.P. Netzer, *Surf.Sci.*, 1996, **352**, 128.
77. G. Koller, S. Surney, F.P. Netzer, M.G. Ramsey, *Surf. Sci.*, 2002, **504**, 11.
78. B.M. Vogelaar, M. Makkee, J.A. Moulijn, *Fuel Processing Technology*, 1999, **61**, 265–277.
79. A.R. Katritzky, R.A. Barcock, M. Balasubramanian, J.V. Greenhill, M. Siskin, W.N. Olmstead, *Energy and Fuels*, 1994, **8**, 498–506.
80. A.E. Skaugset, T.B. Rauchfuss, S.R. Wilson, *Organometallics*, 1990, **9**, 2875–2876.
81. A.R. Katritzky, M. Balasubramanian, M. Siskin, *Energy and Fuels*, 1992, **6**, 431–438.
82. J. Zhang, Y. Wang, D. Wu, *Energy Conversion and Management*, 2003, **44**, 357–367.
83. L.D. Gasper-Galvin, A. T. Atimtay, R. P. Gupta, *Ind. Eng. Chem. Res.* 1998, **37**, 4157-4166, and references within.
84. J. H. Swisher, K. Schwerdtfeger, *J. Mater. Eng. Perform.*, 1992a, ***1*** **(No. 3)**, 399-407, J. H. Swisher, K. Schwerdtfeger, *J. Mater. Eng. Perform.*,1992b, ***1*** **(No. 4)**, 565-571, J. H. Swisher, J.Yang, R. P. Gupta, *Ind. Eng. Chem. Research*, 1995, ***34***, 4463-4471.
85. P.R. Westmoreland, D.P. Harrison, *Environ. Sci. Technol.*, 1976, **10**, 659.
86. R.P. Gupta, S.K. Gangwal, S.C. Jain, *Energy Fuels*, 1992, **6**, 21-27.
87. G. D. Focht, P.V. Ranade, D. P.Harrison, *Chem. Eng. Sci.*, 1988, **43** (No. 11), 3005-3013.
88. P. R. Westmoreland, J. B. Gibson, D.P. Harrison, *Environ. Sci. Technol.*, 1977, **11**, 488, and P. R. Westmoreland, P. D Harrison, *Environ. Sci. Technol.* 1976, **10**, 659.
89. M. Pineda and J. M. Palacios, F. Tomas, C. Cilleruelo, E. Garcia, and J. V. Ibarra, *Energy & Fuels* 1998, **12**, 409-415.
90. S.S. Cole, W. Nelson, *J. Phys. Chem.*, 1938, **42**, 245.
91. M. Pineda, J. L. G. Fierro, J.M. Palacios, C. Cilleruelo, E. Garcia, J.V. Ibarra, *Appl. Surf. Sci.*, 1997, **119**, 1.
92. S. Lew, A.F. Sarofim, M. Flytzani-Stephanopoulos, *Chem. Eng.Sci.*, 1992, **47**, 1421, and E. Sasaoka, *Energy Fuels*, 1994, **8**, 763.
93. E. A. Efthimiadis, S.V. Sotirchos, *Chem. Eng. Sci.*, 1993, **48**, 1971.
94. a) M. C. Woods, S. K. Gangwal, K. Jothimurugesan, D.P. Harrison, *Ind. Eng. Chem. Res.*, 1990, **29**, 1160, b) K. Jothimurugesan, D.P. Harrison, *Ind. Eng. Chem. Res.*, 1990, **29**,1167, c) S. Lew, A.F. Sarofim, M. Flytzani-Stephanopoulos, *Ind. Eng.Chem. Res.*, 1992, **31**, 1890.
95. (a) S. K. Gangwal, J.M. Stogner, S.M. Harkins, *Environ. Prog.*,1989, **8**, 26, (b) S.K. Gangwal, S. M. Harkins. M. C. Woods, S.C. Jain, S.J. Bossart, *Environ. Prog.*, 1989, **8**, 265, (c) W. Mojtahedi, K. Salo, J. Abbasian, *Fuel Process. Technol.*1994, **37**, 53.
96. S. Lew, A.F Sarofim, M. Flytzani-Stephanopoulos, *Chem. Eng. Sci.*, 1992, **47** (No. 6),1421-31.
97. A. T. Atimtay, L.D. Gasper-Galvin, J.A. Poston, *Environ. Sci. Technol.*, 1993, **27** (No. 7), 1295-1303.
98. T. Kyotani, H. Kawashima, A. Tomita, A. Palmer, E. Furimsky, *Fuel, 1989*, **68** (No. 1), 74-79.
99. S. S. Tamhankar, M. Bagajewicz, G.R. Gavalas, P. Sharma, M. Flytzani-Stephanopoulos, *Ind. Eng. Chem.Process Des. Dev.*, 1986, **25**, 429-437.
100. M. Desai, F. Brown, B. Chamberland, V. Jalan, *Fuel Chem.*, 1990, **35** (No. 1), 87-94.
101. G. Sick, K. Schwerdtfeger, *Trans. B*, 1987, **18B**, 603-609.
102. M. Flytzani-Stephanopoulos, G.R. Gavalas, S. S Tamhankar, *U.S. Patent* **4,729,889**, March 8, 1988.
103. G. E. Voecks, P.K. Sharma, Hot Gas, *U.S. Patent* **5,252,528**, Oct. 12, 1993.

Chapter 2

Characterization Methods

This chapter details the characterisation methods employed in this PhD project to investigate structural morphologies and to examine the stability of the synthesized porous materials, both before and after doping. Furthermore we introduce the methods utilized to determine the cluster size of metals, the methods used by which we determined the location of such metal clusters within their host structure and finally the methods employed to examine the sorption properties of our synthesized porous solids.

2.1 Characterization Methods

2.1.1 X-Ray Diffraction (XRD)

Low-angle X-ray diffraction studies show that MCM-41 has a framework with long-range order; the few reflections being indexed to a two dimensional hexagonal unit cell as indexed in figure 2.1 below that is similar to the lyotropic hexagonal phase templating material employed.

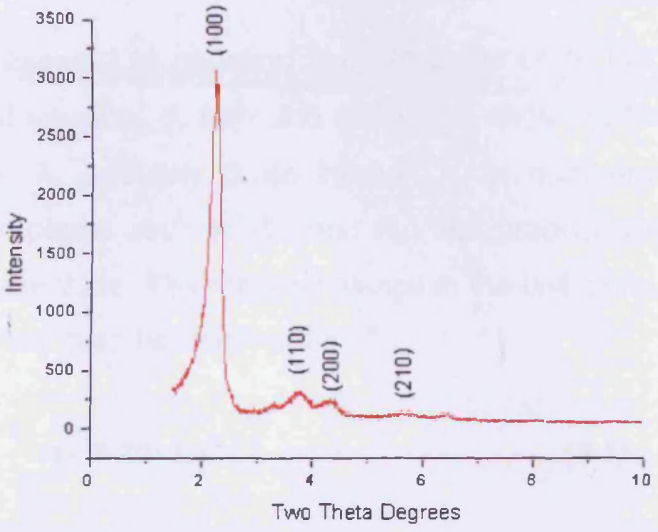

Figure 2.1 X-Ray diffraction pattern of MCM-41 with two-dimensional hexagonal symmetry, plane group *p6mm*

The reflections are a consequence of the hexagonal packing of cylinders structure surrounded by amorphous silicate or aluminosilicate walls as presented in figure 2.2a. It is usual to see between 1 and 4 reflections for MCM-41 in the low-angle region; however, Edler and White[1] have previously observed 7 reflections.

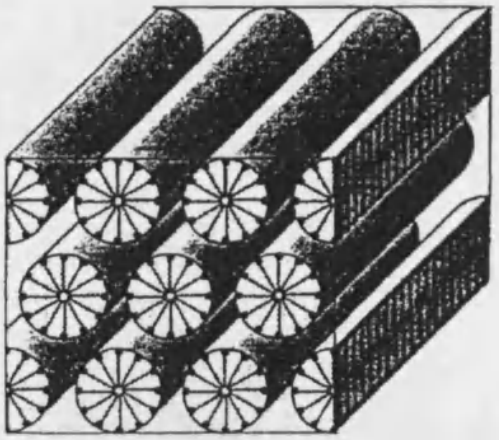

Figure 2.2a. A representation of pores distribution and the cylindrical packing before removal of templating materials [3]

Bragg's law presented in equation 2.1 can be used to calculate the plane separation or d spacing, *d*, from the diffraction angle, θ, the wavelength of incident X-rays, λ, and any given integer, *n*, of numbers of constructive wavelengths (in phase such as R_1, and R_2) that produce Bragg's peaks, as illustrated in figure 2.2b. The repeat distance in the unit cell a_0 (= $2d_{100}$ / √3 or = d_{100} / sin 60) may then be determined. [26]

$$n\lambda = 2d\sin\theta \qquad (2.1)$$

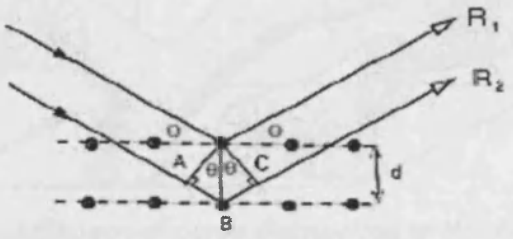

Figure 2.2b. Illustration of Bragg's Law, R_1 and R_2 are diffracted X-rays. The angle θ is the angle of incidence with planes containing the indicated atoms [26]

Cubic mesoporous silicate and aluminosilicate often called MCM-48 exhibit four peaks, which could be indexed to the space group *Ia*3*d*, see figure 2.3, Xu and Luan[2] assigned eight reflections, consisting of short cylinders with interwoven pores as represented in figure 2.4 below.

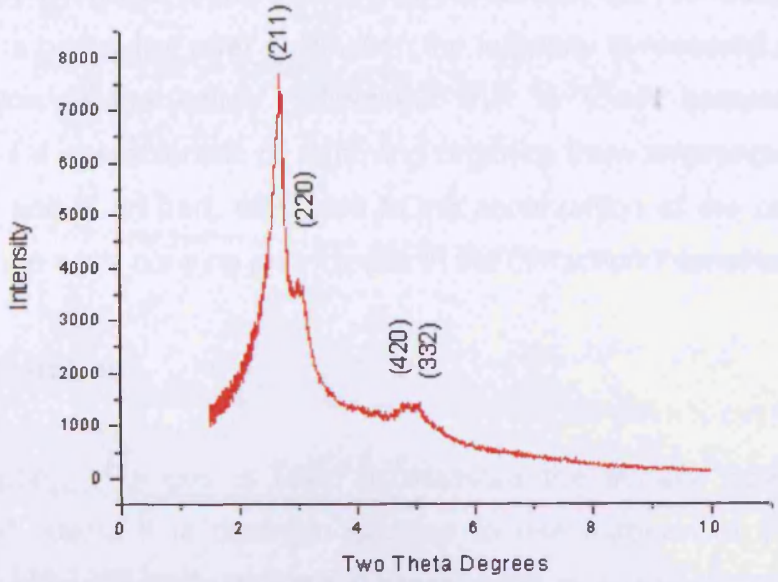

Figure 2.3 X-Ray diffraction pattern of MCM-48 with cubical symmetry, space group *Ia3d*

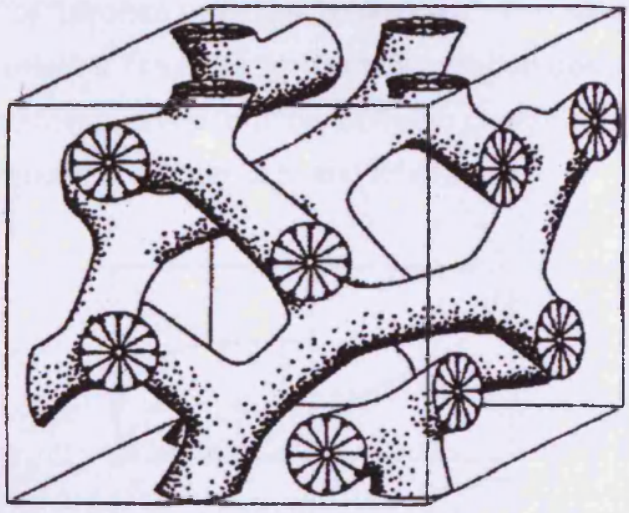

Figure 2.4 Simple representations of pores distribution of MCM-48 before the removal of templating materials[3]

X-Ray powder diffraction (XRD) does not give much information about the structure of the pore walls especially for silicate and aluminosilicate and the apparent lack of ordering at the atomic level infers that the materials do not contain any crystalline inorganic regions, but rather resemble amorphous oxides with low density [4]. However XRD is a useful analytical tool for studying crystalline materials particularly zinc oxide, metallic gold and silver.

In the as-synthesised organic-inorganic composite, the surfactant template occupies the pores, but after calcination the template is removed and there is a contraction in the lattice (reflections shift to lower d-spacing). This shrinkage is a characteristic of removing organics from amorphous materials by heating and is, in part, attributed to the continuation of the condensation process in the walls causing an increase in the diffraction intensities.[5]

2.1.2 Gas Sorption

The adsorption of a gas is used to measure the surface area and pore structure of solids. It is common practice to use nitrogen at 77 K as the adsorbate, although there are many others, and in a typical experiment the amount of nitrogen that a solid adsorbs can be determined at increasing relative pressures. When adsorption is complete, a vacuum may be applied and desorption of nitrogen may be measured.[6] The adsorbed amount is plotted against relative pressure for both adsorption-desorption processes, giving rise to an adsorption-desorption isotherm characteristic of the porosity of the solid as presented in figure 2.5, and table 2.1.

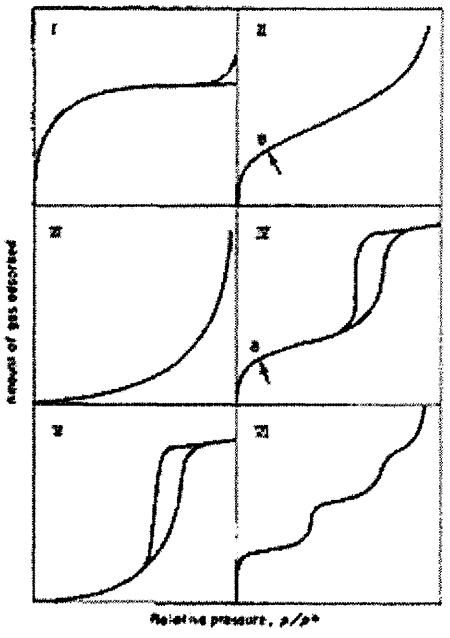

Figure 2.5 Different BET isotherms [6, 7]

Table 2.1 The six types of isotherm in BET classification

Classification	Solid
Type I	Microporous solids
Type II	Non-porous solids
Type III	Non-porous solids, weak adsorbent-adsorbate interactions
Type IV	Mesoporous solids, hysteresis loop
Type V	Meso- or macroporous solids, hysteresis loop and weak adsorbent-adsorbate interactions
Type VI	Adsorption on a uniform surface

Adsorption isotherms are characterised according to the Stephen Brunauer, Paul Emmett and Edward Teller (BET) classification and are dependent on the nature of the surface and the forces (dispersion, repulsive and Coulombic) that exist between the adsorbent and adsorbate by assuming the initial adsorbed layer can act as a substrate for further adsorption creating a multilayer. The BET surface area is derived from the monolayer coverage of the sample and calculated from the adsorption curve by applying the BET equation, 2.2A, where V_{ads} is the volume of gas adsorbed at pressure p, p^{o} is the saturation pressure, V_m is the volume of gas adsorbed at monolayer coverage and c is the BET constant.[19]

$$\frac{p}{V_{ads}(p^{o}-p)} = \frac{1}{V_m c} + \frac{c-1}{V_m c}\cdot\frac{p}{p^{o}} \qquad \textit{(2.2A)}\ ^{19}$$

Mesoporous materials, such as M41S, have specific surface areas in excess of 700 m^2g^{-1} and are characterised by the type IV isotherm. The isotherm has three main parts as presented in figure 2.6A, the first being monolayer-multilayer adsorption on the pore walls in the low-pressure region (A). The first point of inflection corresponds to the effective mean pore diameter and is also the beginning of capillary condensation within the pores (C), the long plateau (D) follows the second point of inflection and corresponds to multilayer adsorption on the external surface of the solid after the pores have filled.[7]

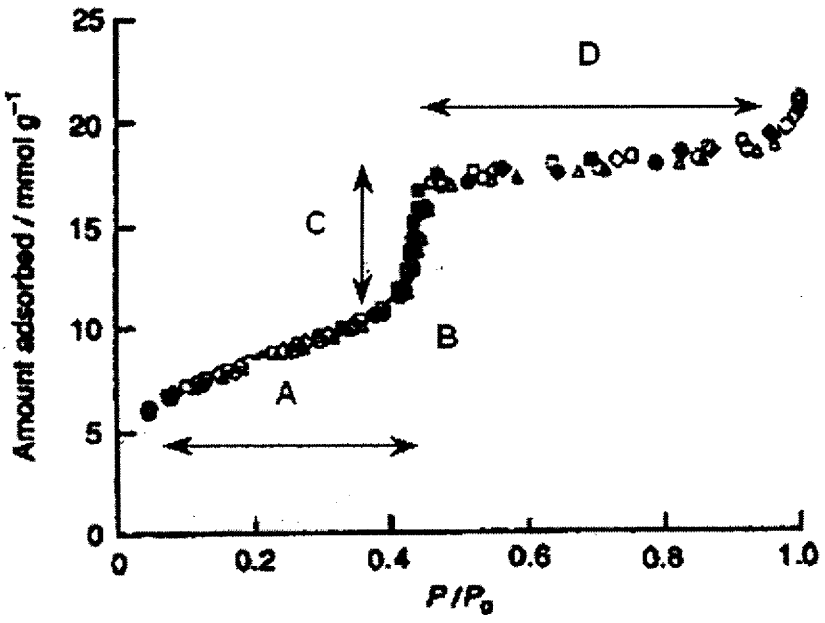

Figure (2.6A) Adsorption-desorption isotherm of nitrogen on MCM-41 at 77 K, filled symbols denote desorption, •■ [8]

A feature often characteristic of the type IV isotherm is the hysteresis loop between the adsorption and desorption branches and it is a function of pore size, [9] temperature[10] and the adsorbate.[11] However, this is not observed for the isotherm in figure 2.6A.

The pore size and pore size distribution are usually calculated from the desorption curve by applying the Barrett, Johner, and Halenda (BJH)[27] equation (2.2B). Generally, the desorption branch of an isotherm is used to relate to the amount of adsorbate lost in a desorption step to the average size of pores emptied in the step. A pore loses its condensed liquid adsorbate (Inner capillary volume) at a particular relative pressure ($\mathbf{P/P_o}$). At any desorption step the inner capillary adsorbate is evacuated in addition to the physically adsorbed layer on the pore wall thickness (**t**).

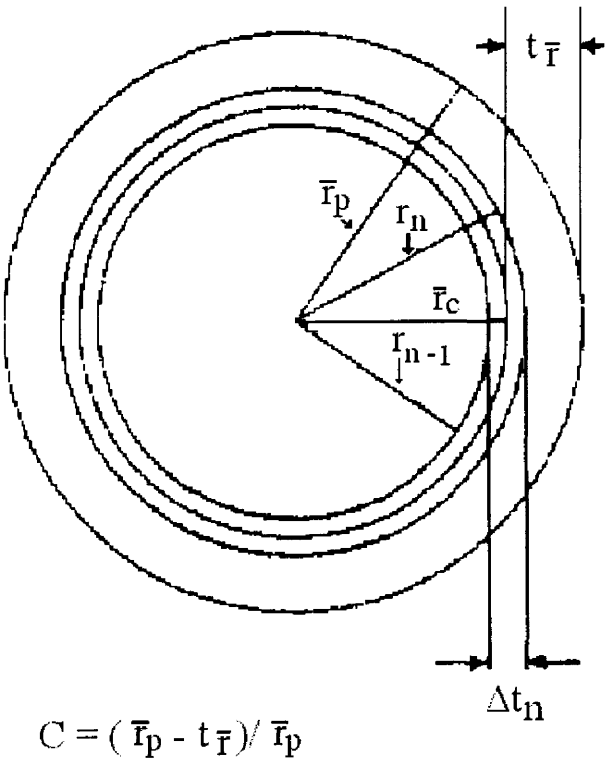

Figure (26B) representation of BJH's assumed desorption mechanism of the adsorbed layers inside the pores, showing the concentric layers and their radii[27]

The quantity of the gas desorbed in a step is composed of a quantity equivalent to the evaporated liquid of the inner capillary volume and that from the physically adsorbed on the walls. BJH's equation depends on two assumptions; 1) the pores are cylindrical, 2) the amount of adsorbate is in equilibrium with the gas phase.

$$V_{p_n} = R_n \Delta V_n - R_n c \Delta t_n \sum_{j=1}^{n-1} A_{p_j} \qquad (2.2B)$$

where ΔV_n is the change in the volume of the desorbed liquid gas by a stepwise decrease that occurs in the thickness of the physically adsorbed layers on the walls Δt_n and from the amount of total liquid-gas volume lost from pores V_{pn}. The area of each pore at any given relative pressure is A_{pj} (the summation of A_{pj} gives the cumulative area of total pores). Whereas **c** is a factor related to the average radii as presented in figure 26B. The other factor is R_n, its value also dependent on the change in the values of r_p, r_k, and

Δt. The inner capillary radius is r_k, can be calculated from Kelvin's[27] equation (2.2C) and the pore radius is r_p is shown in figure 26B. [27]

.

$$\log (P/P_0) = \frac{-2\sigma V}{8.316 \times 10^7 \times 2.303 T r_k} \qquad (2.2C)$$

where 8.316 X 10^7 is the gas constant in ergs/ degree, σ is the surface tension of liquid gas (N_2), V is liquid molar volume (N_2), r_k is the radius of capillary and T is the absolute temperature in °K.

The wall thickness of the material can then be calculated from the difference between the lattice parameter presented previously in equation 1, from XRD peaks and the pore size from BET analysis. However, whilst these values are useful tools in explaining the properties of these materials, they should only be considered as estimates.[19]

2.1.3 Scanning Electron Microscopy / Energy Dispersive X-Ray Spectroscopy

Scanning electron microscopy (SEM) provides detailed information about the topography of a sample's surface. In SEM a finely focused electron beam probe moves from one point to another on the specimen to form a raster pattern forming the electronic image.[12]

Energy dispersive X-ray spectroscopy (EDX) has been used in conjunction with SEM to determine the composition of the mesoporous walls. When a high-energy beam of charged particles such as electron beam of X-rays, is focused into the sample to be characterized. At rest, an atom within the sample contains ground state electrons situated in discrete energy levels (shells) bound to the nucleus. The incident beam may excite an electron in an inner shell, prompting its ejection and resulting in the formation of an electron hole within the atom's electronic structure. An electron from an outer, higher-

energy shell then fills the hole, and the difference in energy between the higher-energy shell and the lower energy shell is released in the form of an X-ray. The X-ray released by the electron is then detected and analysed by the energy dispersive spectrometer. These X-rays are characteristic of the difference in energy between the two shells, and of the atomic structure of the element, from which they were emitted.[12]

2.1.4 Transmission Electron Microscopy (TEM)

Electron beams differ from X-rays in two aspects; 1) electron beams have smaller wavelength, 2) electron beams possess a charge. The smaller the wavelength the smaller the Bragg angles that will make it possible to record extensive sections of the reciprocal lattice and have high resolution power. Due to the charge, electron beams interact with the atoms more strongly than in the X-ray, which makes it record electron diffraction patterns almost instantaneously.[12, 13] The amount of sample to be analysed is much smaller for electron microscopy than in the X-Ray diffraction method.[14]

The imaging of the surface structure of a porous material allows the pore size, symmetry and shape to be determined, as well as the thickness of the pore walls. In this way, a good image can be used to confirm the values calculated by XRD and gas sorption. Transmission Electron Microscopy (TEM) was used in the first characterisation of MCM-4, and it is now widely used as the definitive technique for the confirmation of bulk structure for new materials. Kresge *et al.*[15] used TEM to confirm the hexagonal symmetry of MCM-41 with different pore sizes as seen in figure 2.7 below.

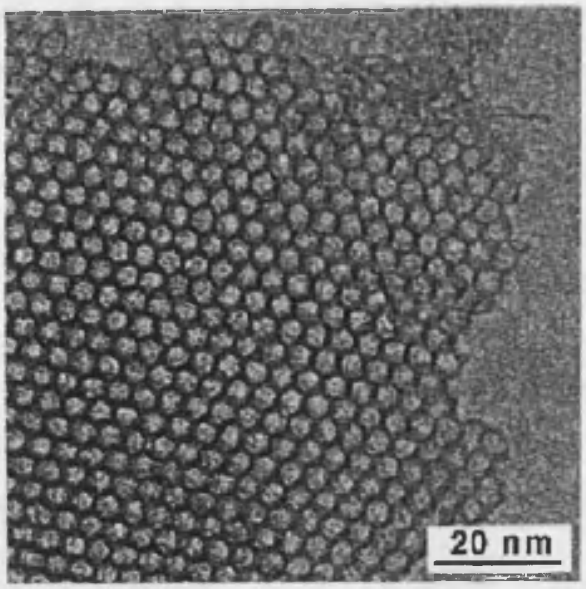

Figure 2.7 TEM of MCM-41 with 30 Å pore sizes [15]

2.1.5 Thermogravimetric Analysis (TGA) or Thermogravimetry (TG)

The definition of Thermal Analysis by International Confederation for Thermal Analysis (ICTA) is "A group of techniques in which a physical property of a substance is measured as a function of temperature while the substance is subjected to a controlled temperature program".

Thermogravimetry quantitatively measures weight change for a sample exposed to a temperature program. It is the most commonly used thermal technique, it measures weight changes in a material as a function of temperature (or time) under a controlled atmosphere. Its principal uses include measurement of a material's thermal stability and composition.

2.1.6 Differential Scanning Calorimetry (DSC)

Differential scanning calorimetry (DSC) uses heat to measure the progress of a chemical or physical process, which occurs over a range of temperatures. The technique of calorimetry involves recording the energy necessary to establish a zero temperature difference between a substance and a reference

material against either time or temperature as each specimen is subjected to an identical temperature program.

During a DSC experiment, a sample is heated over a range of temperature. At some point, the material starts to undergo a chemical or physical change that releases or absorbs heat. As the temperature increases, the process continues to completion. The ordinate value at any time or temperature is related to the difference in heat flow between a standard sample and the unknown; this is related to the kinetics of the process. Integration of the area under the heat flow curve yields the enthalpy change associated with the thermal event of interest.

DSC is the most used thermal analysis technique, and measures heat flows and temperatures associated with exothermic and endothermic transitions. It is routinely used for investigation, selection, and comparison performance of materials. DSC is used in academic, industrial and government research facilities, as well as quality control and production operations. Material properties that are routinely measured include glass transitions, crystallization, phase changes, melting, crystallization, and product stability.

2.1.7 Mass Spectroscopy

A compound is injected into a mass spectrometer, where it will be vaporized and bombarded with a high-energy beam of electrons (*ca* 70 eV), which in turn knock an electron out of the compound forming a 'molecular ion', radicals, cations, and neutral fragments. A molecular ion is a 'radical cation' that processes a positive charge and an unpaired electron. All of the positively charged fragments will be accelerated through negatively charged focusing plates into the analyser tube, except for the neutral fragments that are discharged. The analyser tube is surrounded by a magnetic field that causes the positive charge fragments to travel in a circular path depending on their mass to charge ratio (m/z) where they are collected and recorded in a mass spectrum.[17]

2.1.8 Ultraviolet-Visible Spectroscopy

Ultraviolet-visible spectroscopy (UV/ VIS) uses light in the visible and adjacent ultraviolet (UV) ranges. In this region of energy molecules undergo electronic transitions between bonding, nonbonding, and antibonding orbitals, or from atomic electronic energy levels. Ultraviolet light is electromagnetic radiation with wavelength ranging from 180 – 400 nm and visible light ranges from 380 – 700 nm. Each colour absorbs a specific range of wavelengths as shown in Table 2.2. [18] These colours are particularly important to analyse compounds or certain metals such as gold and silver that give surface plasmon resonance (SPR) phenomena when their sizes reach a quantum-size[23, 24].

Table 2.2 represents colour observed and the wavelength absorbed

Wavelength absorbed (nm)	Colour
620 – 700	Red
580 – 620	Orange
530 – 580	Yellow
470 – 530	Green
420 – 470	Blue
300 – 420	Violet

2.1.9 Nuclear Magnetic Resonance (NMR)

Solid state NMR is a powerful non-invasive analytical technique that provides quantitative and qualitative information about solid complex matrices.

Nuclear magnetic resonance (NMR) spectrometry is a form of absorption spectrometry. Under appropriate conditions in a magnetic field, a sample can absorb electromagnetic radiation in the radio frequency region at frequencies governed by the characteristics of the sample, as a function of a certain nuclei in the molecule. A plot of the frequencies of the absorption peaks versus peak intensities constitutes an NMR spectrum. [20, 21]

2.1.9.1 Magnetic Properties of Nuclei

All nuclei carry a charge. In some nuclei this charge spins on the nuclear axis, and this circulation of the nuclear charge generates a magnetic dipole along the axis. The angular momentum of the spinning charge can be described in terms of quantum spin numbers ***I***; these numbers have values of 0, ½, 1, and so on (***I*** = 0 denotes no spin). The intrinsic magnitude of the generated dipole is expressed in terms of nuclear magnetic moment, μ. [20]

Spectra of several nuclei can be readily obtained (e.g. ^{1}H, ^{13}C, ^{15}N) since they have spin numbers of ½ and a uniform spherical charge distribution. Nuclei with a spin number ***I*** of 1 or higher have a non-spherical charge distribution. This asymmetry is described by an electrical quadrupole moment, which affects the relaxation time and consequently the linewidth of the signal and the coupling with neighbouring nuclei.[20]

2.1.9.2 Generation of NMR Spectrum

In the absence of an external magnetic field, the magnetic moments of the individual nuclei in a compound are randomly oriented. However, when an external magnetic field is applied to these nuclei, the magnetic moments of the nuclei with spin + ½, orient themselves so they are in the same direction (α-spin) as the applied magnetic field. Those with -½ orient themselves opposite (β-spin) the applied field. When electromagnetic radiation of correct energy is applied to nuclei, a nucleus in the α-spin state will absorb the radiation, flipping its spin and entering the β-spin state. This absorption is detected, resulting in a signal in the NMR spectrum by the difference in energies between α and β states. The energy difference between the two spin states depends on the externally applied magnetic field strength ($B0$) defined by equation 2.3.[20]

$$\Delta E = (h\gamma / 2\pi) B_0 \quad ..... \quad (2.3)^{20}$$

where, h is plank's constant. This simply states that ΔE is proportional to B_0 since h, γ, and π are constants.

2.1.9.3 Advantage of Solid State over Solution State NMR

There are many advantages of solid state NMR over the liquid state method. Some of these are; all solid state NMR methods do not contain solvent effect, for example dissolution, aggregation, and dissociation, because the sample is analysed directly in the NMR instrument in its solid form; the sample in solid state NMR does not need to be extracted or treated representing the coordination of specific element in the original sample; solid state NMR is able to analyse highly insoluble samples such as black carbon. It is useful to analyse heterogeneous samples directly especially if the sample loses some of its components when transferred to liquid (leaching). Moreover, minimum amount of sample required is typically 300 mg or less when tested by solid state NMR, which is extremely important if the sample is scarce. In addition, solid state NMR could be used to measure internuclear distances, quantitatively, which might enable us to determine the conformation of a molecule, the length of a hydrogen bond, or determine a significant bond angle[22]. Solid state NMR can be used effectively in inhomogeneous or amorphous systems [22].

2.9.1.4 Magic Angle Spinning (MAS)

Magic angle spinning (MAS) is a technique often used to perform experiments in solid state NMR spectroscopy. This is usually performed by spinning the sample at 70 KHz at the magic angle (54.7°) see figure (2.8).

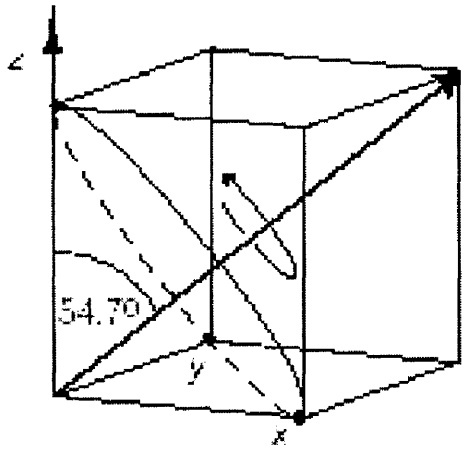

Figure (2.8) A schematic representation of the magic angle spinning technique illustrate the angle between the spinning axis and the magnetic field (the magic angle)[21]

MAS is used to alleviate line broadening to a large extent, if not entirely, due to chemical shift anisotropy (CSA), which arises from a non-spherical electron density distribution around the nucleus as well as, to some level, line broadening due to dipole - dipole interactions. In both cases these effects are removed in liquid-state NMR by the rapid and random tumbling of molecules induced by Brownian motion. In the solid state this rapid and random molecular tumbling does not occur.[21]

2.1.9.5 Solid State NMR Decoupling

The most obvious way to remove interactions between, for example, a carbon and a proton spin is to irradiate one spin (in this case the protons). Thus the broad line for a single ^{13}C resonance is narrowed by proton irradiation. It should be noted that the efficiency of decoupling depends on the position of the applied decoupling field relative to the resonance frequency of the nucleus to be decoupled, so that the axis of quantisation for the protons is in the x, y plane at 90° to the z-axis.[16]

2.1.9.6 Solid State NMR Cross Polarisation (CP)

The cross polarisation technique is used usually to increase the signal intensity. The signal intensity of, for example, ^{13}C NMR is weak due to several

factors; a) it is a low abundance nucleus (1 %) with small magnetic moment, b) long polarisation times in solids (spin- lattice relaxation time T_1 about 1000 s), c) the sensitivity is reduced due to dipolar coupling which causes line broadening.

2.1.10 Gas Chromatography

Chromatography is an analytical method that is used for the separation, identification, and determination of a chemical component in a mixture. It contains two main phases, stationary and mobile phase. The stationary phase is that fixed on a planar surface or in a column. The mobile phase is that which moves over or through the stationary phase, carrying the analyte. The analyte is the substance that is to be separated during chromatography. [25]

2.1.10.1 Chromatographic methods

There are two main chromatographic methods: column chromatography and planar chromatography. Column chromatography is a separation technique in which the stationary bed is fixed within a tube. Differences in rates of movement through the medium are calculated to different retention times of the sample. Planar chromatography is a separation technique in which the stationary phase is present on a plane. The plane can be paper, or impregnated by a substance as the stationary bed of solid particles spread on a support such as a glass plate. [25]

2.1.10.2 Classification of Chromatography

There are three major classes of chromatography: liquid (mobile phase is liquid), gas (mobile phase is gas), and supercritical-fluid chromatography (SFC). Each class can be further subdivided according to their stationary phases.[25]

2.1.10.2.1 Gas Chromatography

Gas chromatography (GC), also sometimes known as Gas-Liquid chromatography, (GLC), is a separation technique in which the mobile phase is a gas (usually inert gas like helium). Gas chromatography is always carried out in a column, which is typically "packed", or "capillary". The stationary phase could be liquid adsorbed on a solid, or organic species bonded to a solid, or solid. [25] We used a CP-Sil 5 CB column that contains a 100% dimethylpolysiloxane phase in which separation is almost entirely based on boiling points.

2.1.10.2.2 Pulsed Flame Photometric Detector

The Pulsed Flame Photometric Detector (PFPD) was developed in the early 1990's. Unlike the traditional flame photometric detector, which has a continuous flame, the PFPD is based on a pulsed flame for the generation of flame chemiluminescence. The detector operates with a fuel rich mixture of hydrogen and air. This mixture is ignited and then propagates into a combustion chamber three to four times per second where the flame front extinguishes. The PFPD can detect many elements but we are interested in sulphur for this project.

2.2 Characterization Instruments

X-ray diffraction (XRD) was performed using a *D4* multi sampler, using a copper target (k_α = 1.5418 Å) 40 kV, and 40 mA, low-angle scan parameters step size 0.01°, numbers of steps 659.00 and time of each step is 0.50 s, wide-angle scan step size 0.01°, number of steps 7700.00, time of each step is 0.20 s, both scans had diversion slits 0.05° and the ant scattering slit 0.50°.

All NMR experiments were carried out on a (Bruker) MSL300MHz NMR spectrometer, with a 7.05 T wide-bore magnet. Highresolution solid-state ^{27}Al and ^{29}Si spectral were recorded at 78.21 and 59.62 MHz, respectively. High-

resolution solid-state ^{29}Si NMR spectra were recorded using cross-polarization (CP), direct observation was used for both ^{29}Si NMR and ^{27}Al NMR measurements. Typical operating conditions for ^{29}Si MAS experiments were: ^{29}Si 45° pulse duration = 2.3 μs; recycle delay = 30s. Typical operating conditions for ^{27}Al MAS experiments were: ^{27}Al single pulse = 0.7 μs; recycle delay = 0.5 s. The ^{29}Si NMR and ^{27}Al NMR chemical shifts are given relative to tetramethylsilane.

The BET tests were performed using a Micrometrics 2010 instrument using N_2 analysis gas and He back fill gas. Initially, the materials were dehydrated by evacuation at 573 K. The pore size distributions were derived from the desorption branches. It should be noted that calculations of pore-size distributions on the basis of the BJH theory could underestimate the mean pore diameter of small mesopores by up to 1 nm. Owing to this systematic error; such data are no safe basis to discuss absolute values of pore sizes.

The GC (sulphur analysis) used is a Varian CP 3800, has a capillary column (CP-Sil 5CB) that has dimensions of 25 m by 0.25 mm by 1.2 mm containing 100 % dimethyl-poly-siloxane at 50 °C, with a PFPD detector using H_2 and air gasses as fuel, and He as carrier gas, the injector temperature was 300 °C. The TGA/DSC/MS tests were performed by The NETZSCH thermogravimetric analyser TG 409 C connected to QMS 403C Aëolos under He gas cover; heating rate was 3 °C min^{-1}. SEM test imaging was performed using JEOL 6301F 20KV. SEM/DEXS tests were performed using XL 30 ESEM Philips. Low intensity TEM was carried out using JEOL-JEM-CX1002-Microscope 100KV. The UV/VIS test was carried out using SHIMADZU UV-240 IPC using slit size 5.0 nm and medium scanning speed, mesoporous silicate and aluminosilicate used as reference materials accordingly. All the previous tests were performed at University College London (UCL). HRTEM was performed using JEOL-JEM 2010-Microscope 200KV at Imperial College; samples preparation for TEM tests were suspended in alcohol then transferred to the testing grids by capillary glass tubes.

2.3 References

1. K. J. Edler and J. W. White, *Chem. Mater.*, 1997, **9**, 1226.
2. J. Xu, Z. Luan, *Chem. Mater.* 1998, **10**, 3690-3698.
3. K. Schumacher, I. Peter, *Langmuir* 2000, **16**, 4648-4654
4. R. M. Silverstein, F. X. Webster, *Spectrometric Identification of Organic Compounds*, john Wiley& Sons, Inc. sixth Edition, 2-70.
5. C. J. Brinker and G. W. Scherer, *Sol-Gel Science; The Physics and Chemistry of Sol-Gel Processing*, Academic Press, London, 1990.
6. S. J. Gregg and K. S. W. Sing, *Adsorption, Surface Area and Porosity*, 2nd Edn., Academic Press, London, 1997.
7. D. J. Show, *Introduction to Colloid and Surface Chemistry*, Butterworth Heinemann, Fourth Edition, 2000, 115 - 136.
8. P. J. Branton, P. G. Hall and K. S. W. Sing, *J. Chem. Soc., Chem. Commun.*, 1993, 1257.
9. P. L. Llewellyn, Y. Grillet, F. Schüth, H. Reichert and K. K. Unger, *Microporous Mater.*, 1994, **3**, 345.
10. J. Rathousky, A. Zukal, O. Franke and G. Schulz-Ekloff, *J. Chem. Soc., Faraday Trans.*, 1995, **91**, 937.
11. P. J. Branton, P. G. Hall, K. S. W. Sing, H. Reichert, F. Schüth and K. K. Unger, *J. Chem. Soc. Faraday Trans.*, 1994, **90**, 2956.
12. C. N. R. Rao, J. Gopalakrishnan, *New Direction in Solid State Chemistry*, Cambridge University Press, 1986,71-109.
13. D. J. Show, *Introduction to Colloid and Surface Chemistry*, Butterworth Heinemann, Fourth Edition, 2000, 47-53.
14. P.W. Atkins, *Physical Chemistry*, Oxford University Press, Sixth edition, 1998, 855-868.
15. C. T. Kresge, M. E. Leonowicz, W. J. Roth, J. C. Vartuli and J. S. Beck, *Nature*, 1992, **359**, 710; J. S. Beck, J. C. Vartuli, W. J. Roth, M. E. Leonowicz, C. T. Kresge, K. D. Schmitt, C. T-W. Chu, D. H. Olson, E. W. Sheppard, S. B. McCullen, J. B. Higgins and J. L. Schlenker, *J. Am. Chem. Soc.*, 1992, **114**, 10834.
16. M. Wilson, *NMR Techniques and Applications in Geochemistry and Soil Chemistry*, Prgamon Press, England, 1987, page 64.
17. P. Y. Bruice, *Organic Chemistry*, Prentice-Hall International Editions 1995, 522-535.
18. P. Y. Bruice, *Organic Chemistry*, Prentice-Hall International Editions 1995, 684 - 686.
19. M. J. Danks, *PhD theses*, University of Exeter, 2002.
20. P. Y. Bruice, *Organic Chemistry*, Prentice-Hall International Editions 1995, 633-675.
21. R. M. Silverstein, F. X. Webster, *Spectrometric Identification of Organic Compounds*, john Wiley& Sons, Inc. sixth Edition, 144-216.
22. M. Duer, *Introduction to solid state NMR spectroscopy*, First Edition, Blackwell publishing, Oxford UK, 2004, 68-71.
23. H. Bonnemann, W. Brijoux, and Th. Joussen, *Angew. Chem., Int. Ed. Engl.*, 1990, **29**, 273
24. W. P. Haperin, *Rev. Mod. Phys.*,1986, **58**, 533.
25. D. A. Skoog, D. M. West, F.J. Holler, *Fundamentals of Analytical Chemistry*, seventh edition, Saunders College Publishing, 1996, Chapter 28, 661.

26. P.W. Atkins, *Physical Chemistry*, Oxford University Press, Sixth edition, 1998, 625-630.

27. E. P Barrett, L.G. Joyner, and P.P. Halenda, *J. Am. Chem. Soc*, 1951, 73, 373-380.

Chapter 3

Results 1 and discussions

- **Mesoporous syntheses procedures**
- **Modified mesoporous syntheses procedures**
- **Improving mesoporous stabilities**

This chapter discusses the stability of the mesoporous structures prepared during this project, prior to, and after modifications have been made. In order to perform our modifications, we have had to, in detail, examine every step involved in the synthesis including its effects on the final porous product. We show in this chapter how we were able to control these steps and produce stable mesoporous materials that we have employed as hosts for metal clusters (chapter 4) and examined in terms of their sorption capability (Chapter 5).

Mesoporous Syntheses and Modification of Their Procedures

3.1 Host Preparation

Metals and metal oxides should possess a few basic properties before being employed in industries, such as having a high surface area, pore volume percent and sturdiness as well as being economically feasible to produce. Unfortunately, most of the proposed metals and metal oxides are not (see chapter 1). Therefore, alternative routes should be explored to satisfy some of these requirements.

The most common practice of increasing surface area and pore volumes in inorganic materials is by introduction of pores into their structure. For the past few years porous solids were utilised successfully in a wide scope of applications for example, sorption, catalysts, fuel storage, and many other applications. We found that producing porous metals or metal oxides is not easily achieved due to their synthesis complications most transition metals hydrolyse very fast that make them extremely difficult to control during the templating synthesis. Other metals are too expensive to use as parent metals in particular gold and silver. In addition, some metals form a powder-like texture of metal oxides that is soft and impractical to directly employ in an industrial application, for example ZnO. In spite of all the obstacles, a few attempts were carried out to synthesize porous transition metals but the final products did not possess a high surface area such in TiO_2, MnO_2, NiO, ZnO and CaO, their BET surface area was below 300 m^2g^{-1} and failed stability tests[1-8]. Furthermore, structures and sizes of metals and metallic oxides determine some of their properties; some metals and metal oxides should exist as nano-clusters in order to obtain specific properties. [1-8] Gold for example is catalytically inert as a bulk but is active when its size reaches a nanoscale.

One of the proposed routes to overcome some of the obstacles discussed in the previous paragraph is to synthesize a host that is relatively cheap,

contains suitable pore sizes, has a high surface area and is sturdy and reusable, and then selective metals and metal oxides of specific catalytic, and sorption properties can be introduced into its pores. We promoted mesoporous silicate to be used as a host material because it is cheap, quite easy to synthesize and its morphology is easily controlled. In this project three methods of synthesizing porous materials will be tackled: solvothermal reaction, true liquid crystal templating (TLCT), and the precipitating method (ppt).

3.2 Stability of Mesoporous Silicate

Cassiers et al. [9, 10] published a review comparing the stabilities of different mesoporous silicates that had been prepared by various groups. They found that the thermal stability strongly related to wall thickness and type of silica precursor used during synthesis. They also showed that M41S materials prepared with fumed silica were thermally stable to at least 850 °C, whereas materials prepared with tetraeathyl orthosilicate (TEOS) were completely collapsed at a calcination temperature of 750 °C. Nevertheless, the TEOS-made materials claimed to have exactly the same wall thickness and were prepared under the same hydrothermal conditions as the corresponding fumed-silica-made materials. We do not think this is entirely true because the author ignored the role of complexing agents, the pH effects, and aging effects used in some of the synthesis perpetrations. It was found by comparing hexagonal mesoporous structures that the thermal stability descending trends were observed as follows: KIT-1 (colloidal silica) [11], MCM-41 (fumed silica) [12, 13]> FSM16 (layered silicate) [14]> MCM-41 [12, 13] (TEOS), HMS [16] (TEOS). Although SBA-15 [15] is also prepared with TEOS, it showed a much higher thermal stability than HMS and MCM-41 synthesized with TEOS. This was explained by the existence of a thicker wall, which was claimed to be three times thicker.

It was observed that the structural deformation of the examined samples did not follow the same trend after a mild hydrothermal treatment at 400 °C with

25 % steam at 1 atm pressure as it did after thermal treatment. It was observed that the hydrothermal stability was influenced by three factors. First, materials with very polymerised or thicker pore walls were less affected under those steaming conditions. Second SBA-15 and KIT-1 claimed to withstand a more severe test under autogenous pressure, whereas the other molecular sieves were completely destroyed. Under mild steaming conditions, a third factor became more important for all materials with comparable wall thickness. It was observed that the structural degradation of cubic MCM-48 was lower than that of the hexagonal mesoporous materials HMS, MCM-41, and FSM-16, which was explained as a result of its different pore structure and curvature, resulting in a lower affinity toward water for MCM-48. [9, 10]

No remarkable trends were observed for the mechanical stability. The mesoporosity was essentially lost for all mesoporous structures at pelletizing pressures of around 444 MPa. Nevertheless, those ordered mesoporous structures showed mechanical stabilities that are inferior to those of zeolites, which might result from their large porosity and the absence of a stabilizing crystal structure. Finally, it should be mentioned that, despite the interesting features of SBA-15 and KIT-1, none of the (well known) mesoporous materials reported in these papers exhibited superior stability behaviour for all tests [9, 10]. Therefore, much work is still required to utilize, stabilize the existing or develop new mesoporous materials. We gained more experience through this project.

The evaluation of the stability of mesoporous materials should be tested under similar conditions with extra care. Moreover, introducing different metal oxides to the framework or into the pores of the mesoporous silicate materials may improve their overall stability, which will also be investigated in the following paragraphs. All samples discussed bellow are reproducible, and the ones that are not were omitted.

3.3 Preparation Methods of Mesoporous Materials

3.3.1 Synthesis of Mesoporous Silicate

3.3.1.1 True Liquid Crystal Templating Method

Ordered hexagonal mesoporous silicate was synthesised following Attard's [17] procedure of true liquid crystal templating method (TLCT), CTAB (1.25 g, 0.0011 mol) was added to stirring aqueous hydrochloric acid (1.25 cm^3, pH 2) and methanol (2.5 cm^3). The solution was heated, under reduced pressure on a rotary evaporator, at a specific temperature until a viscous solution, on the boundary between isotropic liquid and hexagonal mesophase, was obtained. Tetramethoxysilane (2.36 cm^3, 0.016 mol) was added and the solution heated further, under reduced pressure, at the same temperature until the hexagonal mesophase was reformed. Then the hydrolysed precursor and the mesophase were aged for 24 hours at room temperature, and calcined at 550 °C in flowing air for 6 hrs.

Modifications were employed during the aging stage by holding the as synthesised product for various periods of time, temperatures and calcination conditions; see results and discussions in the section below.

3.3.1.2 Solvothermal Method

Solvothermal reaction was employed to produce Hexagonal and cubic mesoporous silicate as follows:

3.3.1.2.1 Hexagonal Mesoporous Silicate

Hexagonal mesoporous silicate samples were prepared by the hydrolysis of (C_{16}TAB) and tetraethyl silicate (TEOS) in a basic solution, the final composition was 1.0 CTAB: 7.5 TEOS: 1.8 NaOH: 500 H_2O (molar ratio), then

solvothermally treated at 110 °C for 60 hrs. Drying gave a white powder, which was calcined at 550 °C in flowing air for 6 hrs giving the products. [18]

3.3.1.2.1 Cubic Mesoporous Silicate

Cubic mesoporous silicate was prepared by stirring 1.0 moles of tetraethoxy silicate (TEOS) and 0.5 moles of KOH in 62 moles of H_2O for 10 min. After adding the cationic quaternary ammonium bromide surfactant (CTAB), 0.65 moles of hexadecylammonium bromide ($C_{16}TAB$); 0.62 moles of octadecylammonium bromide ($C_{18}TAB$) and 10 min of vigorous stirring the white and creamy solution was filled into a Teflon-lined steel autoclave and statically heated at 115 °C for 48 hrs. The resultant white precipitate was filtered and washed several times with deionised water. Drying produced a white powder, which was calcined at 550 °C in flowing air for 6 hrs. [19]

3.3.1.3 Precipitation Method (ppt)

Different amounts of ethanol, methanol, or propanol alcohols were added to obtain a gel with the following composition: 1 TEOS/0.3 $C_{16}TAB$/11NH_3/*x* alcohol/144 H_2O. To synthesize the material, $C_{16}TAB$ was first dissolved in the mixed solution of distilled water, aqueous ammonia, and alcohol by stirring for 15 min; then TEOS was added. The solution was further stirred for 2 hrs; the white precipitate was then collected by filtration and washed with distilled water. Dried samples were calcined at 550 °C with a heating rate of 1 °C/min and kept at this temperature for 6 h to remove the surfactant. [20]

3.4 Results and Discussion

3.4.1 Removal of the Templating Materials

3.4.1.1 Pyrolytic Elimination

Pyrolytic elimination of the surfactant was usually performed by calcination of the as-synthesised solids at 550 °C for 5 - 6 hours under static or dynamic flow of air.

3.4.1.2 Chemical Extraction

Chemical extraction of the surfactant from the as-synthesised solids is usually performed using ethanol solution (ca. 1 g of powder, 100 ml of ethanol 99 %; for 16 – 24 hrs at 60 °C). The final (porous) material was separated by filtration then calcined at 550 °C for 5 hrs at 3 °C min^{-1}. Chemical extraction of surfactants can be performed by two methods: 1) by stirring directly in the solvent, 2) by soxhlet extraction.

The XRD patterns was taken to compare the effects of removing the templates chemically from as-synthesised mesoporous silicate (TLCT), which was first aged for two days at room temperature then; 1) stirred in alcohol directly at 60 °C, 2) or soxhlet extraction, as presented in figure 3.1 below.

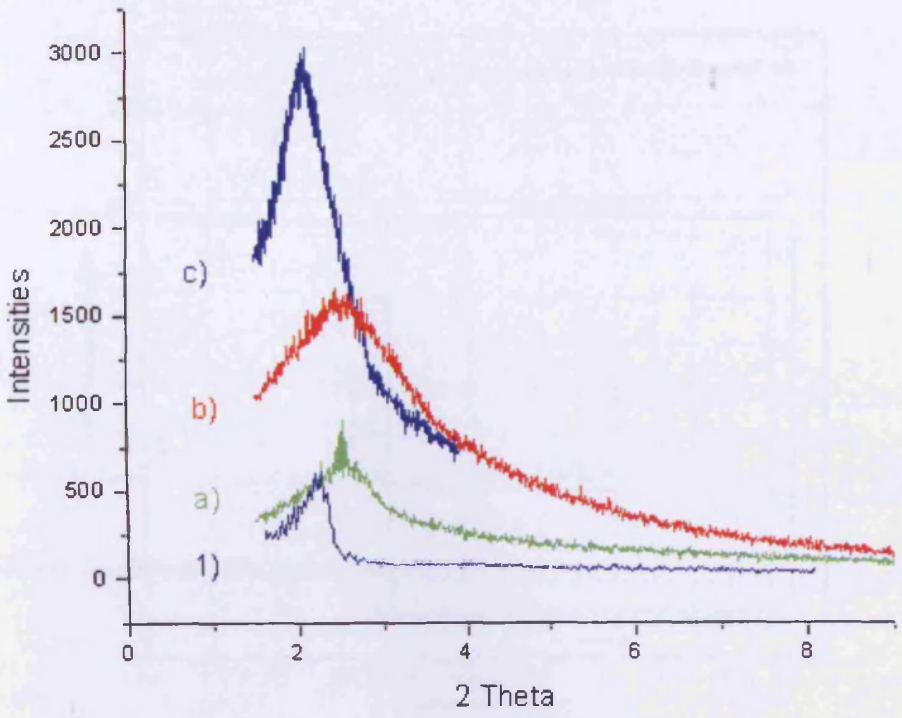

Figure 3.1 XRD patterns of the chemical removal of surfactants of pure silicate hexagonal morphologies prepared using TLCT method, 1) aged for two days at room temperature, then a) stirring in ethanol for 5 hrs, or b) soxhelt extraction for 5 hrs, or c) soxhelt extraction for 15 hrs

The XRD patterns showed very poor framework and low Bragg's peak (100), in the case of stirring the mesoporous silicate in ethanol directly. However soxhlet extraction gave better d spacing after 14 -16 hrs, which shifts the d spacing to a lower diffraction angle, giving d spacing of 40 Å after 5 hours, and it continued to shift to a lower angle after 14 -16 hrs to reach 43 Å, and had a higher peak intensity than sample (a), which is opposite of that directly stirred in alcohol, see figure 3.1. Larger d spacing could indicate increasing the thickness of the walls and or pore diameters.

BET tests were performed for a sample that was aged for one day at room temperature then it was divided into two batches to test the soxhlet extraction effect. The first batch (A) was calcined directly to remove the organic templating materials, and the second batch (B) was soxhlet extracted then calcined as presented in figure 3.2 below.

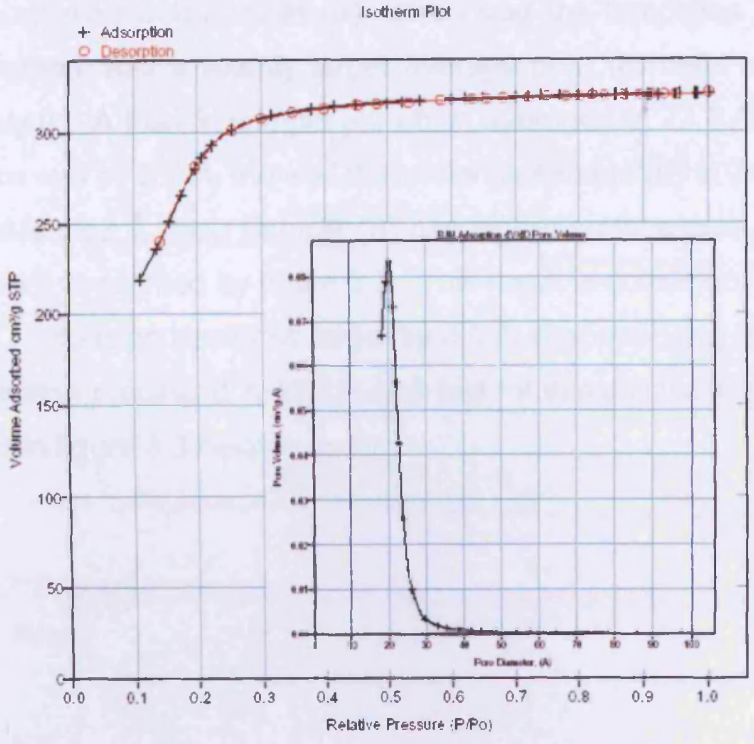

A BJH Adsorption Average Pore Diameter (4V/A): 21.6547 A
BJH Desorption Average Pore Diameter (4V/A): 22.4959 A
average= 22.1 A

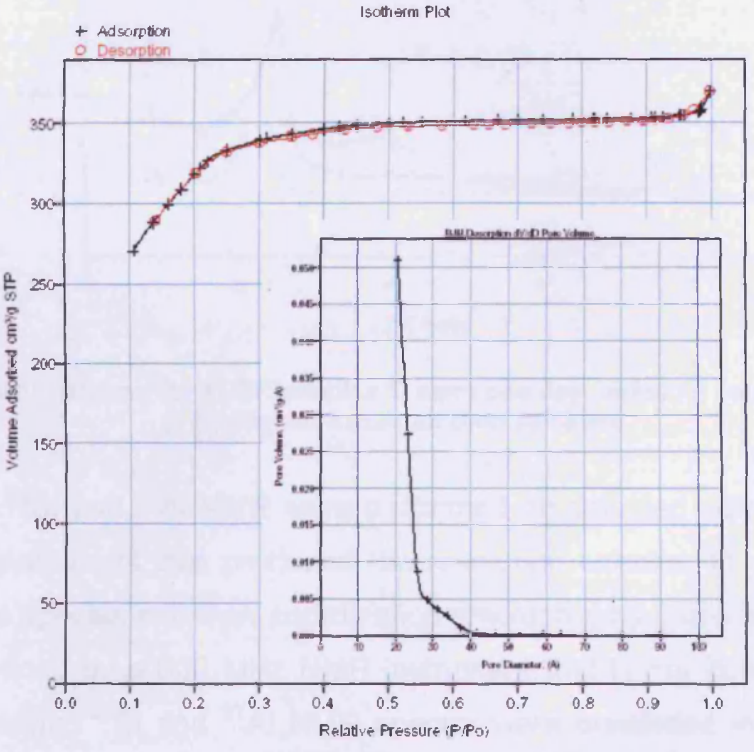

B BJH Adsorption Average Pore Diameter (4V/A): 22.5382 A
BJH Desorption Average Pore Diameter (4V/A): 23.0837 A
average=22.8 A

Figure 3.2 BET N_2 isotherm for mesoporous silicate (TLCT) (A) calcined, (B) soxhlet extracted then calcined

These tests showed that sample (B), which had the templates removed by soxhlet extraction, had a slightly larger average pore diameter of 22.8 Å by approximately 0.7 Å than in sample (A) which averages to 22.1 Å. That gives a thicker pore wall by 5.2 Å, the wall thickness for sample (B) is 24.0 Å and for sample (A) it is 18.8 Å. Also Sample (B) had higher surface area, than that of sample (A) as represented by figure 3.2. This result is consistent with the fact that the XRD d spacing becomes larger by 5.0 Å after exposing the sample to soxhlet extraction process d = 40.6 Å and that for sample (A) is equal to 35.4 Å, presented in figure 3.3 below.

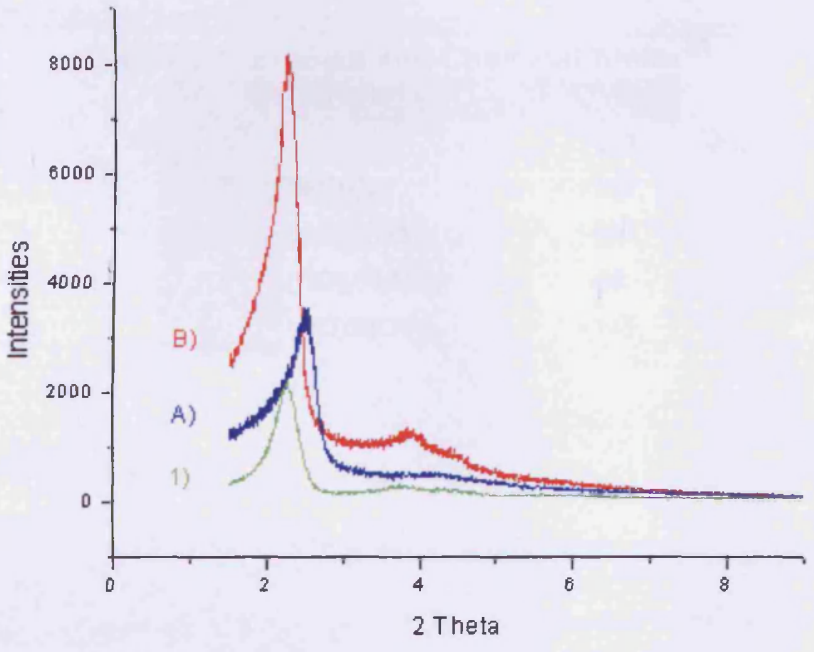

Figure 3.3 XRD patterns for TLCT samples 1) aged one day, either A) calcined directly, or B) soxhlet extracted then calcined

Solid-state ^{29}Si and ^{27}Al NMR were performed on selected samples using a 300 MHz instrument that produced low-resolution spectra. In order to fully quantify the species and their coordination environments these samples need to be examined by a 600 MHz NMR instrument that is not in possession of UCL. Therefore, ^{29}Si and ^{27}Al NMR spectra were presented in this chapter only to demonstrate the existence of these different species. All the relative percentages are measured in term of peaks intensities and presented to give some kind of rationalization to the existence of their different species and

because it was not possible (or have high percentages of error) to deconvolute the decupling spectra for both elements.

Figure 3.4 shows ^{29}Si MAS CP NMR spectra of the calcined only, sample A, and sample B that was soxhlet extracted then calcined. These spectra reveal that Q^4 intensity had increased by 4 % after calcination of the extracted sample (B), than in (A), which was calcined directly with out any extraction. Table 3.1 shows the Q values and the corresponding silicate species verses their chemical shifts. The relation between Q^4 intensities and the stability of the structure will be discussed in the thermal stability section below.

Table 3.1 Q values and Chemical Shifts [21]

Si NMR	Compound	Chem.Shifts
		Ppm
Q^4	$Si(Osi)_4$	-112
Q^3	$(HO)Si(OSi)_3$	-100
Q^2	$(HO)_2Si(OSi)_2$	-92
Al-Si	$(AlO)Si(OSi)_3$	-105

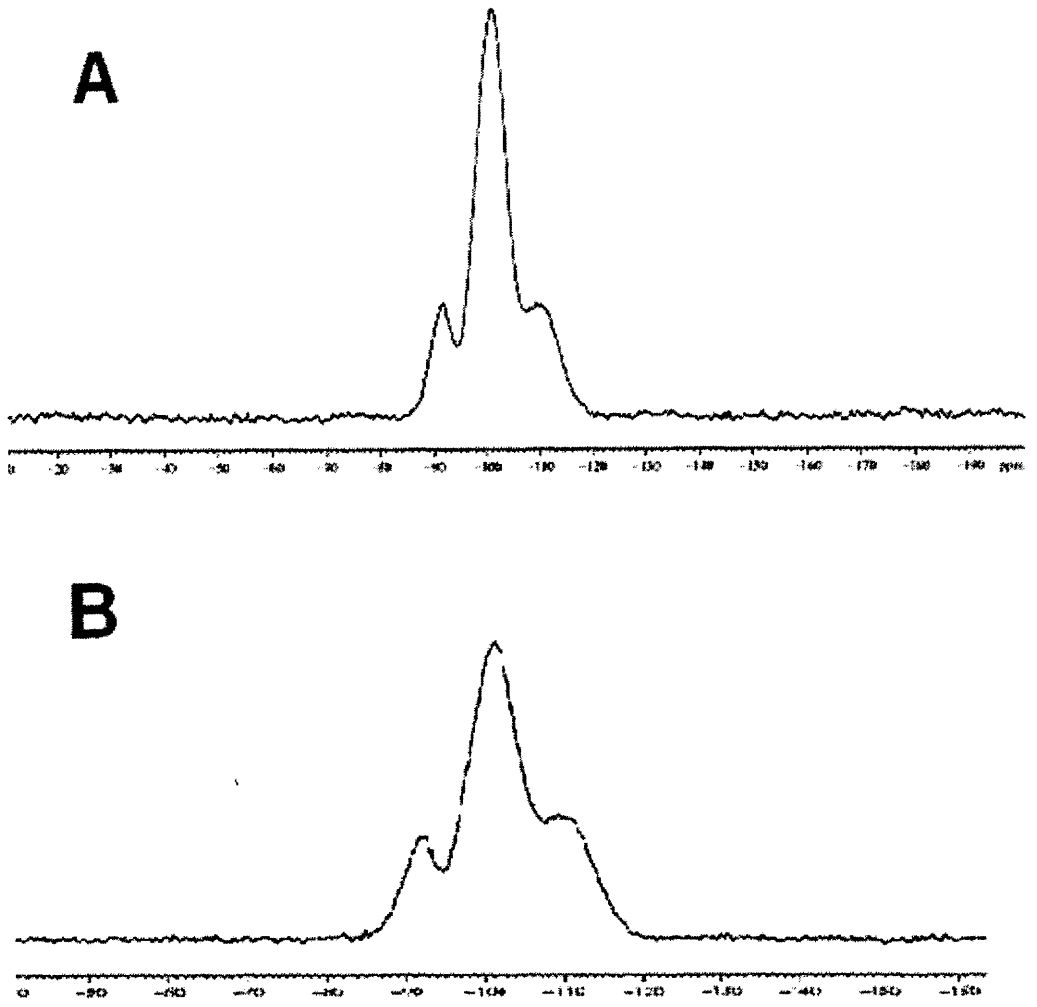

Figure 3.4 ^{29}Si MAS CP NMR spectra of A) calcined directly, B) soxhlet extracted then calcined

Moreover, an additional advantage discovered using soxhlet extraction, which was not published in any article up to date, is the ability to reform the morphology of the aged TLCT sample after its destruction, upon exposing to different solvents at room temperature, before calcination. This phenomenon will be of great use during the incorporation of metals and metal oxides. Notice that the d spacing slightly shifts to a smaller angle even after calcination; usually calcination shifts the d spacing to a larger angle due to pore shrinkage (see calcination effects section in chapter 1, and 2), as presented in figure 3.5.

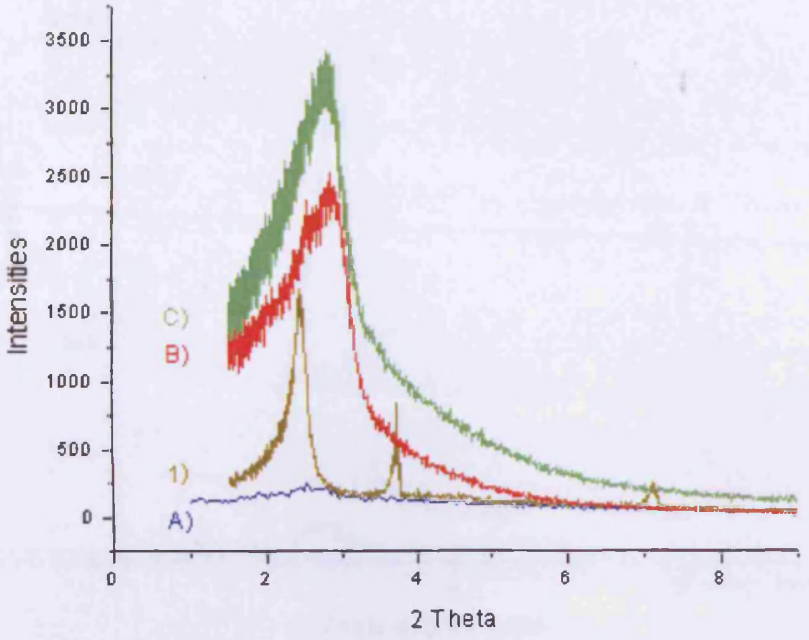

Figure 3.5 The effect of the soxhlet extraction on reforming the overall order of the structure prepared by TLCT method, 1) sample aged for 16 hours at room temperature, A) direct stirring of the aged sample in ethanol destroyed the structure at room temperature, B) reforming the structure integrity after 24 hrs by soxhlet extraction in ethanol, C) further improvement of the structure after calcination

3.4.2 Modifications of Mesoporous Materials Preparation Methods

3.4.2.1 Effect of Heating Rate

During the course of these experiments we discovered that the effect of the heating rate depends on the morphology of the prepared structure and depends upon the synthesis route used; for example a fast heating rate at or above 4 °C min^{-1} could decrease the long-range order or completely destroy the cubic mesoporous structure, as will be discussed in detail in the following paragraphs, as represented by figures 3.6 and 3.7 below.

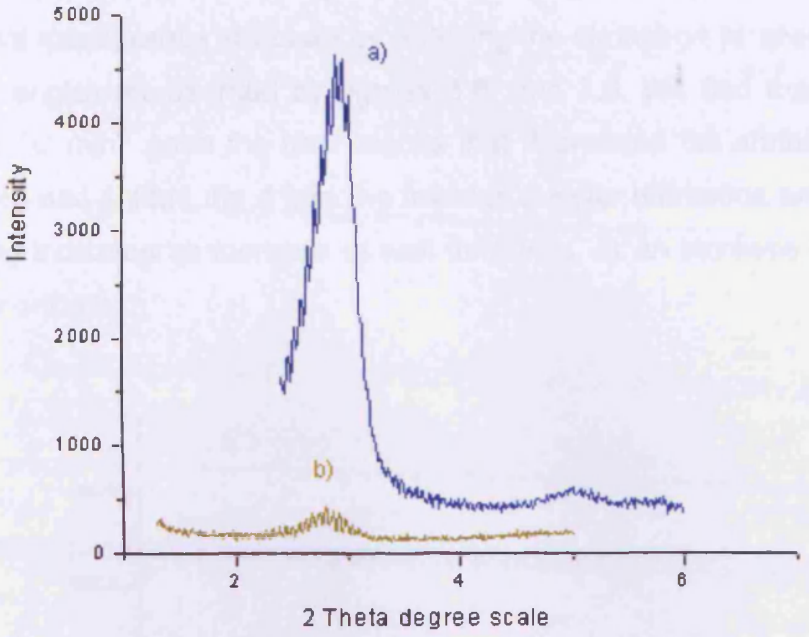

Figure 3.6 The effect of heating rates on cubic mesoporous silicate prepared *via* precipitating method (ppt), a) 3 °C min^{-1}, b) 4 °C min^{-1}

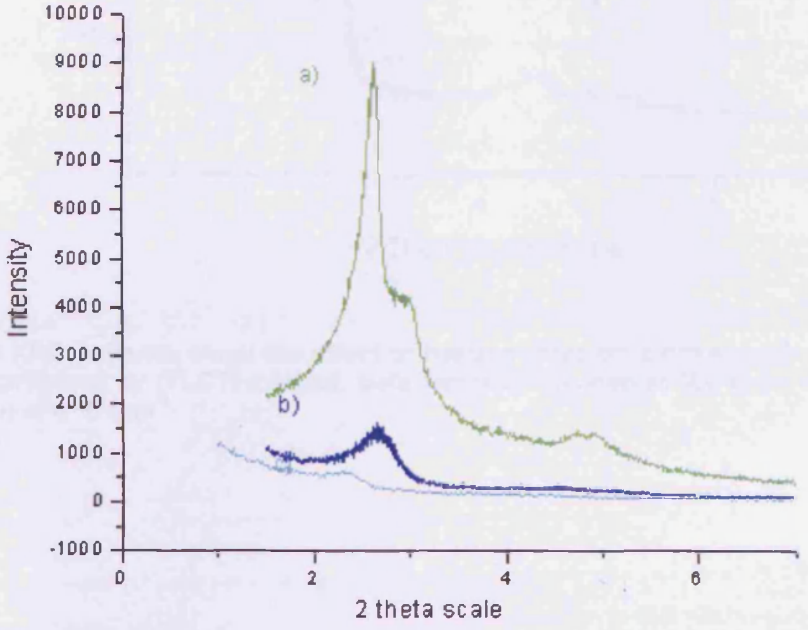

Figure 3.7 XRD patterns represent the effect of heating rates on cubic mesoporous structure prepared by solvothermal method, a) 3 °C min^{-1}, b) 4 °C min^{-1}, c) 6 °C min^{-1}

In contrast, the effect of heating rates between 2 – 4 °C min^{-1} improves the hexagonal mesoporous structure by reducing the shrinkage (d spacing shifted to lower angle) represented by figures 3.8, and 3.9. We find that a heating rate of 3 °C min^{-1} gave the best results that decreased the shrinkage of the pores size and shifted the d spacing towards a lower diffraction angle. Larger d spacing indicates an increase of wall thickness, or an increase in the pore diameter or both.

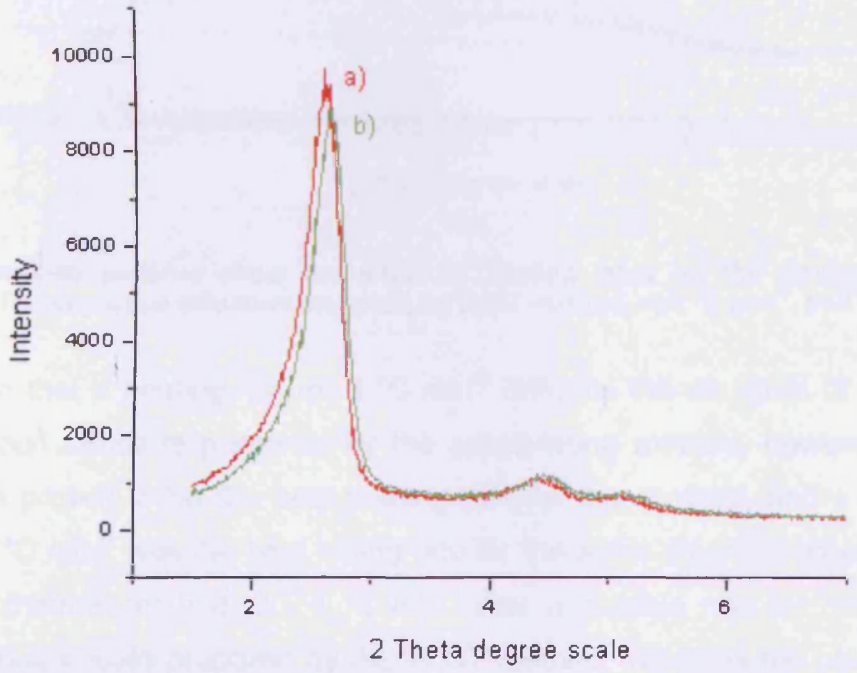

Figure 3.8 XRD patterns show the effect of heating rates on a hexagonal mesoporous structure prepared by (TLCT) method, both samples calcined at 600°C for 5 hrs, a) at 3 °C min^{-1}, b) at 4 °C min^{-1}

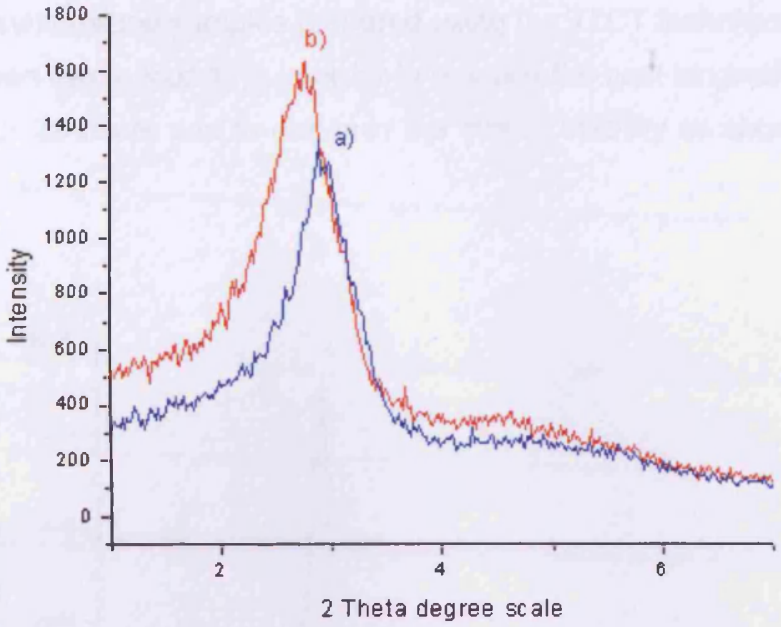

Figure 3.9 XRD patterns show the effect of heating rates on the structure of a hexagonal mesoporous structure prepared by TLCT method, a) 2 °C min^{-1}, b) 4 °C min^{-1}

We found that a heating rate of 3 °C min^{-1} deforms the structure of a cubic mesoporous structure prepared by the precipitating method, however 2 °C min^{-1} has proven to be the best heating rate for this method, and a heating rate of 3 °C min^{-1} was the best hating rate for the same structure prepared by the solvothermal method. 3 - 4 °C min^{-1} was a suitable rate for hexagonal mesoporous silicate prepared by the TLCT method. Whereas the calcination temperature of 550 -600 °C showed an improvement on the long-range order for both structures hexagonal and cubical mesoporous materials.

3.4.2.2 Aging Effect

Aging of the as-synthesised mesoporous materials plays an important role in the overall long-range order by, enhancing the condensation step, and strengthening the framework by forming more metal oxygen bonds. Hypothetically, increasing the temperature at the aging step, to be slightly less than the temperature of the mesophase formation, would improve the stability of the mesoporous framework. It is equally important; to point out that the aging time is strongly dependent on the synthesis procedure employed.

We found by performing repetitive experiments, that the average aging time for the as-synthesised samples prepared using the TLCT technique should be held between two to four days in order to produce the best long-range ordered mesoporous structure and to enhance the overall stability as shown in figure 3.10.

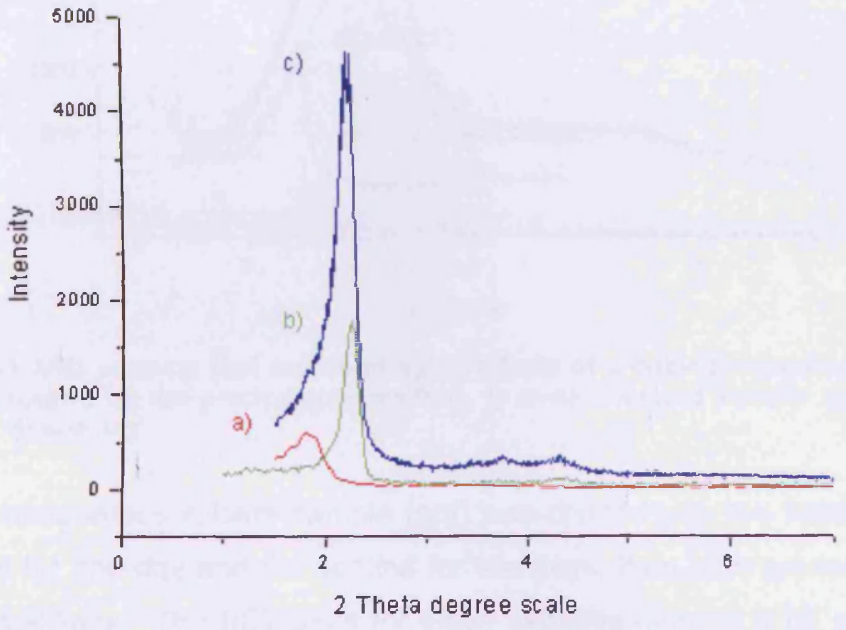

Figure 3.10 XRD patterns representing the aging affect on hexagonal mesoporous silicate prepared *via* the TLCT method, sample a) as-synthesised, b) aged at room temperature for 24 hrs, c) aged for four days

On the other hand, elongated aging times will transform the mesophase or deform the morphology of interests, and could participate in the weakening of the framework rather than strengthening it, for solvothermal preparation methods. One day aging has proven to produce the best cubic mesoporous silicate morphology for both solvothermal and precipitating methods as presented by figures 3.11 – 3.14.

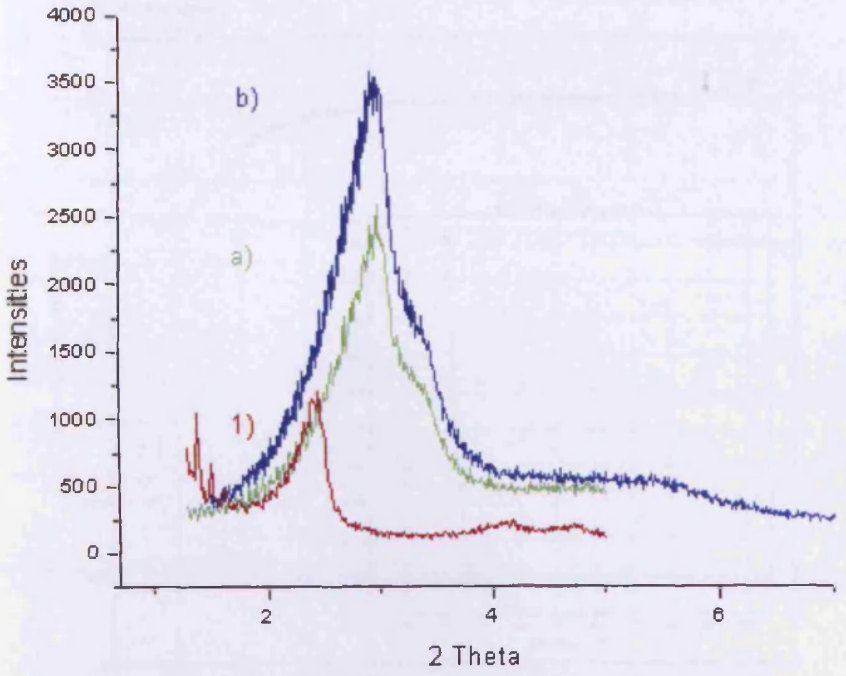

Figure 3.11 XRD patterns that represent aging effects of a cubic mesoporous silicate sample prepared by the precipitating method, 1) as-synthesised sample aged for A) two days, B) one day

A cubic mesoporous silicate sample (ppt) was divided into two batches, one was aged for one day and the second for two days, then both calcined under similar conditions. The BET tests for these samples (figures 3.12, and 3.13) confirmed that elongated aging has a negative effect on the cubic mesoporous structure, which shows that the structure loses about 30 % of its total surface area by only aging an extra day, and produces a wider range of pore sizes, that can be seen in the pores distribution graph (insets), and by the appearance of hysteresis loop of the desorption cycle presence in the BET isotherm. These results agreed with the observed XRD intensities presented in figure 3.11.

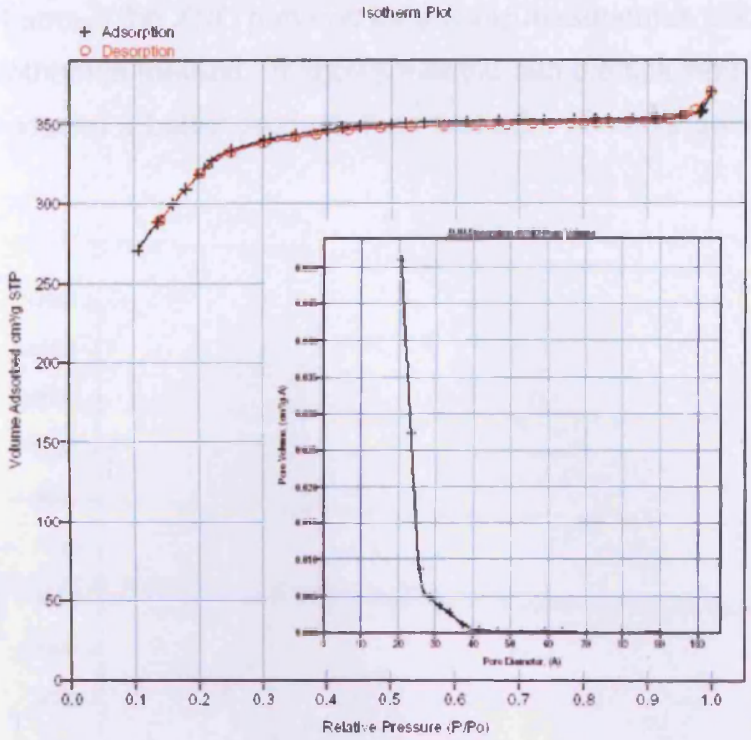

Figure 3.12 A BET test for mesoporous silicate prepared by the precipitating method, aged for one day and then calcined

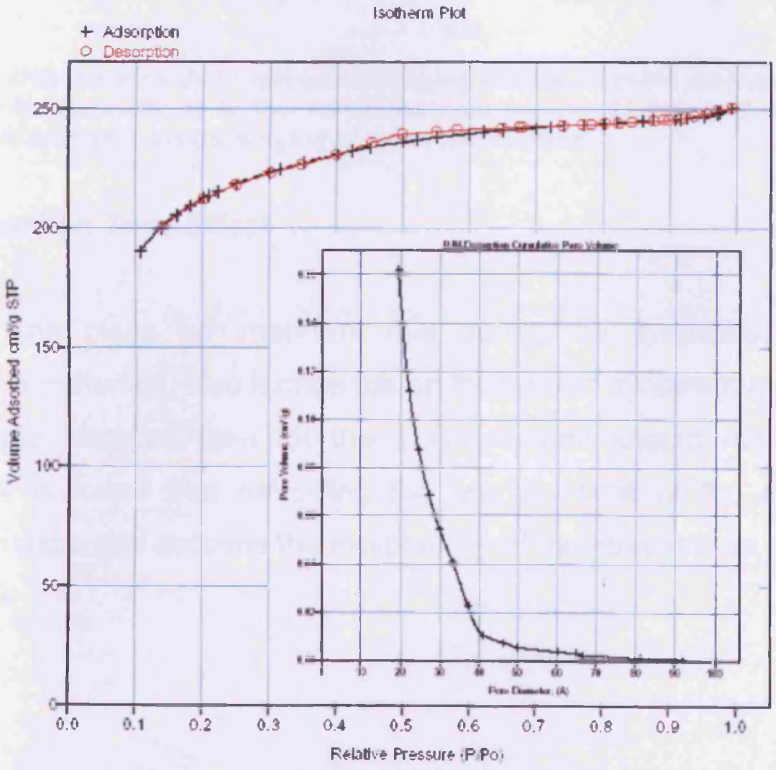

Figure 3.13 A BET test for mesoporous silicate prepared by the precipitating method, aged for two days and then calcined

Figure 3.14 shows the XRD patterns for a cubic mesoporous silicate prepared by the solvothermal method. It shows that the sample calcined after one day of aging produced a better product, than that after six days aging, which was destroyed.

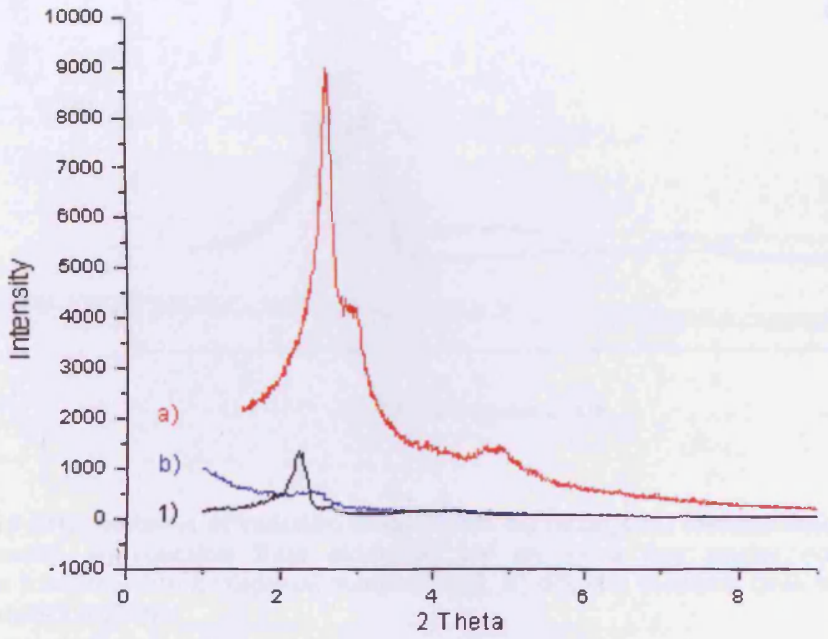

Figure 3.14 XRD patterns that represent the aging effects on cubic mesoporous silicate prepared solvothermally 1) is the as-synthesised sample a) calcined after one day aging, b) calcined after six days aging at room temperature

3.4.2.3 Reaction Time Effect

Reaction time plays an important role during the synthesis of ordered mesoporous materials, also it depends on the type of synthesis method used. For example, reaction time for the TLCT method should not exceed 20 minutes. It is found that extending the reaction time of the solvothermal method an extra day deforms the morphology of the structure as presented in figure 3.15.

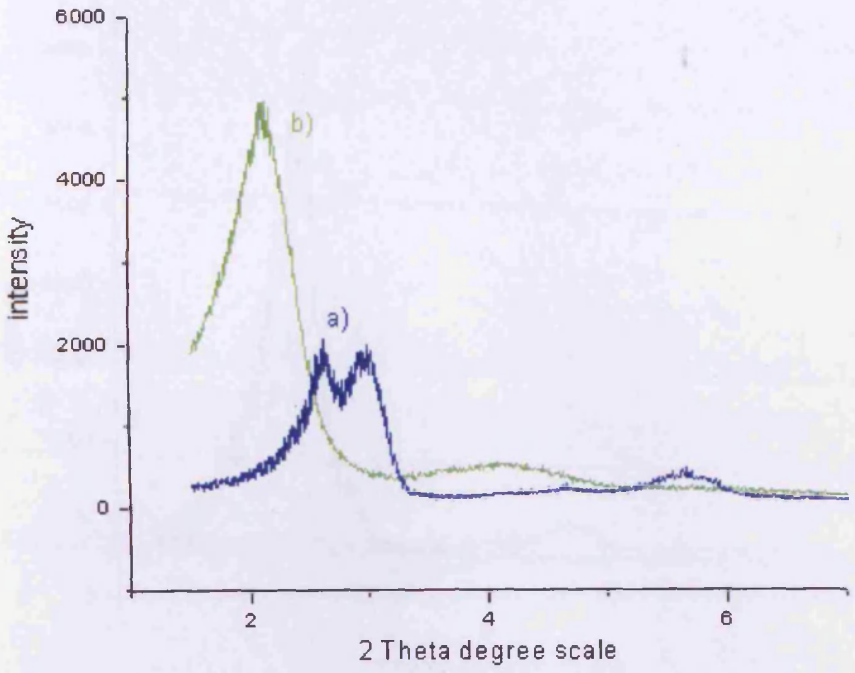

Figure 3.15 XRD patterns of reaction time effects on hexagonal mesoporous prepared solvothermally, a) reaction time extended for an extra day under solvothermal conditions (deforms the hexagonal morphology), b) original reaction time at the same solvothermal conditions

Extending the reaction time for about 16 hrs or more than the original synthesis procedure time, of only two hours, produced higher intensity of the (220) peak. Higher overall intensity of the cubic morphology could indicate more framework condensation occurred employing the precipitating method, as presented in figure 3.16, Higher XRD intensities could indicate higher surface area as was proven by the BET test figure 3.13.

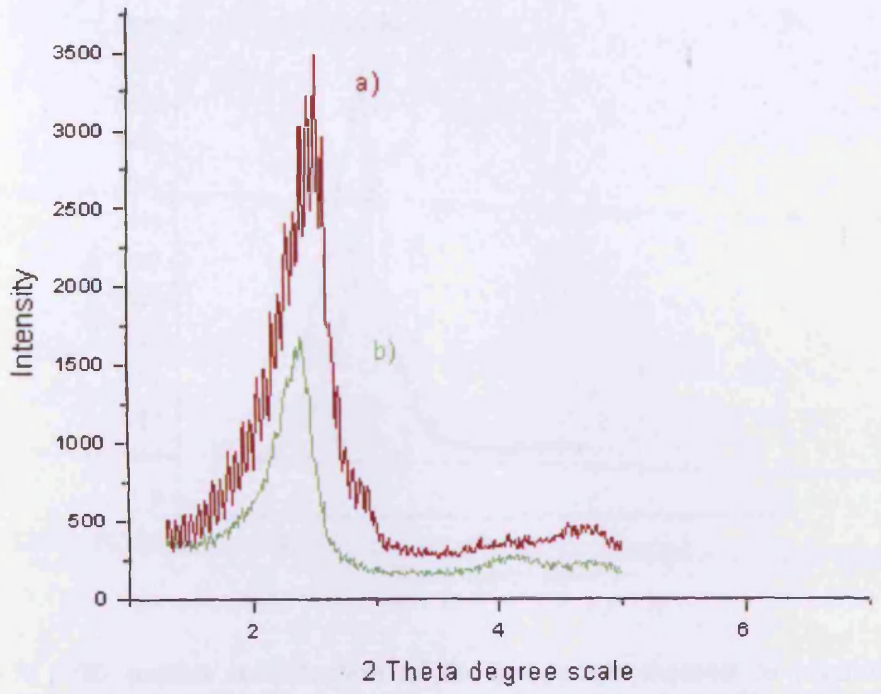

Figure 3.16 XRD patterns of extended reaction time that improved the morphology and the long-range order of the cubic mesoporous structure prepared by the precipitating method, reaction time a) over night, b) 2 hours; following the original method [20]

In general, precipitating experiments conducted proved that aging for one day would produce a better-ordered mesoporous structure than for two days. Moreover, extending the reaction time to overnight rather than only 2 hrs, as described in the original synthesis procedure, produced a better-ordered cubic structure. In addition, using a heating rate that is two degrees a minute shifts the d spacing to a smaller angle, whereas 4 degrees a minute destroys the structure. Similar behaviour was observed for the cubic mesoporous structures that were synthesized *via* solvothermal reaction. Figure 3.17 (a) represents the optimum reaction conditions used to produce cubic mesoporous structure using the precipitating method.

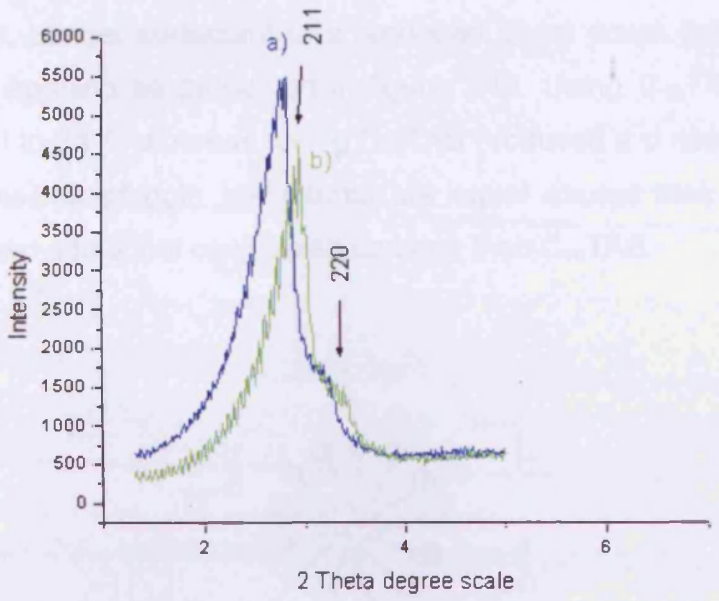

Figure 3.17 XRD patters modification of the precipitate method to produce cubic morphology calcined at 550 °C a) aged for one day calcined at 2 °C min^{-1}, b) aged 2 days at 2 °C min^{-1}

3.4.2.4 Effects of the Surfactants tail length Used on the Product's Morphology

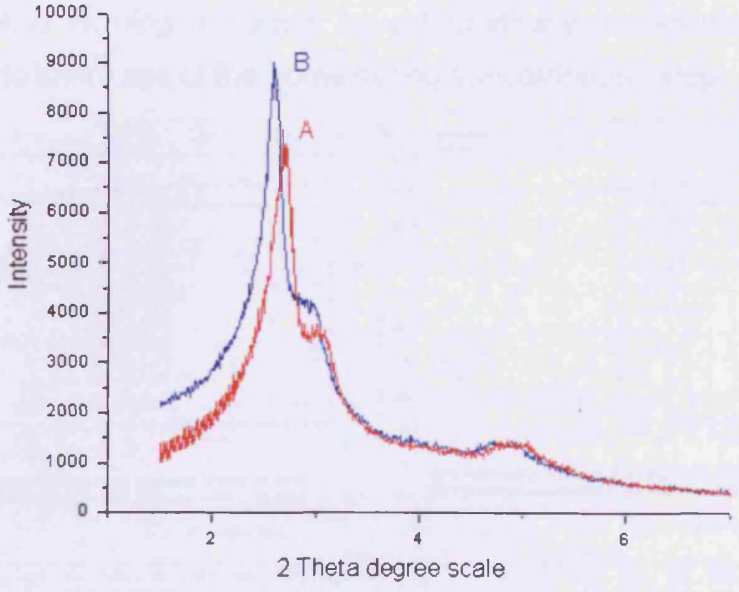

Figure 3.18 XRD patterns of cubic structure (solvothermal); sample a) using C_{16}TAB, b) using C_{18}TAB

The effects of utilizing longer surfactant tails are directly proportional to the d spacing shifts. Longer surfactant tails produced larger pores that contributed to a larger d spacing as presented in figure 3.18. Using C_{18}TAB gave a d-spacing equal to 34 Å; whereas, using C_{16}TAB produced a d spacing of 32 Å. All the dimensions of both surfactants are equal except their tails, where C_{18}TAB has two additional conjugated carbons than C_{16}TAB.

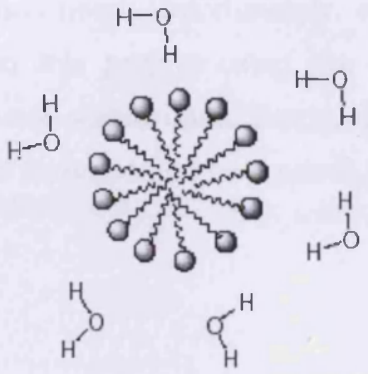

Figure 3.20 Schematic representation of the crossing over of tails of surfactants aggregates during the micelles formation[25]

Moreover, the BET results (figure 3.21) show a difference of 1.0 Å in the average pore diameter between both samples. This difference could be interpreted as a result of an overlapping in the end chain of the tail of each surfactant while forming a micelle as schematically represented by figure 3.20, or due to shrinkage of the pores during the calcination step.

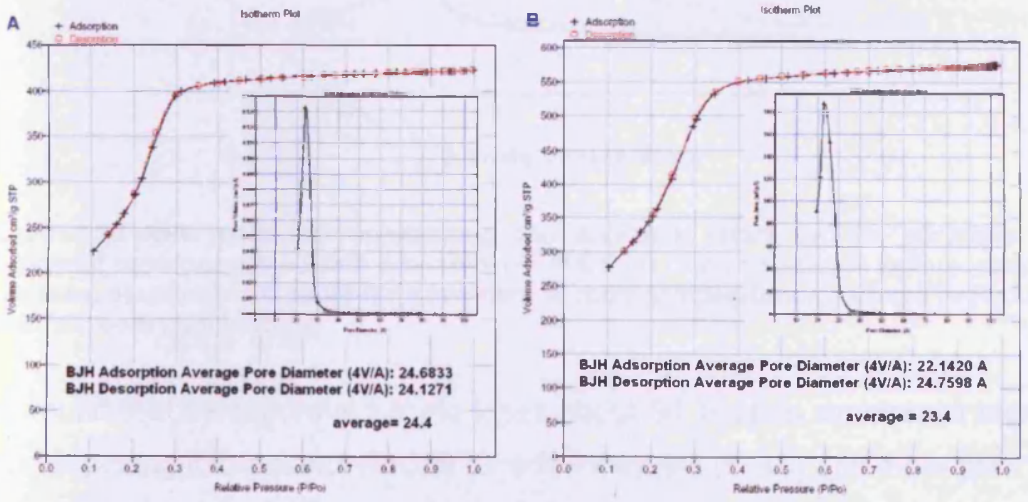

Figure 3.21 BET test for samples prepared using similar conditions except for the length of the surfactant used A) C_{18}TAB, B) C_{16}TAB

3.4.3 Stability Tests of Mesoporous Materials

3.4.3.1 Solvolysis Stability

Solvolysis stability is the ability of a mesoporous material to keep the integrity of its structural morphology and to resist losing some of its framework species upon exposing it to various solvents. When water is used as a solvent then the term "hydrolysis" is often used. Unfortunately, we found that most of the pure silicates prepared in this project using the standard (reported [17-20]) preparation methods are not stable upon exposure to water, alcohols, and solvents that contain water as presented by figure 3.22 below.

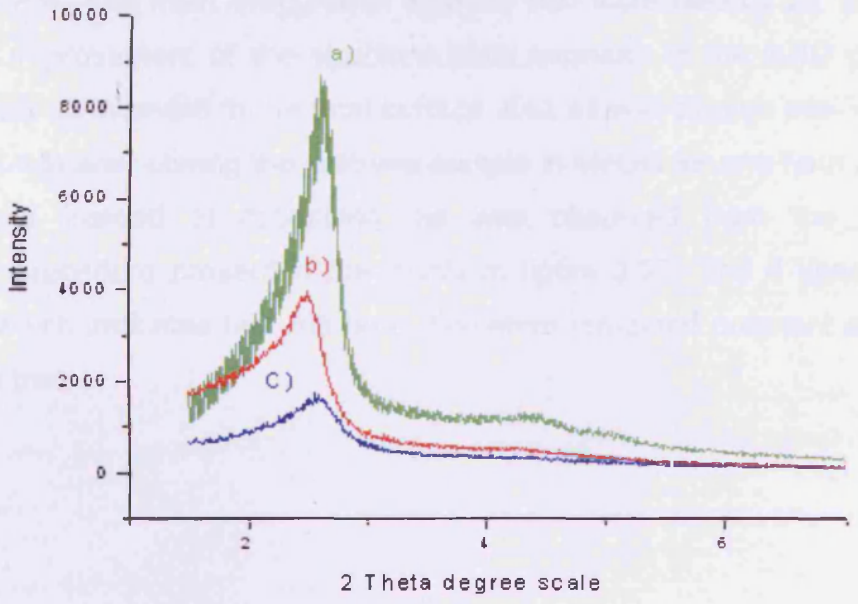

Figure 3.22 XRD patterns representing the solvent's effect on the structure of hexagonal mesoporous silicate prepared *via* TLCT (a) calcined sample before solvent exposure, b) stirred in ethanol for a few min. at room temperature, c) stirred in H_2O for 5 min. at room temperature

We found that mesoporous silicate loses about 50 % of its structural integrity upon exposing it to ethanol (EtOH) for a few minutes (5 -10) and more than 70 % when exposed to deionised water for 5 minutes at room temperature (see figure 3.22). Knowing that crude oil and some untreated petroleum products may contain some amounts of water. In addition, most metal and metal oxide

incorporation methods require the existence of water or alcohol as solvents or as by-products of the hydrolysis step, for example, the hydrolysis of zinc acetate by NaOH or LiOH produces ZnO particles and water, as presented by formula (3.1) below.

$$Zn(CH_3CO_2)_2 + 2NaOH \rightarrow ZnO + 2Na(CH_3CO_2)_2 + H_2O \quad .....(3.1)$$ [22]

3.4.3.1.1 Alcohol Solvolysis Test Performed on Mesoporous Silicate Produced by the Modified TLCT Method

Specially modified TLCT methods were employed to produce mesoporous silicate capable of withstanding the solvolysis test by stirring the calcined sample in methanol (MeOH) for one hour at room temperature, see figure 3.23, curve B. The main Bragg peak intensity had increased by 22 %, which indicates improvement of the structure (total increase in the XRD patterns could mean an increase in the total surface area as was proven previously in figures 11-13) after stirring the calcined sample in MeOH for one hour at room temperature instead of collapsing, as was observed from the original synthesis procedure presented previously in figure 3.22. The d spacing did not shift which indicates that the pore diameters remained constant after the solvolysis test.

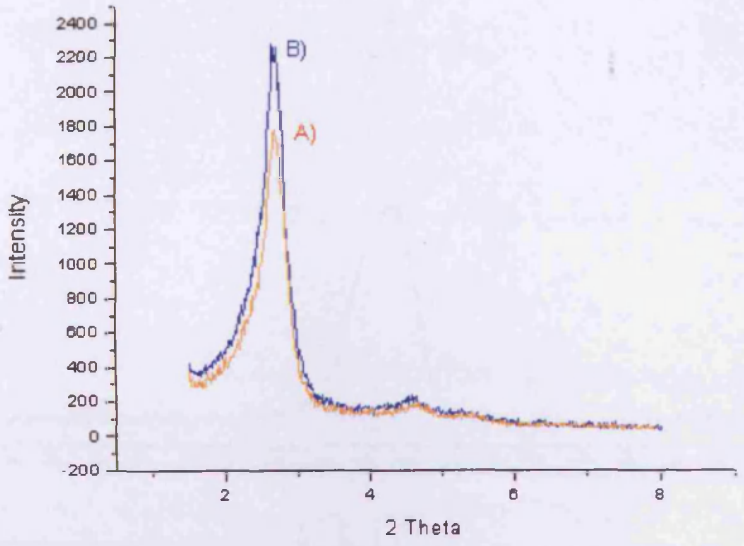

Figure 3.23 XRD patterns of the solvolysis test for the calcined mesoporous silicate (TLCT), A) before the test, B) stirred in MeOH for one hour at room temperate

Figure 3.24 represents solid-state ^{29}Si NMR MAS decoupling spectrum, A) before and B) after the solvolysis test, which reveals that only Q^4 intensity had increased after the solvolysis test, whereas Q^3, and Q^2 intensities decreased. The change in the intensities of Q values could indicate that the framework connectivity is improving due to the increment in Q^4 value which represents the $Si(SiO)_4$ species. This could indicate that the framework undergoes further condensation when exposed to methanol.

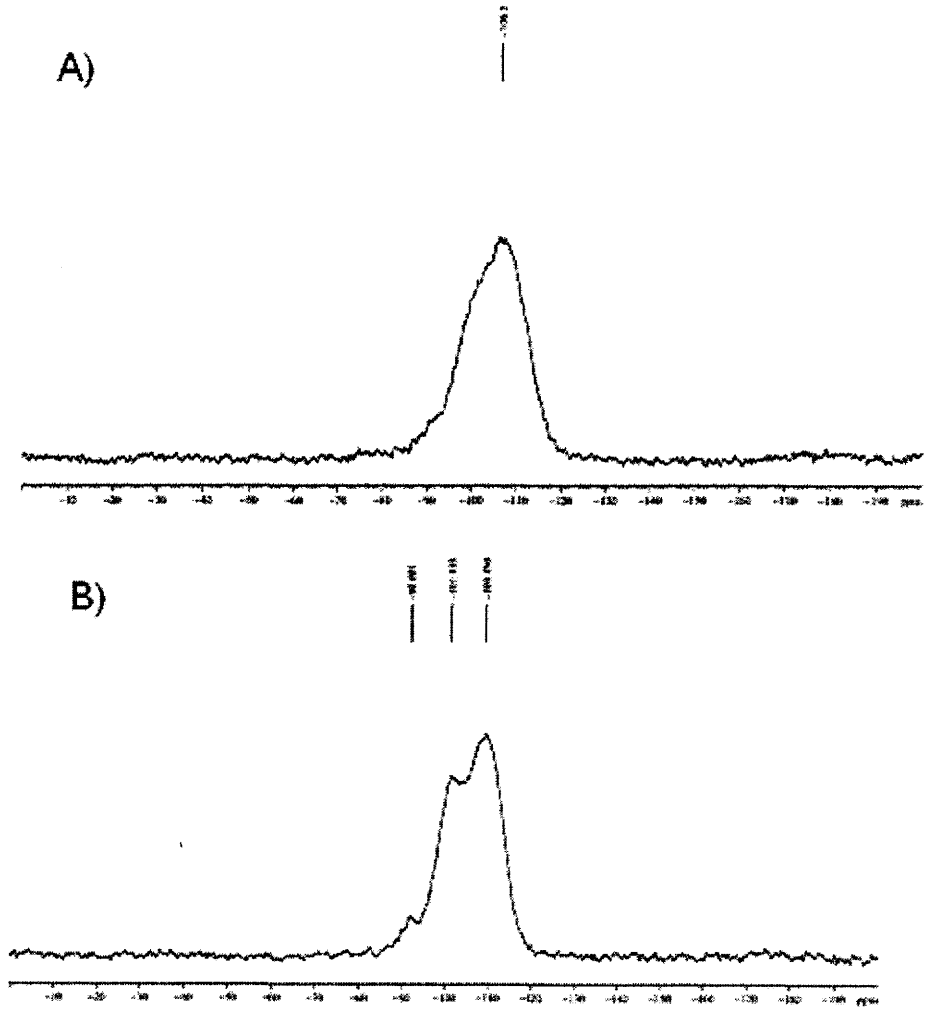

Figure 3.24 ^{29}Si NMR of mesoporous silicate *via* the modified TLCT method, A) calcined sample, B) after the solvolysis test (stirred in MeOH for one hour at room temperate)

3.4.3.2 Mechanical and Thermal Stabilities

Usually, introduction of metals or metal oxides into the pores (impregnation) of mesoporous materials requires multiple heat treatments that include the host material. In addition, heat treatment is required for regeneration cycles of the host after performing sorption or catalytic reactions. Mechanical stability is required for handling and filtration purposes in this project. Therefore, it is not required for the TLCT method because it produces glassy hard mesoporous flakes that need to be broken down or ground to use, as photographed in figure 3.25. Whereas, solvothermal and precipitating methods produce powder like solids that need slight force to form pellets or discs. Therefore,

modifications are required only to improve mesoporous silicate solvolysis, hydrothermal and thermal stabilities.

Figure 3.25 Mesoporous silicate; (Left) as-synthesised, (right) calcined product of TLCT method

Theoretically, strengthening the framework around the pores is the key factor to gain thermal and mechanical stability. On the other hand increasing the hydrophobic property of the framework would increase the hydrolysis stability. Hypothetically, substituting foreign atoms to the framework of silicate might upset the overall neutral charge, which produces an electrostatic attraction force that may pull the framework strongly together. However, what type of atoms and how much should we use? Moreover, how will these foreign atoms affect the morphology of the ordered mesoporous structure? We chose aluminium (Al) atom that also has positive interaction towards sulphur compounds (see fuel desulphurisation section in chapter one).

3.4.3.2.1 Introduction of Aluminium Oxides to Mesoporous Silicate

Introduction of alumina species were performed by two methods, during the synthesis or by post treatment of mesoporous silicate. Different atomic percentages of aluminium / silicon were explored; we find that the aluminium / silicon atomic percent should not exceed 15 %. At 12 - 15 % the mesoporous structure dramatically deforms and loses long-range order, at or above 15 % it collapses as presented in figure 3.26, therefore, all synthesis kept at Al/Si % from 2 – 11 %.

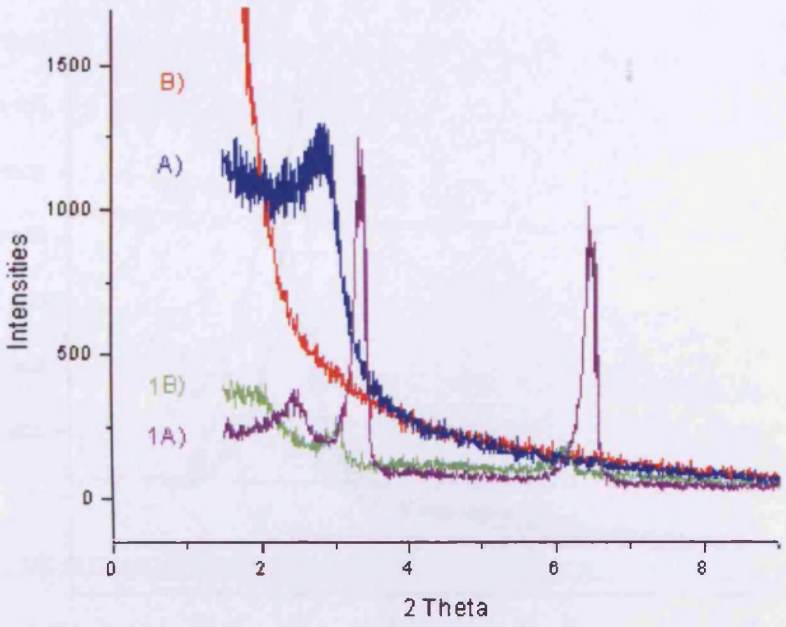

Figure 3.26 XRD patterns of mesoporous aluminosilicate (TLCT) having different Al % wt; 1A) Al_2O_3 11 % wt sample aged one day, A) then calcined, 1B) 15 % wt Al_2O_3 sample aged one day, B) then calcined

3.4.3.2.1.1 Post treatment

Hexagonal mesoporous silicate was prepared *via* the TLCT method, calcined at 550 °C for 5 hours at 3 °C min^{-1} then the alumina precursor (**post** synthesis) was introduced to the framework as described in reference[23]. The XRD patterns in figure 3.27 reveal that the d spacing shifts to a lower diffraction angle, which corresponds to the presence of Alumina species in the framework.

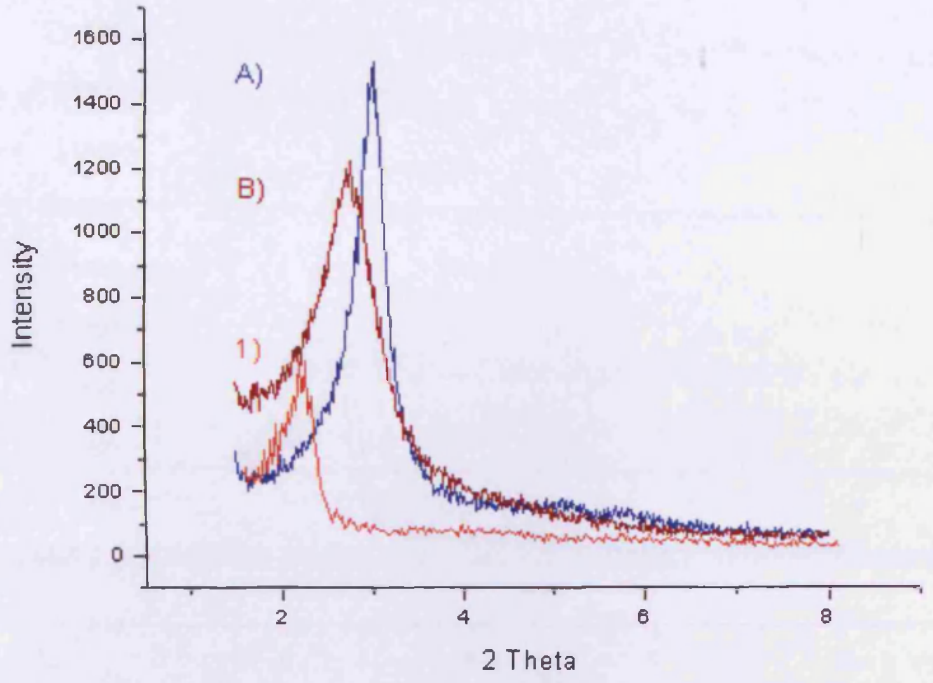

Figure 3.27 XRD patterns of 1) mesoporous silicate (TLCT) aged for 2 days, A) then calcined and B) introduction of Alumina by post treatment

3.4.3.2.1.1.1 Water Hydrolysis Tests for Mesoporous Aluminosilicate TLCT (Post)

A hydrolysis test was performed on post Al substituted mesoporous silicate prepared by the TLCT method (**post**). The XRD results, figure 3.28, show that the structure lost 40 % of its main XRD intensity when stirred in H_2O for 1 hour at 100 °C, and lost 50 % at room temperature. This is a very big improvement compared to the original preparations of mesoporous silicate structure, which lost more than 85 % in five minutes when it was stirred in water at room temperature, as presented previously in figure 3.22. Therefore introducing alumina species to the framework of mesoporous silicate improves its hydrolysis stability.

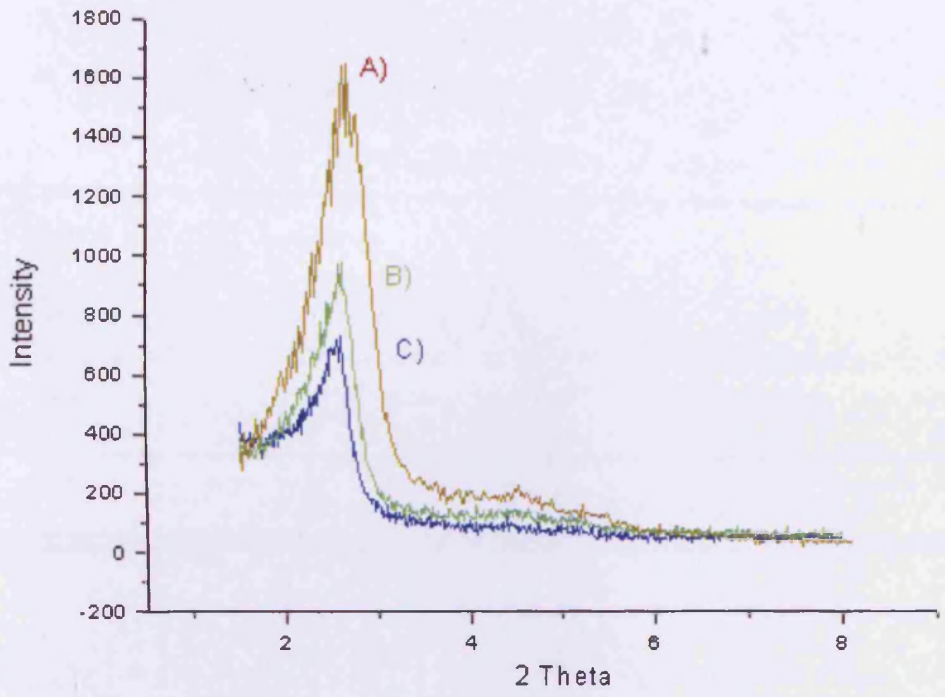

Figure 3.28 XRD patterns of A) hexagonal mesoporous aluminosilicate prepared *via* the (post) treated TLCT method calcined a second time for 4 hrs at 550 °C, stirred at H_2O for 1 hour B) at 100 °C, C) at 25 °C

Moreover, solid state ^{27}Al MAS NMR performed on this sample showed that there are almost equal amount of Al species (comparing their intensities) that possess pentahedral coordination at 32 ppm and octahedral coordinated at 0 ppm (37, and 36 % intensities respectively), which could indicate that 73 % of the incorporated Al_2O_3 precursor may not be entirely substituted in the framework silicate; it might be clustering outside the framework or exist in the framework but also attached to perhaps a bridging atom outside the framework, whereas the rest about 27 % of the Al species exist in tetrahedral coordination environment, at 51 ppm peak [23], [24]. This could indicate only 27 % of the incorporated Al_2O_3 precursors were definitely substituted in the framework silicate of the mesoporous matrix as presented in figure 3.29.

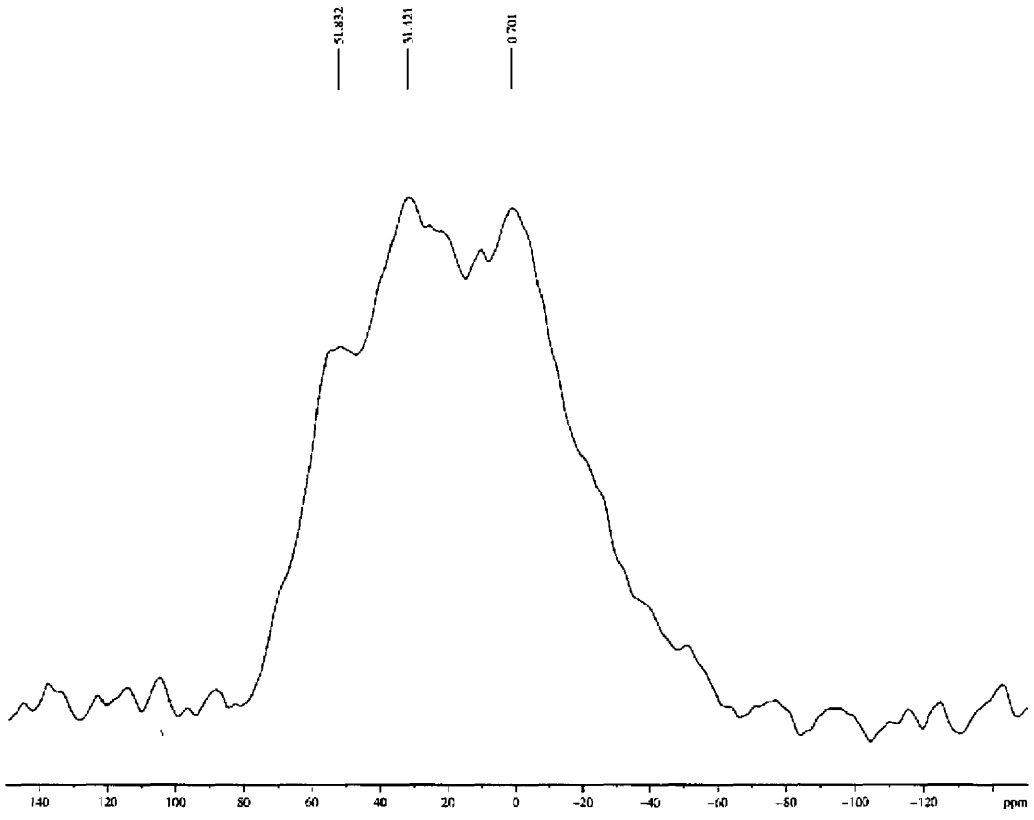

Figure 3.29 Solid-state ^{27}Al MAS NMR spectrum of mesoporous aluminosilicate prepared by the Al- post treatment of TLCT product

3.4.3.2.1.1.2 Alcohol Solvolysis Tests on Mesoporous Aluminosilicate (post)

Solvolysis tests were performed on the mesoporous aluminosilicate that had been prepared by the post treated TLCT method, by stirring one batch in methanol (MeOH) and the second batch in ethanol (EtOH) for one hour at room temperature. This sample showed high solvolysis stability against methanol and ethanol as analysed by XRD tests presented in figure 3.30, in which the peak intensity did not change as well as the d spacing.

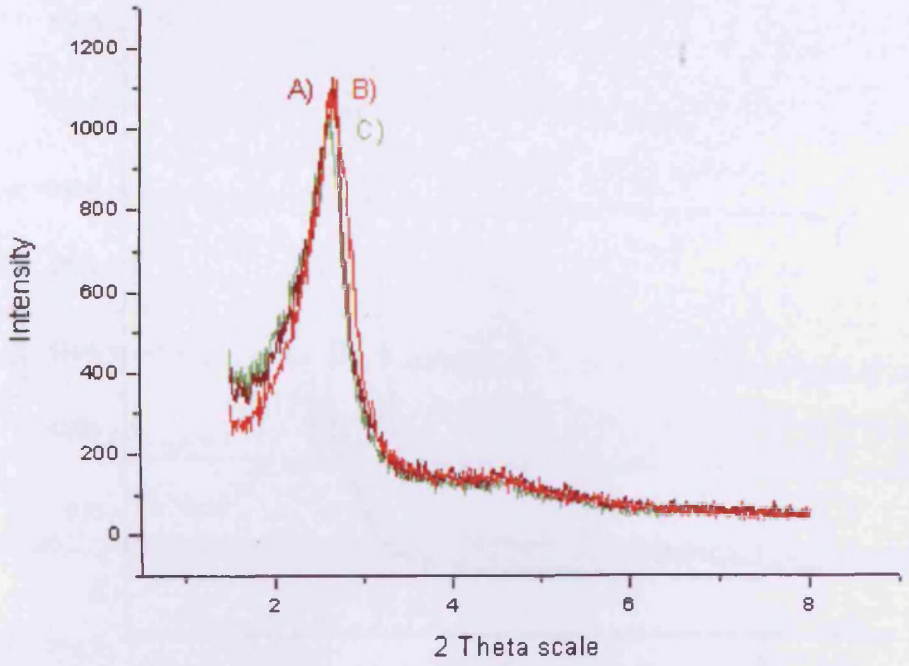

Figure 3.30 XRD patterns of the solvolysis tests at room temperature for one hour on mesoporous aluminosilicate TLCT (post) A) calcined sample, B) stirred in MeOH and C) stirred in EtOH

3.4.3.2.1.2 Substituting Alumina During the Synthesis of Mesoporous Materials

3.4.3.2.1.2.1 Hydrolysis Test for Mesoporous Aluminosilicate Prepared by the TLCT Method

Hexagonal mesoporous aluminosilicate material was synthesized by the especially modified TLCT method in which both precursors (SiO_2/Al_2O_3) were introduced to the liquid crystal phase, **during** the synthesis, as presented in sample (A) in figure 3.31. This sample was stirred at room temperature for one hour in deionised water indicated by (B) in figure 3.31, after which the sample lost 55 % of its overall XRD peaks intensity, however the d spacing shifted to a smaller angle which could indicate pore expansion.

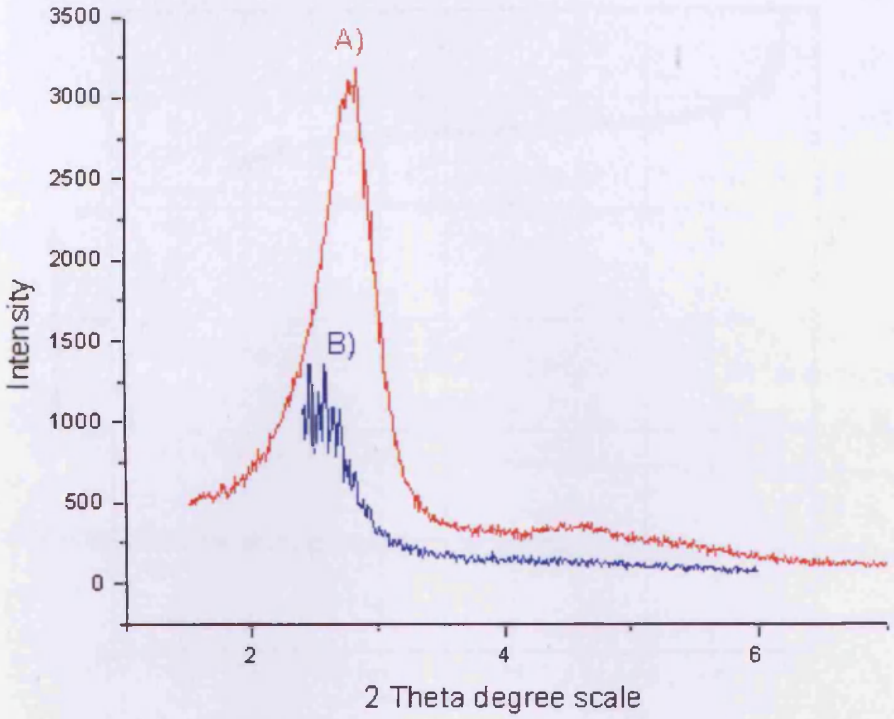

Figure 3.31 XRD patterns of hexagonal mesoporous aluminosilicate (during) prepared *via* the modified TLCT method A) calcined sample, B) stirred in deionised water for 1 hour at RT

BET tests of this sample revealed that the average pore diameters had increased after the hydrolysis test by approximately 2 Å (20 –22 Å respectively). Looking at the isotherms of the sample before and after the hydrolysis test, presented in figure 3.32, one can observe the following: a) the dry sample had more surface area than the hydrolysed sample, comparing the amount of volume adsorbed (Y axes) at any given relative pressure (X axes), b) the dry sample did not show a hysteresis loop, which indicates that the pores were uniform in their average shapes and sizes. On the other hand, after performing the hydrolysis test, the sample showed a hysteresis loop that indicates that variation in the pores shapes and sizes occurred, in agreement with the shift of the d spacing observed at the XRD peak shown in figure 3.31 and discussed in the previous paragraph.

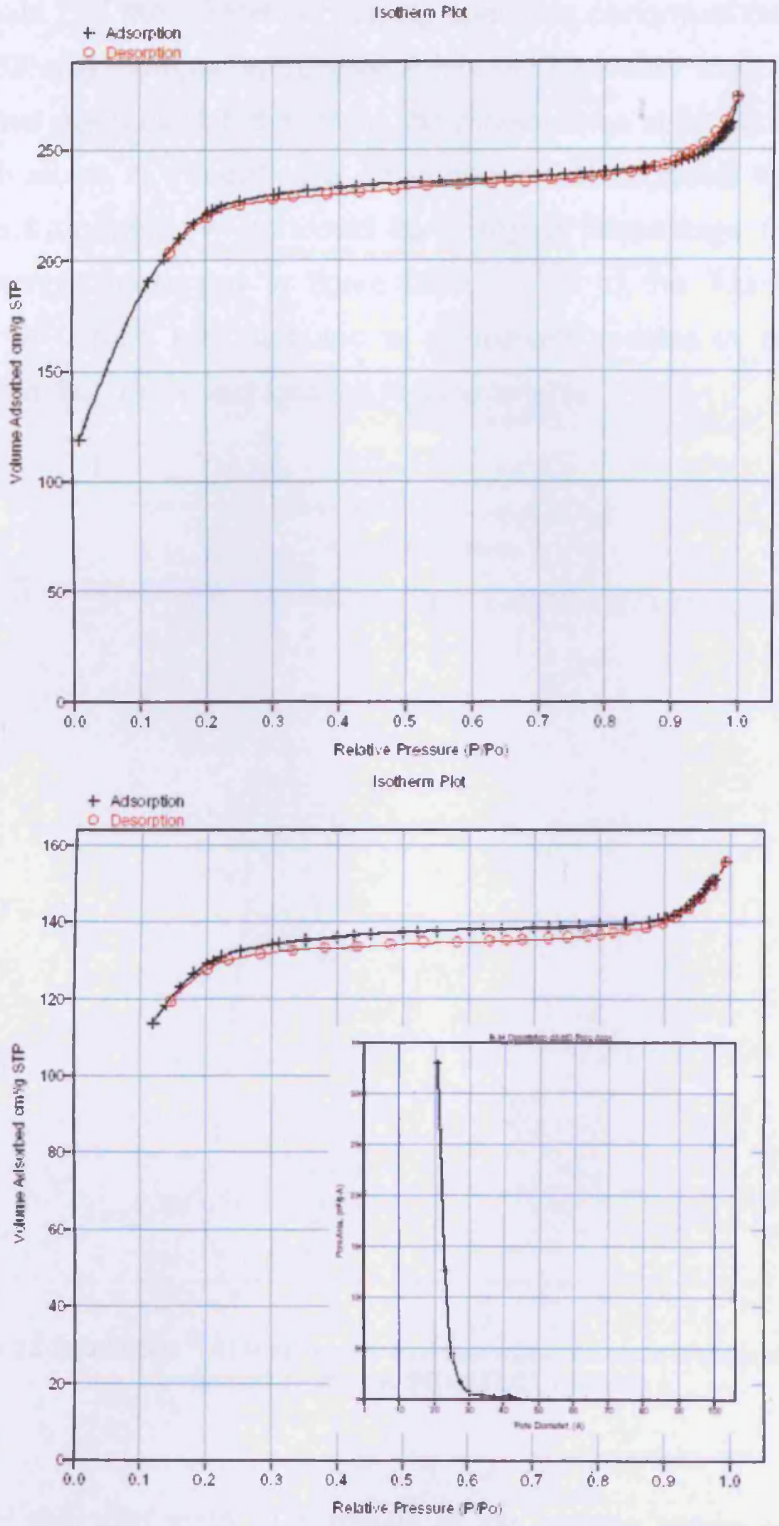

Figure 3.32 BET tests of the calcined aluminosilicate mesoporous sample (TLCT) before hydrolysis (top), sample was stirred in deionised water for 1 hr at room temperature (bottom)

A solid state ^{27}Al MAS NMR decoupling spectrum performed on this sample, figure 3.33, (by comparing relative intensities) reveals that 65 % of the incorporated Al_2O_3 exhibited a single sharp resonance at 50 ppm indicative of aluminium atoms in a tetrahedral environment that suggests their formation within the framework, which could be a higher percentage than the post treated sample presented in figure 3.29. 35 % of the Aluminium atoms observed at 0 ppm are attributed to Aluminium species in an octahedral environment; but their exact location is questionable.

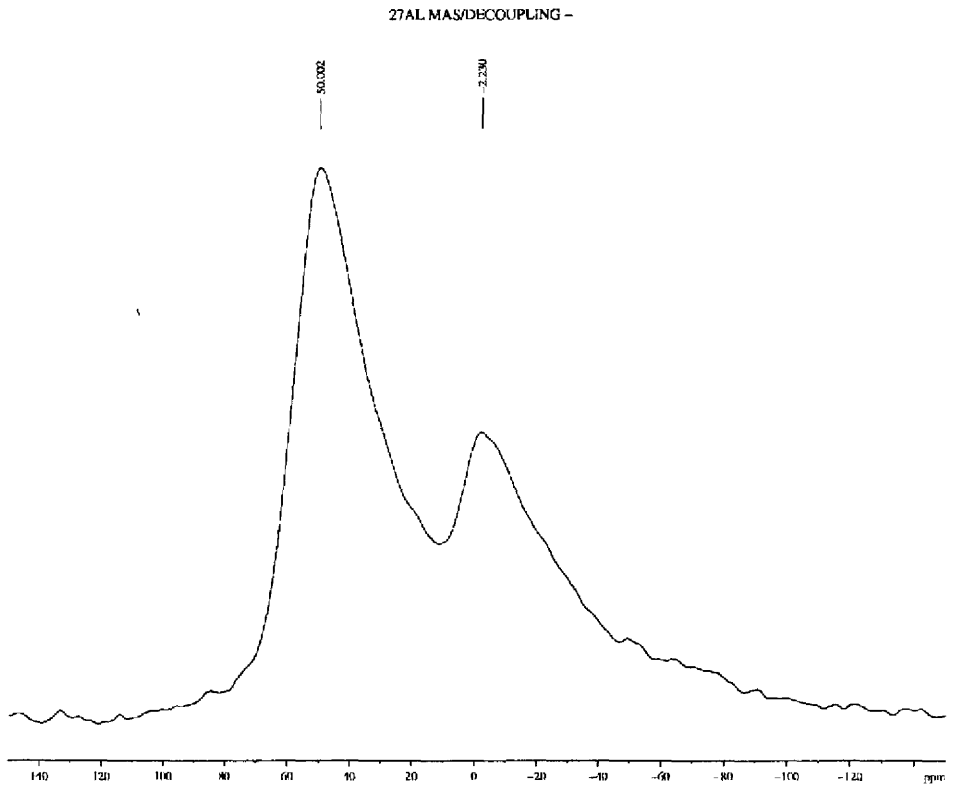

Figure 3.33 Solid-state ^{27}Al NMR spectra of mesoporous aluminosilicate (during) prepared by the modified TLCT method

Analysis of the solid state EDX results of this sample before and after the hydrolysis test, is presented in tables 3.2 and 3.3. The percentage of silicon atoms decreased after the hydrolysis tests while that of the aluminium atoms increased. This indicates that the silicate species are leaching out of the framework during the hydrolysis test, which confirms the weak hydrolysis stability of pure mesoporous silicate prepared by the standard method, and

gives a reasonable explanation for the partial loss, or sometimes the total collapse, of the mesoporous structure observed in the beginning of this project (see figure 3.22). Notice, the increment of the aluminium atomic percentage is due to the rounding up of the SEM/EDX instrument's software. Only carbon peaks were omitted from the tests (see figure 3.34) because carbon film is added on top of the sample prior to the SEM/EDX test.

Table 3.2 EDX results before the hydrolysis test

Element	Weight%	Atomic%	Compd%	Formula
1st Scan				
Al K	4.57	3.40	8.64	Al_2O_3
Si K	42.71	30.50	91.36	SiO_2
O	52.72	66.10		
2ndScan				
Al K	4.89	3.64	9.24	Al_2O_3
Si K	42.42	30.30	90.76	SiO_2
O	52.68	66.06		
3rd Scan				
Al K	4.53	3.37	8.55	Al_2O_3
Si K	42.75	30.53	91.45	SiO_2
O	52.73	66.11		

Table 3.3 EDX results after the hydrolysis test

Element	Weight%	Atomic%	Compd%	Formula
1st Scan				
Al K	5.23	3.89	9.89	Al_2O_3
Si K	42.12	30.09	90.11	SiO_2
O	52.64	66.02		
2ndScan				
Al K	5.42	4.03	10.24	Al_2O_3
Si K	41.96	29.97	89.76	SiO_2
O	52.62	65.99		
3rd Scan				
Al K	5.33	3.96	10.07	Al_2O_3
Si K	42.04	30.03	89.93	SiO_2
O	52.63	66.01		

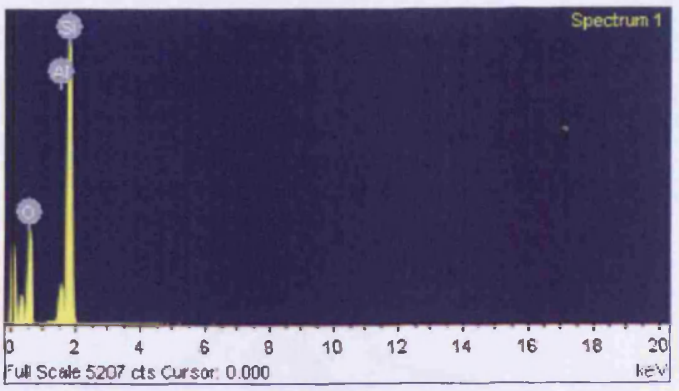

Figure 3.34 EDX peaks detected for the mesoporous aluminosilicate sample prepared by the modified TLCT method

3.4.3.2.1.2.1 Precipitating Method

We found that doping the mesoporous silicate sample with Al_2O_3 species (10 % Al/Si atomic ratio) **during** the synthesis, of the precipitating method increased the structural ability to resist hydrolysis when exposed to deionised water at different temperatures for one hour. The structure retains about 75 % of its main XRD peak intensity, which could be correlated to its structural integrity, at 100 °C, 60 % at 50 °C, and 50 % at room temperature as shown in figure 3.35. In addition we found that increasing the temperature during the hydrolysis test improves the structural resistance to hydrolysis. This sample exhibits by far the strongest hydrolysis stability compared to previous samples.

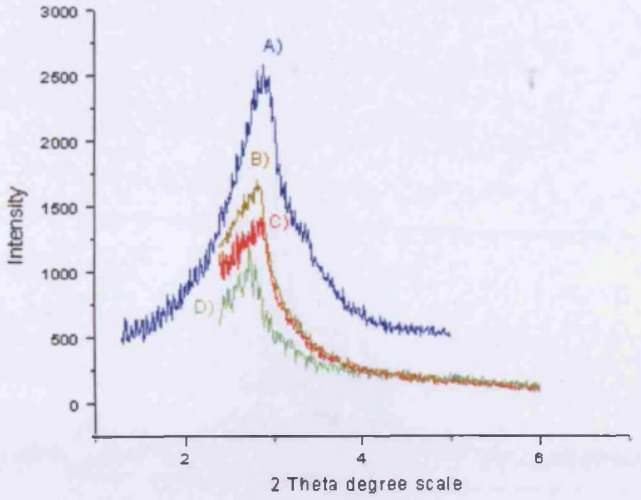

Figure 3.35 XRD patterns of the hydrolysis test on the cubic mesoporous aluminosilicate structure prepared *via* the modified precipitating method A) calcined sample dry, then stirred in deionised water for 1 hour at different temperatures, B) at 100 °C, C) 50 °C, D) 25 °C

Figure 3.36 shows the ^{27}Al MAS NMR spectrum of the cubic mesoporous aluminosilicate structure, of sample (A) in figure 3.35, that has a high peak of Aluminium atoms existing in a tetrahedral coordination environment at a chemical shift of 51 ppm, which is three times higher in intensity than of the octahedral coordination at 0 ppm. This could indicate that 75 % of Al_2O_3 species may be present in the framework. Whereas 25 % of the Alumina fragments' location is questionable comparing the ^{27}Al MAS NMR of a sample prepared by the same procedure containing only 2 % Al / Si atomic ratio, which reveals that the Alumina tetrahedral environment is only two times (relative intensities, 66.6 %) larger than the octahedral one (33.3 %) (see figure 3.37). These NMR results suggest that increasing the aluminium / silicate atomic ratio to 10 % could increase the contribution to the tetrahedral environment of the alumina species.

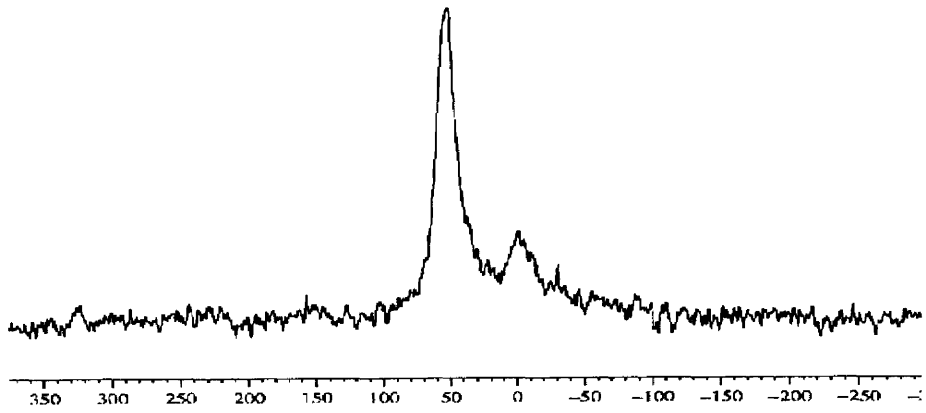

Figure 3.36 ^{27}Al MAS decoupling NMR spectra for the 10% Al/Si sample (A)

2.0% Al/Si

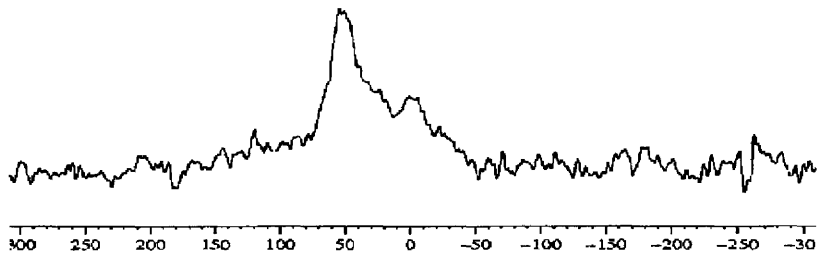

Figure 3.37 represents ^{27}Al MAS decoupling NMR spectra for 2 % Al/Si sample

SEM-EDX tests were performed on the calcined sample (A in figure 3.35) and after undergoing the hydrolysis test at 100 °C (sample B). These results are presented in tables 3.4, and 3.5 respectively; we did not observe a significant change in the atomic percentages for any of the elements, which indicates that there is minimum leaching and loss of the framework species during the hydrolysis test. This may be another reason for this sample's extra stability.

Table 3.4 EDX results before the hydrolysis test

Element	Weight%	Atomic%	Compd%	Formula
Scan 1				
Al K	5.44	4.04	10.27	Al_2O_3
Si K	41.94	29.96	89.73	SiO_2
O	52.62	65.99		
Element	Weight%	Atomic%	Compd%	Formula
Scan 2				
Al K	5.15	3.83	9.72	Al_2O_3
Si K	42.20	30.14	90.28	SiO_2
O	52.65	66.03		

Table 3.5 EDX results after the hydrolysis test

Element	Weight%	Atomic%	Compd%	Formula
Scan 1				
Al K	5.85	4.35	11.05	Al_2O_3
Si K	41.58	29.71	88.95	SiO_2
O	52.57	65.94		
Element	Weight%	Atomic%	Compd%	Formula
Scan 2				
Al K	5.35	3.98	10.11	Al_2O_3
Si K	42.02	30.02	89.89	SiO_2
O	52.63	66.00		

3.4.3.3 Hydrothermal Stability Results

Hydrothermal stability is the ability of a porous material to resist degrading or collapsing when exposed to humidity and heat simultaneously for a specific period of time. This test is essential to introduce, and synthesize some of the metal oxides, which will be discussed in chapter 4. The hydrothermal time required for metal incorporation is 30 minutes but we will explore extended time periods to study its effect on the structure of the prepared porous materials in the following section.

3.4.3.3.1 Hydrothermal Test for Mesoporous Silicate Prepared by the Modified TLCT Method

Mesoporous silicate prepared by the modified TLCT method was hydrothermally tested by heating the sample at 280 °C for 1 hour and under a flow of humid air emitted from bubbling deionised water. Intensities of the XRD patterns show that the material lost 28 % of its structure integrity (which may correspond to loss from the total surface area) after the test (see figure 3.38). The d spacing did not shift which means that no changes occurred in the pore diameters or the wall thickness.

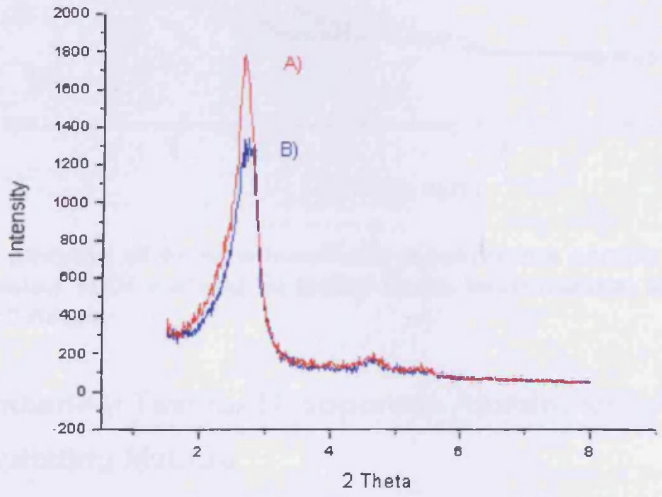

Figure 3.38 XRD patterns of A) mesoporous silicate sample prepared by the modified TLCT method, B) tested under hydrothermal test at 280 °C and humid airflow for 1 hour

3.4.3.3.2 Hydrothermal Test for Mesoporous Aluminosilicate Prepared by Post-treated Product of the TLCT Method

A hydrothermal test was performed on mesoporous aluminosilicate prepared by post-treated TLCT product at 290 °C for 2 hours under humid airflow. The XRD intensities show that the structure lost 40 % of its total surface area after this test, see figure 3.39. The 40 % lost was expected because of the duration of this test, which was extended to two hours, however lesser time periods were used for the other samples. Even though an extended time period was

used during the hydrothermal test of this sample, the d spacing did not shift so the pore diameter and the wall thickness did not change.

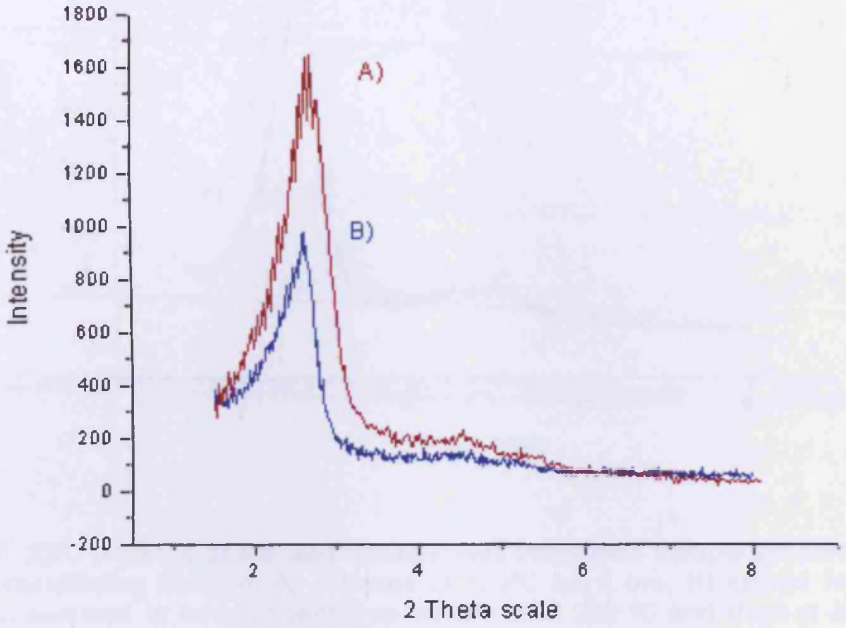

Figure 3.39 XRD patterns of A) Aluminosilicate mesoporous sample prepared by the modified post treated TLCT method B) tested under hydrothermal test at 290 °C and humid airflow for 2 hours

3.4.3.3.3 Hydrothermal Test for Mesoporous Aluminosilicate Prepared by Modified Precipitating Method

The mesoporous aluminosilicate (Al substituted **during** the synthesis) prepared by the modified precipitating method was subjected to two combined tests. First, the solvolysis test was applied by stirring the sample in MeOH at room temperature for one hour and dried at 50 °C then the hydrothermal test was performed at 280 °C for 30 minutes under humid airflow, and then calcined at 400 °C for 5 hrs under airflow. The Bragg intensities of the XRD patterns show that the structure lost only 10 % of its total intensity that could reflect the change that occurred in the total surface area, and there were slight d spacing shifts after calcination, which was expected due to pore shrinkage in figure 3.40.

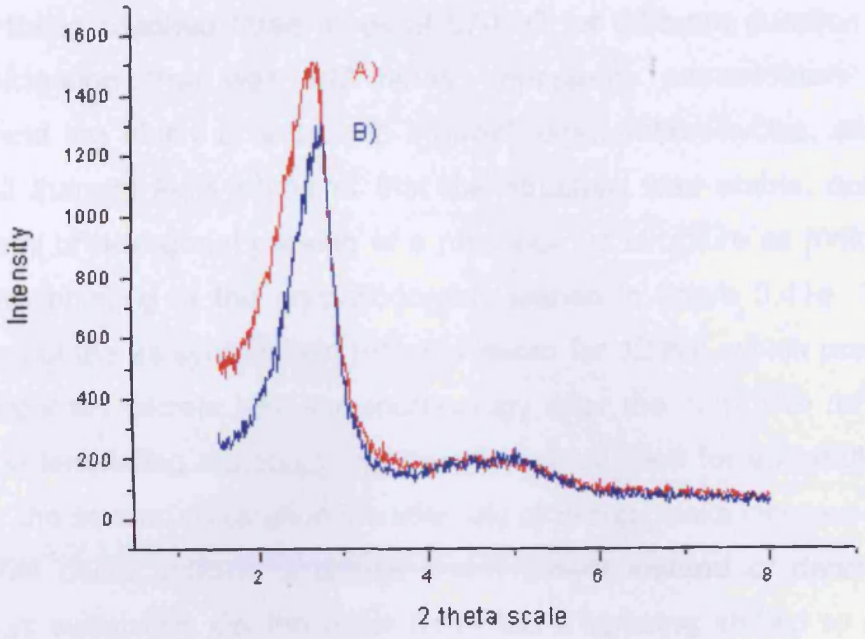

Figure 3.40. XRD patterns of the mesoporous aluminosilicate sample prepared by the modified precipitating method, A) calcined at 550°C for 6 hrs, B) stirred for 1 hr in MeOH, then calcined in humid conditions for 0.5 hr at 280 °C and then at 400 °C for 5hrs under dry air

3.4.3.4 Thermal Stability Results

Our definition of thermal stability for porous material, for this project, is the ability of a porous material to hold its morphology after the removal of the supporting templating materials. Elemental analyses have proven that calcining the material at a temperature above 450 °C for 5 hours with a sufficient flow of air will completely remove the organic templating materials leaving a carbon percentage of ~0.1 % or less. Other definitions are: a) the highest temperature at which porous materials would withstand and do not collapse; this definition ignores duration (time). b) The longest time a porous material can withstand at a given temperature. c) The ability of a porous material to hold its integrity after multiple heat treatments cycles, in other words, regeneration by heat treatments. Our modified preparation methods produced acceptable thermally stable mesoporous materials that could pass all thermal tests to fulfil the purpose of this project, which will be discussed in the following paragraphs.

A hexagonal mesoporous silicate was prepared by the modified TLCT method. Being calcined three times at 570 °C for different duration periods (total calcination time was 102 hours) represents extraordinary thermal stability and the ability to withstand thermal regeneration cycles, see figure 3.41. All thermal tests revealed that the structure was stable, holding its morphology of hexagonal packing of a mesoporous structure as indicated by the arrows pointing at the crystallographic planes in figure 3.41a. The first calcination of the as-synthesised material lasted for 12 hrs, which proves that the mesoporous silicate held the morphology after the complete removal of supporting templating materials and then it was calcined for an additional 45 hrs. After the second calcination the intensity of Bragg peaks increased (figure 3.41b) that could indicate structural improvement instead of deteriorating, which was surprising. On the other hand the d spacing shifted to a larger angle, which was expected due to pore shrinking. Then the sample was calcined for another 45 hrs, the d spacing stopped shifting and the material XRD intensity lost less than 10 % of its original structure (compare the intensity's heights of curves (a) and (c) in figure 3.41.

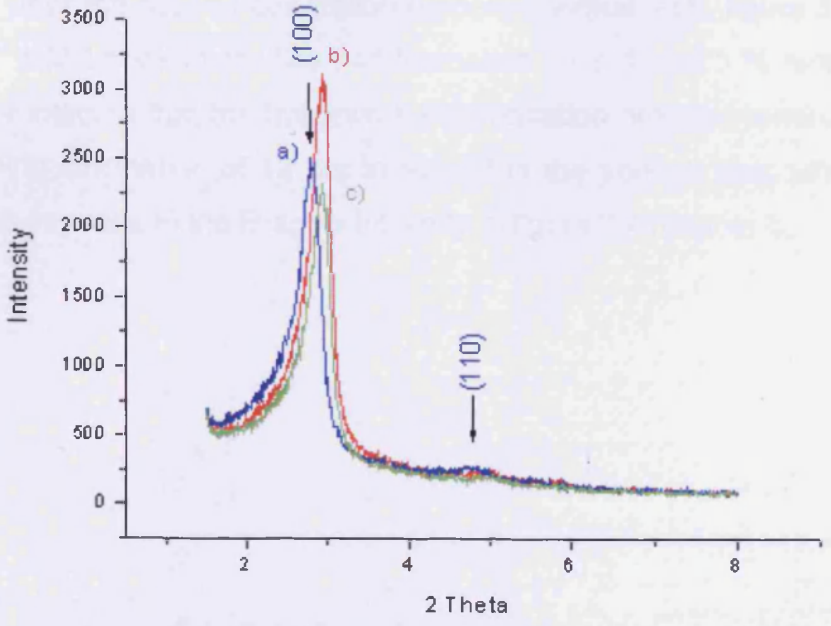

Figure 3.41 XRD patterns showing the effect of multiple calcination at 570 °C for different durations of hexagonal mesoporous silicate that had been prepared using the modified TLCT method, a) 12 hrs, then b) additional 45 hrs, then c) additional 45 hrs

Figures 3.42 to 3.44 present ^{29}Si MAS CP NMR spectra performed to analyse the thermal stability tests. Figure 3.42 presents the NMR spectrum for the 12 hours calcined sample, in which there is an equivalent intensities of 20 % of Q^4 [$Si(SiO)_4$] at δ –112 ppm and Q^2 [$(OH)_2Si(SiO)_2$] at δ – 92 ppm but 60 % of Q^3 [$(OH)Si(SiO)_3$] at –100 ppm.

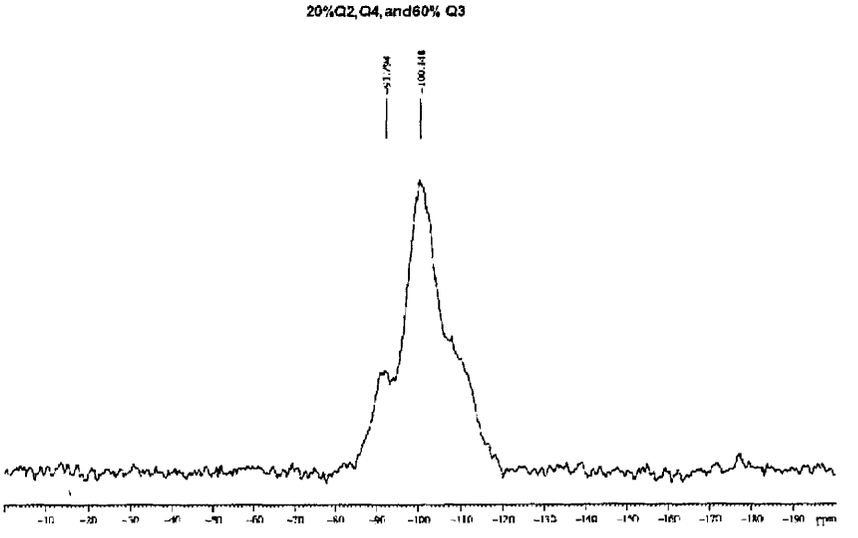

Figure 3.42 ^{29}Si CPMAS NMR spectra of the sample that calcined for 12 hours

However, after the second calcination (second thermal test), figure 3.43, both Q^2 and Q^4 NMR peak intensities had increased by 2 % and 3 % respectively, which may indicate that the framework condensation process continued even after the first calcination of 12 hrs to extend to the second one, which could explain the increase in the Bragg's intensity in figure 3.41caurve b.

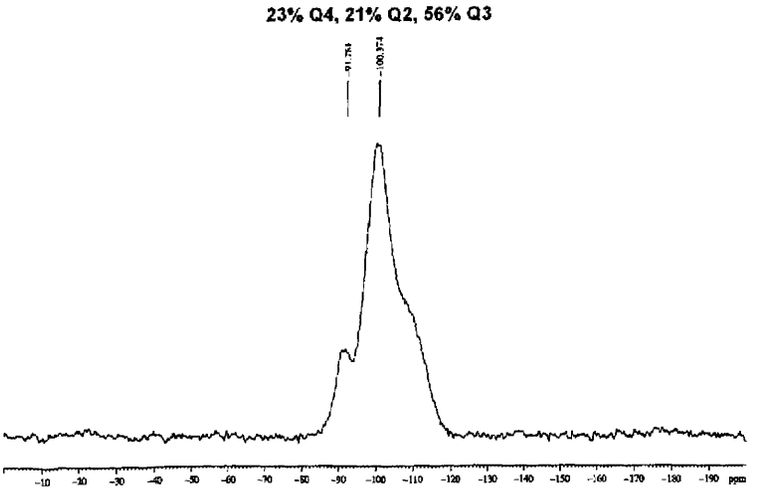

Figure 3.43 ^{29}Si CPMAS NMR spectra of the sample, after 57 hrs calcination

Figure 3.44 shows that Q^4 intensity decreased by 0.4 % after the third calcination (third thermal test). The thermal tests results suggest that the change in Q^4 value NMR intensities mimic the behaviour of the sample's Bragg peak main intensities after calcination as presented in figure 3.41.

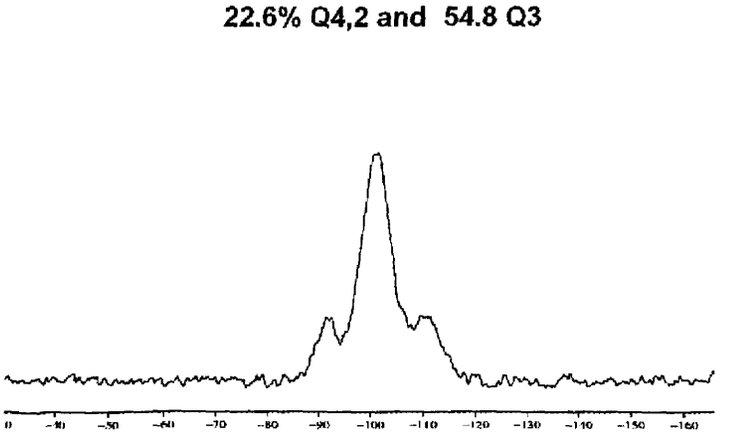

Figure 3.44 ^{29}Si CPMAS NMR spectra of the sample, after 102 hrs calcination

3.5 Summary

The effect of the heating rate depends on the morphology (hexagonal or cubic pore packing) of the prepared structure and depends upon the synthesis route used, for example a fast heating rate at or above 4 °C min^{-1} could decrease the long-range order or completely destroy the cubic mesoporous structure. We found that a heating rate of 3 °C min^{-1} deforms the structure of a cubic mesoporous structure prepared by the precipitating method, however 2 °C min^{-1} was proven to be the best heating rate for this method, and a heating rate of 3 °C min^{-1} was the best rate for the same structure prepared by the solvothermal method. 3 - 4 °C min^{-1} was a suitable rates for a hexagonal mesoporous silicate prepared by the TLCT method, whereas, the calcination temperature of 550 - 600 °C showed an improvement in the long-range order for both structures hexagonal and cubic mesoporous.

Aging of the as-synthesised mesoporous materials plays an important role in the overall long-range order by enhancing the condensation step and strengthening the framework by forming more metal oxygen bonds. We find that increasing the temperature at the aging step; to be slightly less than the temperature of mesophase formation, improves the stability of the mesoporous framework. It is equally important; to point out that the aging time is strongly dependent on the synthesis procedure employed.

We found that the average aging time for the as-synthesised samples prepared using the TLCT technique should be held between two to four days in order to produce the best long-range ordered mesoporous structure and to enhance the overall stability. On the other hand, elongated aging times will transform the mesophase or deform the morphology of interests, and could participate in the weakening of the framework rather than strengthening it, for solvothermal preparation methods. One day aging is proven to produce the best cubic mesoporous silicate morphology for both solvothermal and precipitating methods.

Hydrolysis, thermal and hydrothermal tests are essential to determine the stability of the mesoporous materials. The products of the standard methods [17 - 20] of synthesizing mesoporous silicate failed the stability tests prepared for this project. Understanding and controlling the individual preparation steps helped to produce better mesoporous material. Only modified samples showed acceptable stability to fit the purpose of this project. Moreover, mesoporous materials prepared by various methods behave differently under given conditions. Monitoring the structural and morphological changes of these materials upon exposing them to different conditions will provide a better understanding of their behaviour during doping and sorption reactions. Modified TLCT and precipitating (ppt) methods are more suitable to be employed for this project and will be employed in the following chapters.

3.6 References

1. G. Ramakrishna and H.N. Ghosh, *Langmuir*, 2003, **19**, 3006-3012.
2. S. Sakohara and M. Ishida, *J. Phys. Chem. B*, 1998, **102**, 10169-10175.
3. F. I. Mikrajuddin, and K. Okuyama, *J. Appl. Phys.*, 1 June 2001, **Vol. 89**, No. 11.
4. N. S. Pesika, K. J. Stebe, and P. C. Searson, *J. Phys. Chem. B*, 2003, **107**, 10412-10415.
5. N. S. Pesika, Z. Hu, K. J. Stebe, and P. C. Searson, *J. Phys. Chem. B*, 2002, **106**, 6985-6990.
6. M. Gratzel, *Current Opinion in Colloid & Interface Science*, 1999, **4**, 314-321.
7. R. F. Silva, M. E.D. Zaniquelli, *Thin Solid Films*, 2004, **449**, 86-93.
8. R. F. Silva, M.E.D. Zaniquelli, *Colloids and Surfaces A, Physicochem. Eng. Aspects*, 2002, **198–200**, 551–558.
9. K. Cassiers, T. Linssen, M. Mathieu, M. Benjelloun, K. Schrijnemakers, P. Van., P. Cool, and E. F. Vansant *Chem. Mater.*, 2002, **14**, 2317-2324.
10. T. Linssen, K. Cassiers, P. Cool, E.F. Vansant, *Advances in Colloid and Interface Science*, 2003, **103**,121–147.
11. R. Ryoo, J.M.Kim, C.H. Ko,C.H. Shin, *J. Phys. Chem.*, 1996, **100**, 17718.
12. P. Van Der Voort, M. Mathieu, F. Mees, E.F. Vansant, *J.Phys. Chem. B* 1998, **102**, 8847.
13. O. Collart, P. Van Der Voort, E.F. Vansant, D. Desplantier-Gescard, A. Galarneau, F. Di Renzo,F.Fajula, *J. Phys. Chem. B*, 2001, **105**, 12771.
14. K. Beneke, G. Lagaly, *Am. Mineral.*, 1977, **62**, 763.
15. D. Zhao, J. Feng, Q. Huo, N. Melosh, G.H. Frederickson, B.F. Chmelka, G.D. Stucky, *Science*, 1998, **279**, 548.
16. S. A. Bagshaw, E. Prouzet, T.J. Pinnavaia, *Science*, 1995, **269**, 1242.
17. G. S. Attard, J. C. Glyde, C. G. Goltner, *Nature* 1995, **378**, 366 – 368.
18. W. Zhang, J. Shi, L. Wang, and D. Yan, *Chem. Mater.*, 2000, **12**, 1408-1413.
19. M. Thommes, R. Kohn, M. Froba, *J. Phys. Chem. B*, 2000, **104**, 7932-7943.
20. S. Liu, P. Cool, O. Collart, *J. Phys. Chem. B*, 2003, **107**, 10405-10411.
21. D. Das, C. Tsai and S. Cheng, *Chem. Commun.*, 1999, 473–474.
22. B. Liu and H. Chun Zeng, *Langmuir*, 2004, **20**, 4196-4204.
23. R. Mokaya, *Angew. Chem. Int. Ed.*, 1999, **38**, No. 19.
24. S. A. Bagshaw and T. J. Pinnavaia, *Angm Chem. In/. Ed. Engl.*, 1996. **35**, No.I 0.

Chapter 4
Results 2 and discussion

- **Incorporation of Metals and Metal Oxides into Mesoporous Hosts**
- **Determination of Metals and Metal Oxide Sizes**
- **Improving Metals and Metal Oxide Syntheses**

This chapter includes a short review on metal and metal oxide preparation, with particular emphasis on nano-scale zinc oxide, gold and silver clusters. We have furthermore examined the host material and report the structural effects caused by these clusters. We further provide details of the sizes and nature of the incorporated gold and silver nano-particles. The chapter ends by describing details of a more efficient way to synthesize such materials.

Incorporation of Metals and Metal Oxides into Mesoporous Materials

4.1 Improving Sorption Properties of Mesoporous Silicates and Aluminosilicate by Impregnation with Selected Metals/ Oxides

There are currently relatively few articles to be found discussing the interaction of impregnated silver and gold particles in mesoporous structures with sulphur [1-8]. The examination of gold and silver incorporation into porous silicate is included only towards the end of this chapter, and due to the expense involved in working with gold and silver, the scope of this work is limited. Nevertheless, the incorporation of nano clusters of gold, silver and zinc oxide particles into the pores of mesoporous silicate and aluminosilicate impregnation methods has been examined in this chapter, with the aim of improving the sorption ability of these hosts towards sulphur compounds, which will be discussed in chapter 5.

4.1.1 Zinc Oxide

Zinc Oxide (ZnO) is amongst the most recommended of materials used to adsorb sulphur compounds. ZnO is a soft powder that has a low surface area, estimated to be less than 50 m^2g^{-1}. Whilst many groups have claimed to have synthesized porous ZnO, that possesses a relatively high surface area of around 100 m^2g^{-1}, no evidence has been published examining the mechanical stability and compressibility of those claimed structures [9-12]. This is a most important factor since the compressibility and mechanical stability of a porous material determines its overall strength, and hence its ability to retain its structural integrity after being shaped into pellets or discs. Furthermore, such examinations provide vital information about the rigidity of the pore walls, and therefore, give an indication as to whether these pores can be accessed by diffusing species that can then move to active regions within the structure where catalytic reaction may occur. This is especially important considering that transforming ZnO from its powder state into pellets or sphere-like forms

makes it industrially more applicable in terms of handling, loading, and filtering-out during operational processes. Due to the highlighted reasons regarding the unconfirmed stability and synthesis of porous ZnO, a different approach that can yield a catalytically active, and mechanically stable analogue has been taken in this research work. Specifically our work was focused on creating a sturdy host of cheaper elements, such as silicate, and then to introduce ZnO particles within the pores of the host.

There are very few published articles claiming the incorporation of ZnO into porous silicates[13, 14]. This subject is also controversial since not enough evidence is supplied in current published works to certify whether ZnO particles reside within the pores, or in the outer surface of their porous host. It is also not clear whether zinc oxide particles remain attached or dislodge during exposure to fluids (depletion). Their distribution within their host system (silicate for example) also remains elusive; this is a most important point considering that metal oxides can form aggregates and may concentrate in a limited area of the host. In this particular case, it would be difficult to get a representative sample to perform the catalytic reactions. Other points of consideration that highlight the complexity of these materials, and the little knowledge we possess on them, stem from the irreproducibility of the published procedures[13, 14]. Finally, in-line with some of the published works on porous ZnO, no study has yet examined the stability of the porous host before, during, and after the incorporation of ZnO particles [13-17]. It is therefore very clear that there is much to be done on those systems to fully characterise and understand them. Only then can their maximum potentials be explored.

4.1.1.1 ZnO Preparation Methods

In the early stages of this project, standard preparation procedures were applied to produce ZnO clusters in a manner adhering to Spanhel's method[18]. Which consists of two parts: 1) the zinc oxide precursor is prepared by refluxing zinc acetate in alcohol for few hours, and 2) the prepared precursor is then hydrolysed with aqueous lithium or sodium hydroxide following equation 4.1.

$$Zn(CH_3CO_2)_2 + 2NaOH \rightarrow ZnO + 2Na(CH_3CO_2)_2 + H_2O \quad .....(4.1)$$

Before ZnO incorporation into the mesoporous substrates it was important to determine the pores' percentage volume. This measurement was necessary because it represents the availability of sites that can accommodate metals or metal oxides. A further reason to measure the pores' percentage volume is to assign limits to the maximum incorporation a substrate can accommodate before structural reconstructions occur. Such structural reconstructions include: 1) a complete blockage of the internal pores at high levels of incorporation which leads to a dramatic decrease in the total substrate surface area, and hence minimise the number of particles, that are exposed to the outer surface for reaction purposes, 2) the formation of a layer around the silicate framework, especially at high incorporation levels of metal oxides especially ZnO[14] as seen in figure 4.1, 3) increasing the concentration of some metal oxides species within the porous substrate may lead to a structural collapse of the host if the inserted metal oxide particles grew during the initial nucleation step and later during calcination, as seen by the flattening of the main Bragg peaks (curve (c) in figure 4.2).

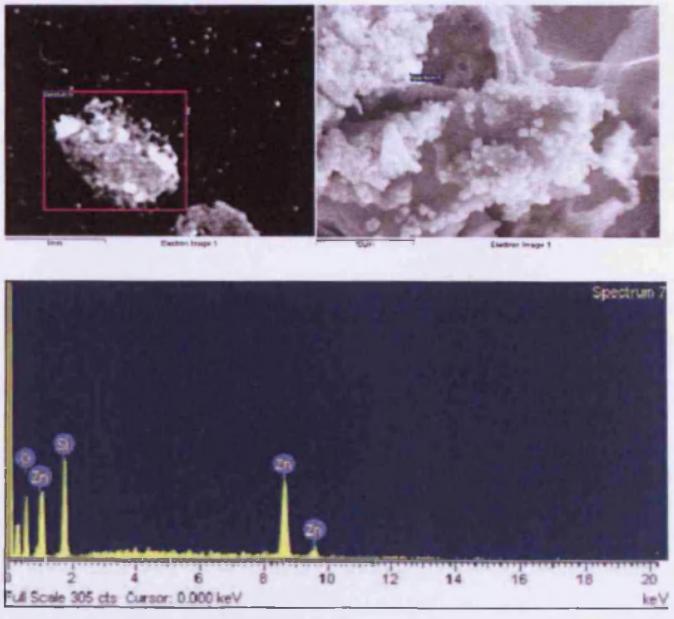

Figure 4.1 SEM-EDX spectra showing ZnO particles (intense weight colour) particles on the outside surface of MCM-41 silicate

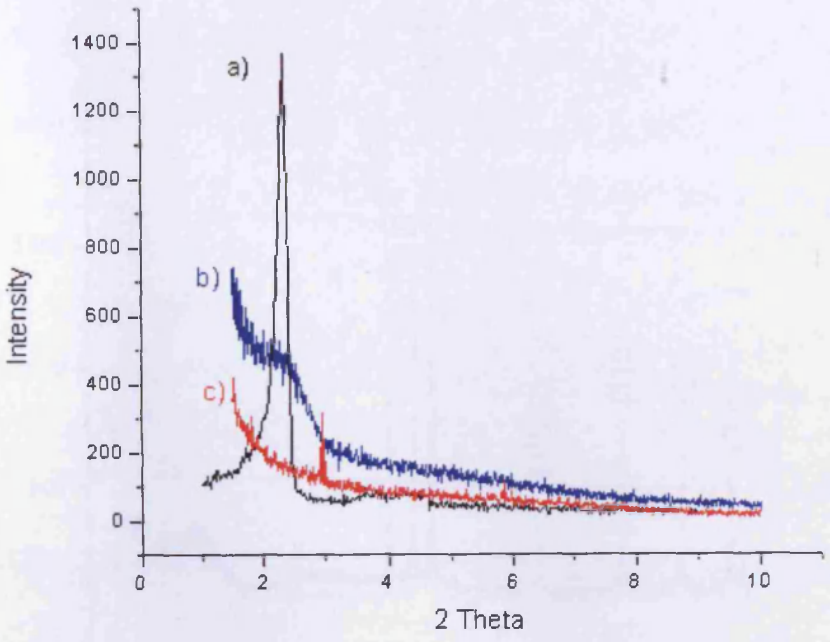

Figure 4.2 XRD patterns of low angle scan a) pure mesoporous silicate (TLCT) and; ZnO forming through: b) thermal treatment specially modified to avoid exposure to water during hydrolysis and c) hydrolysis using LiOH

Figure 4.3 presents XRD patterns of a wide angle scan for the intensities of the crystallographic planes for sample (C). These are higher, and their bases, are narrower than those for sample (B). Thus indicates that the ZnO particles forming in sample (C) are more crystalline and larger in size than in (B).

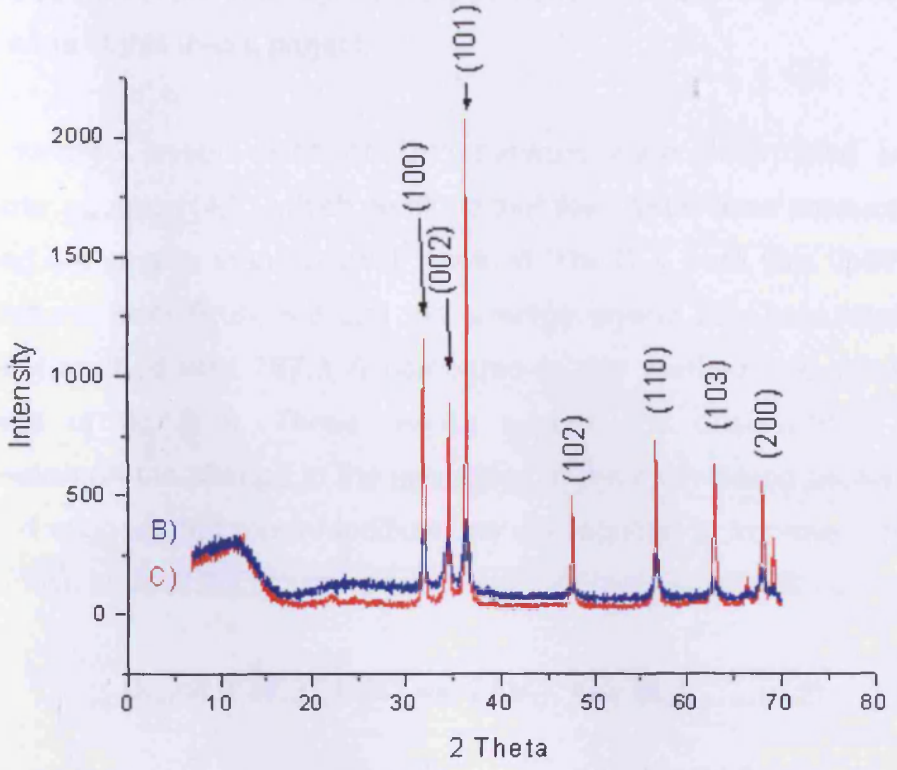

Figure 4.3 Wide-angle scan XRD spectra showing crystal planes, and the three distinctive peeks of ZnO (100) (002)(101), B)ZnO prepared *via* thermal formation, and C) using LiOH

4.1.1.1.1 Structural Deformation of the Host Morphology

The hexagonal structure of mesoporous silicate has been deformed dramatically or been completely lost upon the formation of ZnO using the Spanhel[18] method. 70 % of the host's structure is lost upon heat treatment, and 75 % upon the hydrolysis formation of ZnO, see figure 4.2. There are two likely reasons for this: 1) the pure silicate mesoporous framework has initially weak hydrolysis stability (as discussed in Chapter 3) and 2) the high concentration of the ZnO precursor used which destabilises the structure. The latter point is actually very interesting; many groups claimed to have synthesized ZnO particles in MCM matrix with unfortunately concentrations that are too low to have significant catalytic applications (0.001 - 0.01) M [13-17]. In this project the maximum allowable ZnO incorporation levels into mesoporous hosts will be tackled that keeps the integrity of the host and

produces practically the highest sorption effect. In fact this is amongst the main aims of this thesis project.

The average crystal sizes of ZnO particles were determined using the Scherrer equation (4.2), which confirms that the crystal sizes produced by our method are smaller than Spanhel[18] method. The D_{100} peak was used in these calculations from figure 4.3 and the average crystal size calculated for the Spanhel method was 787.3 Å compared to our method that produced an average of 387.3 Å. These results support the observations and the discussion on the change in the intensities of the main Bragg peaks in figure 4.2 and suggest that more modifications are required to improve our method to produce smaller ZnO clusters.

$$D_{hkl}=0.9*57.3*(1.542 =\lambda) / (\beta/_2) *\cos (\theta/_2) \ldots\ldots(4.2)$$

where 57.3 is a conversion factor from degree to rad, β is the breadth of maximum peak intensity.

4.1.1.2 Modifying the ZnO Preparation Procedure

Since the standard method of preparing ZnO particles results in destabilisation of the mesoporous host structure, a new synthesis route was designed in this work. This was carried out by firstly dissolving zinc precursor (acetate or nitrate) in alcohol before heat-treating the mixture to form zinc oxide. This step did not require the presence of a catalyst such as NaOH or LiOH. Before continuing, and for "good practice" the synthesized ZnO was compared to its commercial analogue. This was done employing absorption techniques; especially UV/VIS spectra. A comparison of the zinc oxide samples is shown in figure 4.4.

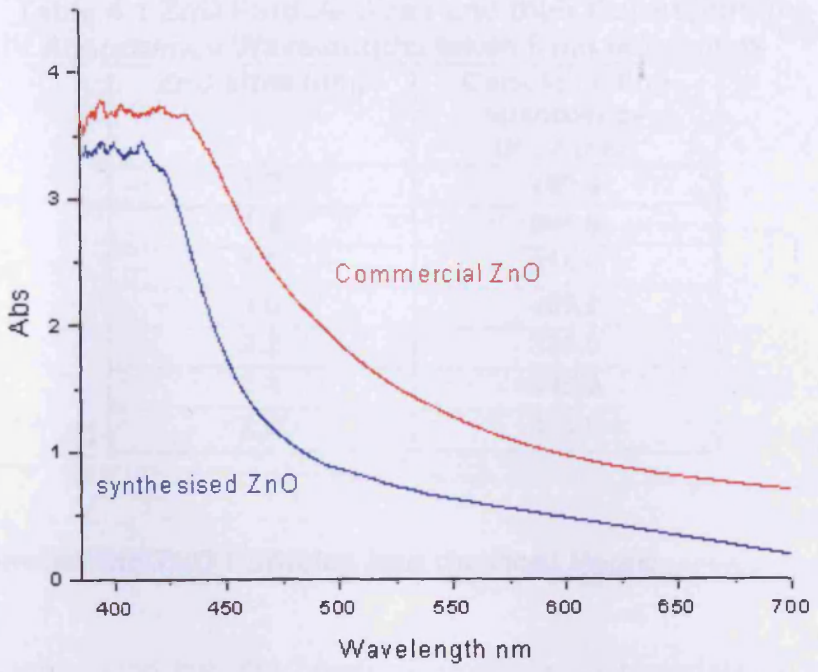

Figure 4.4 Solid-state UV/VIS spectra comparing commercial ZnO (red), with that synthesised in this project (blue), the Ultraviolet part 200-380 nm were omitted because the peaks intensities were over the absorbance scale

The results in figure 4.4 show that both "types" of zinc oxide have very similar peaks in the range 350 - 440 nm; this is characteristic of zinc oxide. The difference between the two samples' absorbance is attributed to the differences in their relative thickness arising while pressing the materials into UV-discs. Nevertheless our sample possesses a narrower UV/VIS peak than the commercial analogue. Moreover wavelengths between 250 – 350 were omitted from figure 4.4 due to the absorption intensities going off the scale.

Table 4.1 ZnO Particle Sizes and their Corresponding UV Absorbance Wavelengths taken from references [19(a,b)]

ZnO sizes (nm)	Corresponding absorbance UV. λ (nm)
1.2	285.0
1.4	295.0
1.6	315.0
1.8	325.0
2.2	335.0
2.4	345.0
2.6	355.0

4.1.1.3 Introducing ZnO Particles Into the Host Pores

ZnO was introduced into the pores of mesoporous materials by stirring the mesoporous host in an alcohol solution containing a specific amount of dissolved zinc acetate at room temperature for 30 minutes. Following this, the sample was filtered and heat-treated to 400 °C for 4 hours. This was performed to convert zinc acetate into ZnO.

4.1.1.3.1 ZnO Clustering in Mesoporous Silicate Prepared by the Modified TLCT Method

The XRD method was used to examine the phenomena of zinc oxide clustering in the host samples synthesized in this work. Figure 4.5 represents the corresponding low-angle XRD patterns of (A) modified TLCT mesoporous silicate before the introduction of ZnO and (B) after the introduction of 3 % ZnO.

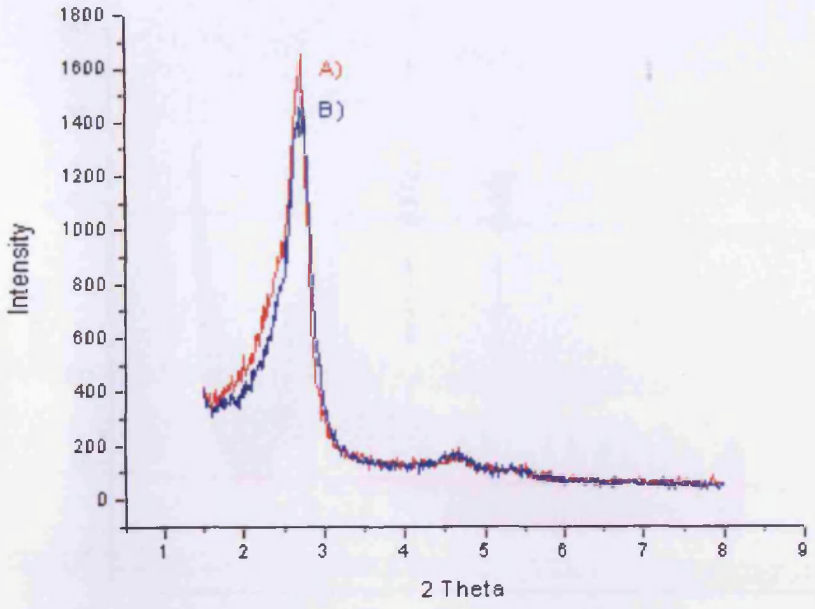

Figure 4.5 Low angle XRD patterns of A) mesoporous silicate (TLCT) and B) after introduction of 3 % ZnO

Figure 4.5 indicates that the incorporation of 3 % ZnO resulted in a 10 % loss in the intensity of the main peak representing the porous silicate structure. No d spacing shifts are observed, and no deformation of the host structure is detected. This loss of intensity is therefore attributed to a reduction in the total surface area of the silicate host, which is indicative of ZnO clustering within the mesoporous host.

A wide-angle XRD pattern test was performed in an analogous manner, which is represented in figure 4.6 below.

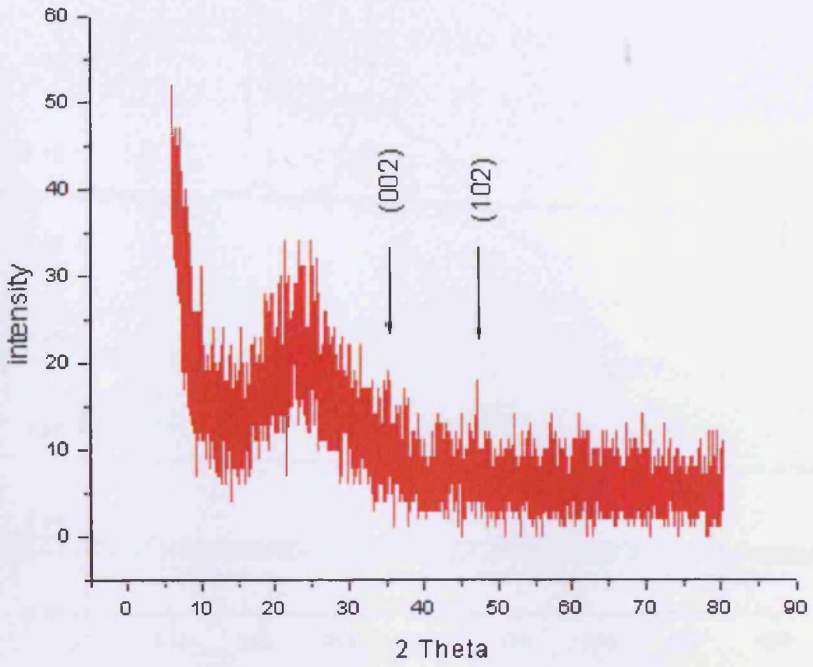

Figure 4.6 Wide-angle XRD patterns of mesoporous silicate (TLCT), B) after introduction of 3% ZnO

The peaks indicated in figure 4.6 of the crystal planes are not easily determined since it is difficult to distinguish those from the base-line noise (of the amorphous mesoporous silicate). That could reflect that the particles sizes of ZnO are too small to be detected by the wide-angle XRD test.

A final test performed to probe the synthesized mesoporous silicate containing 3 % ZnO clusters, using a solid-state UV absorbance examination. This is shown in figure 4.7.

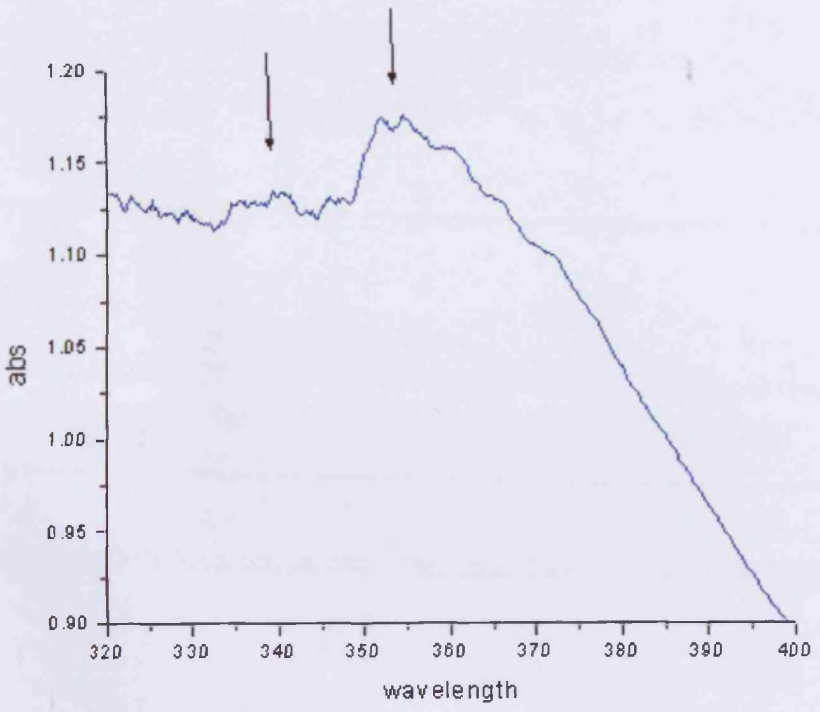

Figure 4.7 UV spectra of 3 % ZnO in mesoporous silicate (TLCT)

Two peaks are shown in figure 4.7 at 355 nm and 335 nm. The first peak corresponds to ZnO particles of dimensions < 30 Å [19 a,b], and the second peak represent ZnO clusters size of approximately 20 Å [19 a,b]. This evidence gives high probability of having these clusters inside the pores.

4.1.1.3.2 ZnO Clustering in Mesoporous Aluminosilicate Prepared by Post Treated TLCT Method

Post Al-treated TLCT mesoporous aluminosilicate was impregnated with 5.3 % of ZnO and then it was calcined at 500 °C for 4 hours. The corresponding low-angle XRD pattern is shown in figure 4.8 for the sample before impregnating (A), and (B) after impregnation below.

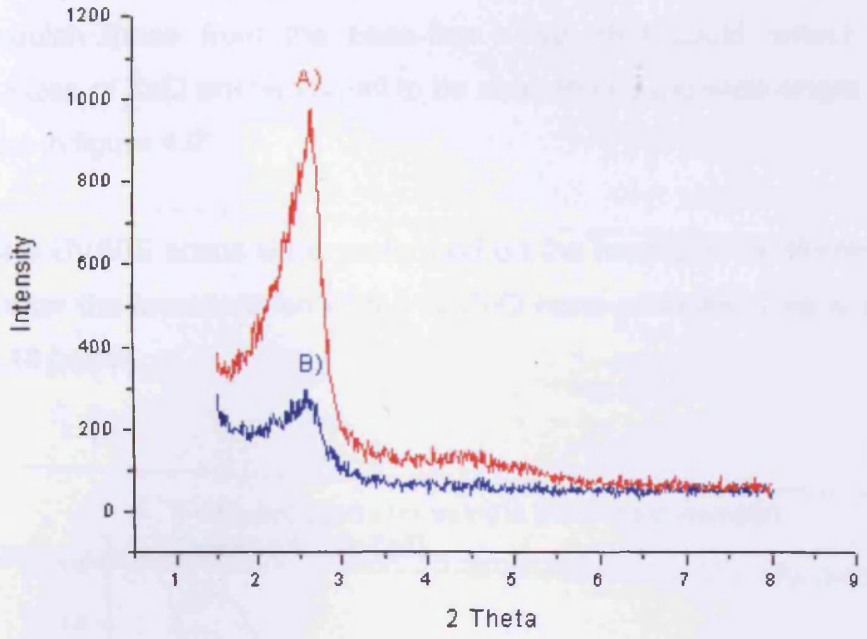

Figure 4.8 Low-angle XRD pattern of aluminosilicate (TLCT) sample before (A), and after (B) 5.3 % ZnO incorporation

Figure 4.8 indicates that there is a 70 % drop in intensity attributed to ZnO clustering within the pores of the aluminosilicate. No d spacing shift is observed indicating that no deformation of the structure occurred.

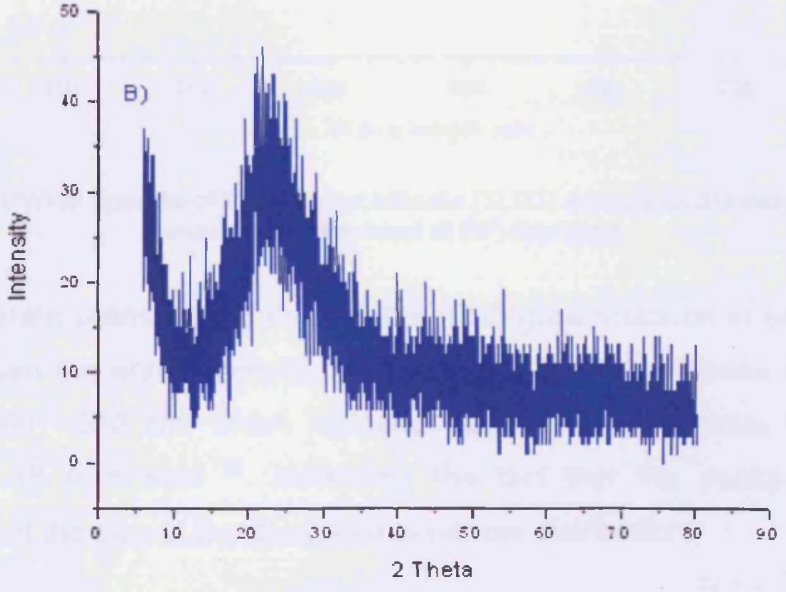

Figure 4.9 Wide-angle XRD patterns of aluminosilicate (TLCT) sample after 5.3 %ZnO impregnation

The distinctive ZnO crystal planes are not easily determined since it is difficult to distinguish those from the base-line noise, that could reflect that the clusters sizes of ZnO are two small to be detected by the wide-angle XRD, as presented in figure 4.9.

Solid state UV/VIS scans were performed on the mesoporous aluminosilicate sample after the incorporation of 5.3 % ZnO nano-particles. This is shown in figure 4.10 below.

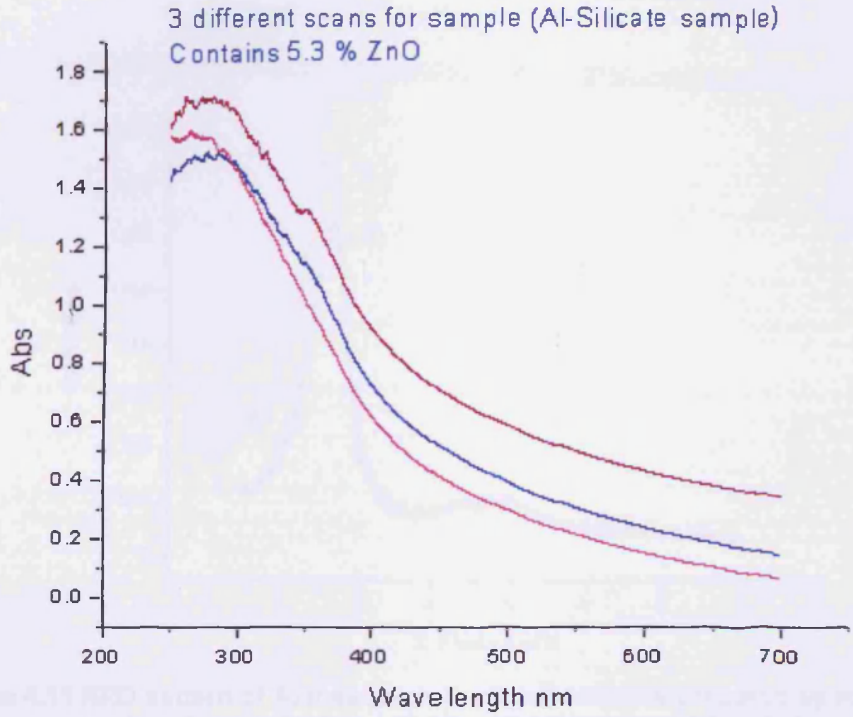

Figure 4.10 UV/VIS spectra of the aluminosilicate (TLCT) sample containing 5.3 % ZnO, scan was performed at 90° rotations

Three separate scans were carried out at 90-degree rotations to each other in order to scan the entire sample. In figure 4.10 the three peaks are located between 260 - 330 nm, which indicates that the ZnO particles formed are around 5 -18 Å in size [19]. Moreover, the fact that the peaks are sharp indicates that the size of the clusters has narrow distribution.

4.1.1.3.3 ZnO Clustering in Mesoporous Aluminosilicate Prepared by the Modified Precipitation Method

In the next stage of the investigation, ZnO clustering was examined in the mesoporous aluminosilicate structure when the host was prepared by the modified precipitating (ppt) method (alumina introduced **during** the synthesis). Figure 4.11 presents the low-angle XRD patterns of: A) mesoporous aluminosilicate prepared by modified precipitating method before impregnation and B) the same sample after impregnation of 5 % ZnO that was calcined for an extra 4 hours at 500 °C.

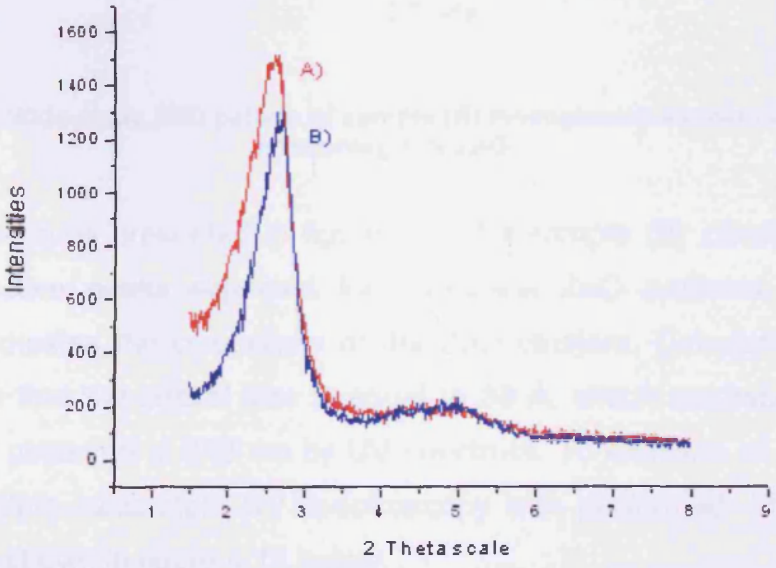

Figure 4.11 XRD pattern of A) mesoporous aluminosilicate prepared by modified precipitating method and B) after impregnation of 5 % ZnO

This sample lost 15 % of its main peak intensity as a result of impregnation with 5 % ZnO particles as presented by curve (B) in figure 4.11, which indicates that the ZnO particles are mainly within the mesopores of the host.

The wide-angle XRD pattern of sample (B) is presented below in figure 4.12; thus was done to obtain a better gauge of the formation of ZnO particles.

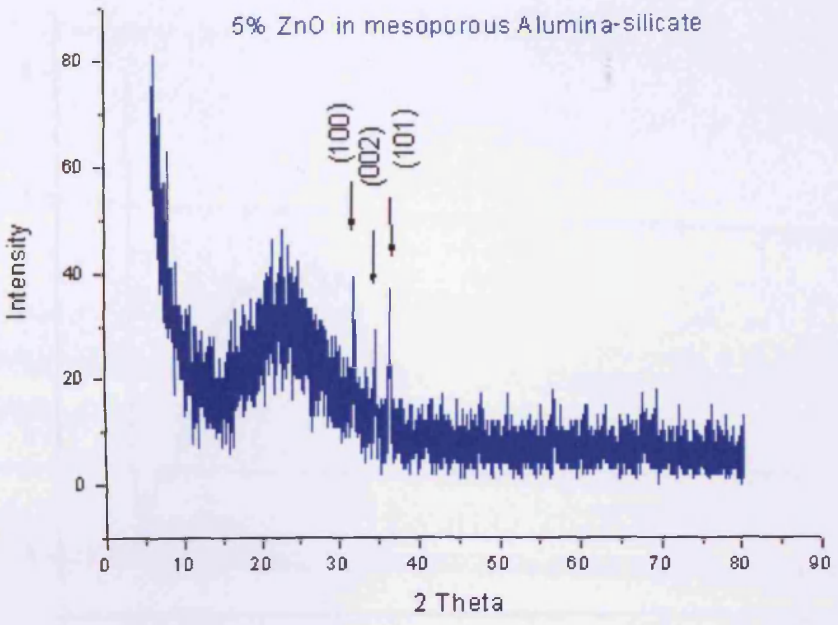

Figure 4.12 Wide-angle XRD pattern of sample (B) mesoporous aluminosilicate (ppt) containing 5 % ZnO

The XRD patterns presented in figure 4.12 for sample (B) clearly show the three distinctive peaks expected for crystalline ZnO particles; this result therefore indicates the crystallinity of the ZnO clusters. Calculation of (100) peak shows that the crystal size is equal to 38 Å, which corresponds to the largest size observed at 380 nm by UV spectrum. To examine all dimensions of ZnO clusters, solid-state UV spectroscopy was performed. The obtained spectrum is shown in figure 4.13 below.

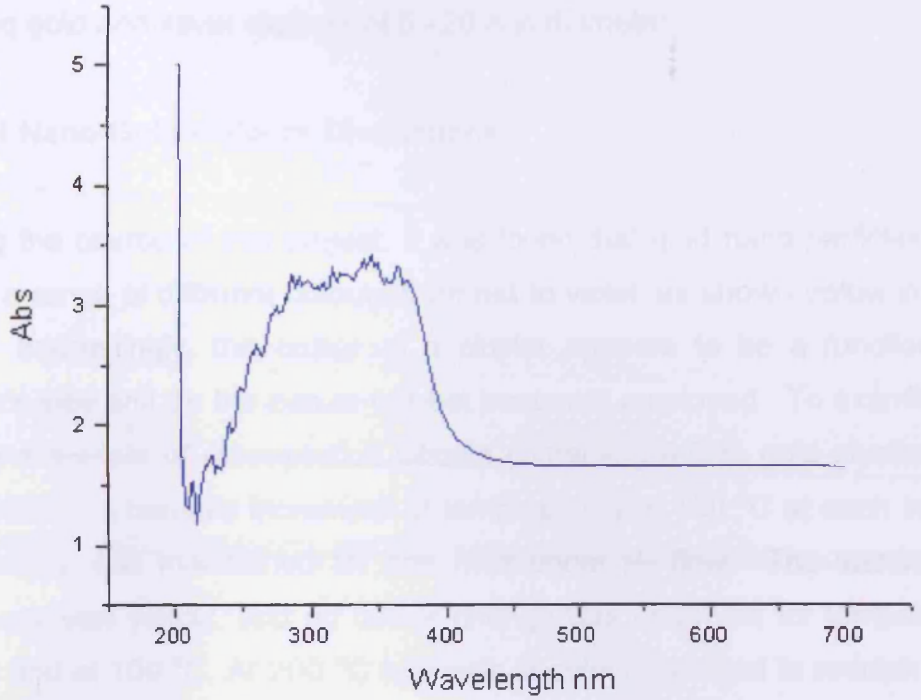

Figure 4.13 UV/VIS spectrum of sample (B) mesoporous aluminosilicate (ppt) containing 5 % ZnO

Figure 4.13 presents the UV/VIS spectra of the mesoporous aluminosilicate containing 5 % ZnO i.e. sample (B) and shows that a wide peak is observed in the range 250 - 380 nm. This result indicates that the ZnO aggregates of different sizes exist in this sample (see table 4.1); the 250 nm peak suggests that particle sizes of down to 10 Å are possible [19].

4.1.2 Introduction of Gold Clusters

There are few articles discussing introduction of gold and silver cluster into the pores of mesoporous materials [20-24]. These methods tend to involve ultrasonic irradiation of gold (or silver) precursors, chemical reduction methods, or hydrogen reduction under heat treatments. These methods however are not found effective and usually include soaking the mesoporous material in metal precursor solutions for two to three weeks [22, 24]. Also those methods result in the formation of large clusters between 100 - 500 Å in diameter[20-21]. Due to these reasons, in this section of this chapter, the details of a new intuitive method for the incorporation of gold and silver into porous

hosts are discussed. This technique, as will be highlighted, is capable of forming gold and silver clusters of 5 - 20 Å in diameter.

4.1.2.1 Nano-Gold Colours Distinctions

During the course of this project, it was found that gold nano-particles could adapt a range of different colours from red to violet, as shown below in figure 4.14. Interestingly, the colour of a cluster appears to be a function of a cluster's size and on the nature of heat treatment employed. To examine this further a sample of mesoporous silicate containing 0.5 % gold clusters was subjected to a periodic increment of temperatures of 100 °C at each interval, the sample was maintained for one hour under H_2 flow. The starting gold precursor was yellow, and no colour change was observed for temperatures below and at 100 °C. At 200 °C however, a colour changed to reddish black, was observed which changed to violet at 300 °C. At temperatures in the range of 300 to 700 °C no further colour change was observed. Interestingly, subjecting the sample to air rather than H_2, in the temperature range of 500 – 700 °C, turns the gold particles' colour to magenta. Furthermore, upon increasing the concentration of gold to 2 % wt host, the colour changes to red at 500 °C, as shown in figure 4.14.

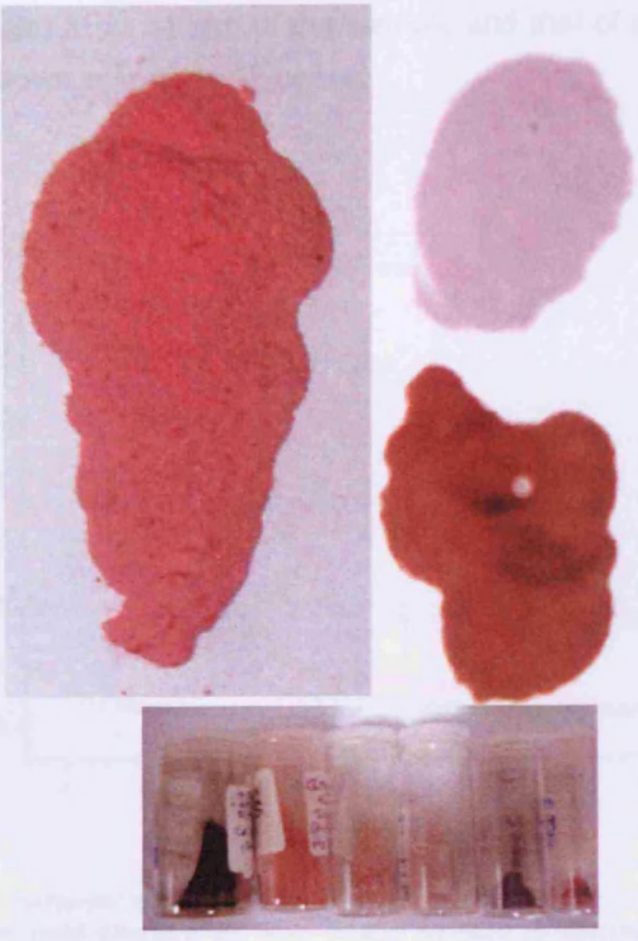

Figure 4.14 Different colours of the nano-gold clusters prepared

The aforementioned results can also be observed *via* UV spectroscopic techniques when violet has a wavelength in the range of 300 - 420 nm and red in the range of 620 - 740 nm (as listed in table 2.1, chapter 2); magenta can be described as a mix of the wavelengths blue and red in the visible spectrum. This will become more relevant in the next few sections.

4.1.2.2 Introducing Gold Clusters into Mesoporous Silicate

The initial step necessary to introduce gold clusters into porous hosts was performed by stirring mesoporous silicate in methanol / sodium tetrachloaurate (III) solution at room temperature for one hour. Following this, the sample was dried at 55 °C and then calcined under hydrogen gas at 500 °C for 30 minutes. Hydrogen was finally removed and the product kept under ambient air at 500 °C for 270 minutes. This sample denoted as sample (B).

The low-angle scan XRD pattern of this sample and that of pure mesoporous silicate host is shown in figure 4.15 below.

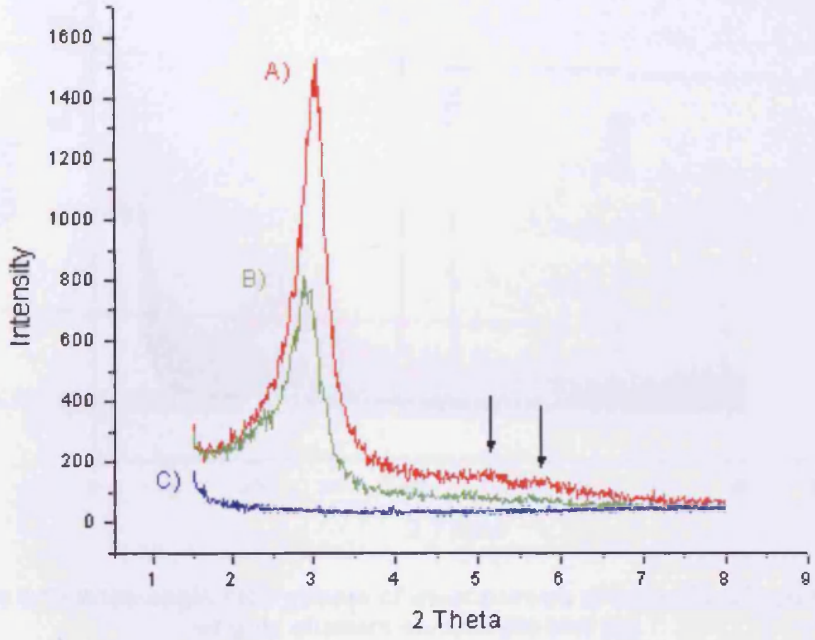

Figure 4.15 XRD patterns of mesoporous silicate (TLCT) A); mesoporous silicate containing 2 % wt gold clusters B); and finally sample B calcined 5 hrs at 600 °C without H_2 gas C)

Figure 4.15 shows that the intensity of the main peak decreases by 50 % with a slight d spacing shift towards lower angle, which indicates that gold clusters occupy 50 % of the total surface area of the mesoporous structure without causing deformation of the host structure. In another examination, portions of this sample (i.e. sample B) were calcined at 600 °C for additional five hours under ambient air referred to as sample (C). Sample (C) appears to have completely collapsed. This therefore indicates that H_2 gas is essential not only to reduce the gold precursor but also to stop the diffusion of gold clusters during heat treatments.

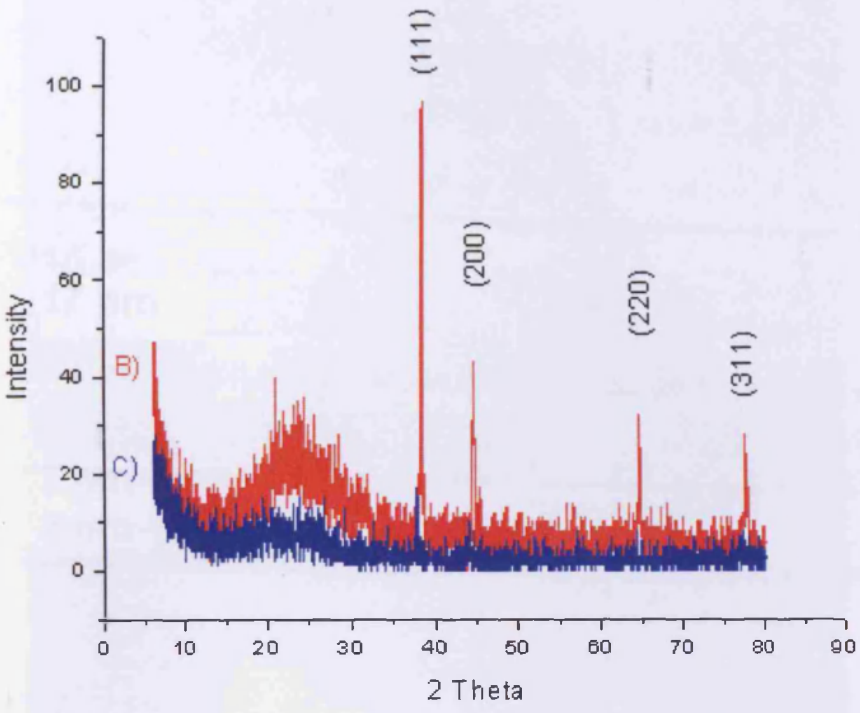

Figure 4.16 Wide-angle XRD patters of mesoporous silicate (TLCT) containing 2 % wt gold clusters sample (B) and (C)

To gauge the characteristics of the gold nanoparticles for samples (B) and (C), wide-angle XRD scans were performed. These are shown in figure 4.16 and indicate that sample (B) has sharper peaks representing crystallographic planes, than that of sample C. This shows that gold clusters in sample B are more uniform than in C.

To check the distribution of the gold clusters inside the host pores, Transmission Electron Microscopy (TEM) imaging technique were employed at low KV. The TEM of sample B shows a good distribution of gold clusters ranging in diameter from 20 - 30 Å that are spreading all around (figure 4.17). There is also an isolated large cluster of 170 Å in diameter that appear outside the pores, i.e. on the surface of the sample, it seems like covering three other 20 Å clusters underneath it (figure 4.17).

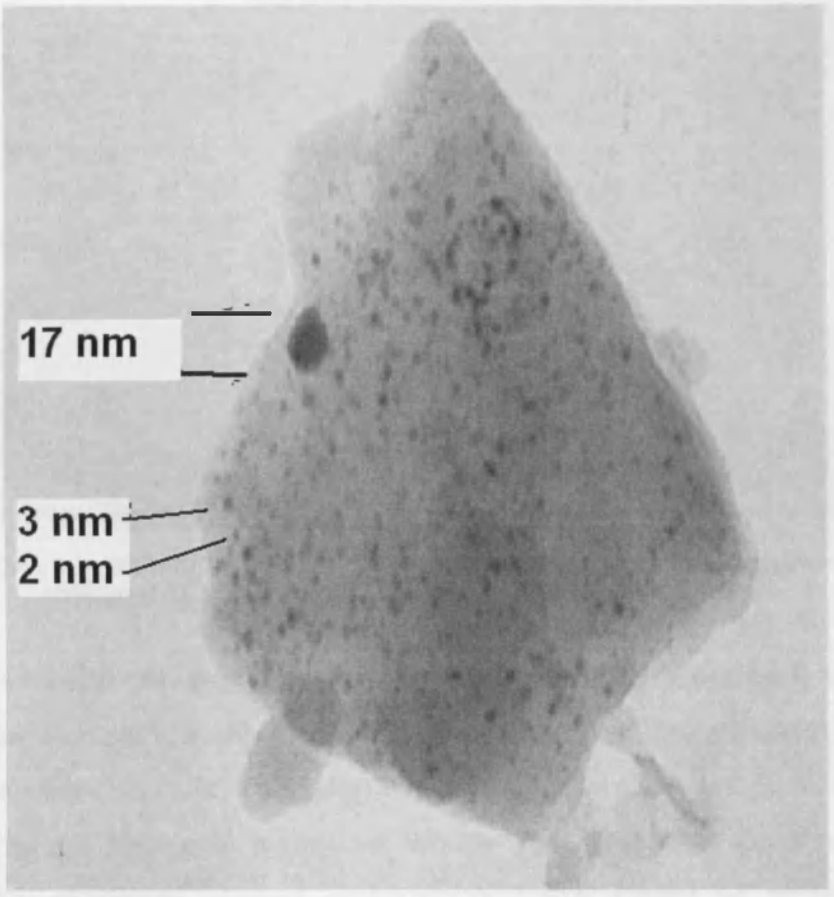

Figure 4.17 Low intensity TEM image of mesoporous silicate (TLCT) containing 2 % wt gold clusters, sample (B)

To maximise the information that could be gathered about the nature of gold particles within the porous silicate, high-resolution transmission electron microscopy (HRTEM) images were obtained. The (HRTEM) images, shown in figure 4.18 indicate that the pore channels (typical of hexagonal packing) extend throughout the sample, which confirms the long-range X-ray diffraction peaks, highlighted in figure 4.15. This indicates that impregnation did not affect the pore structure.

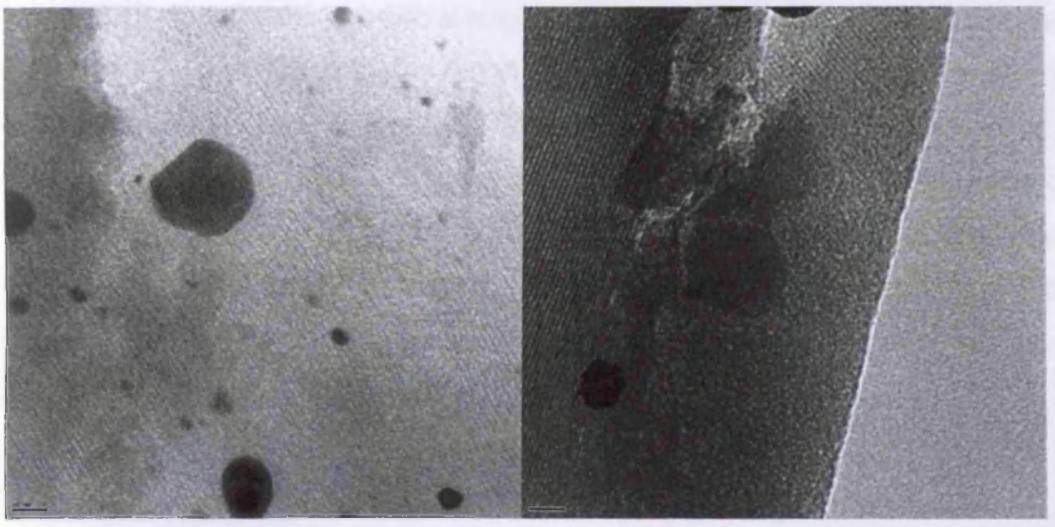

Figure 4.18 High-resolution TEM images showing the channels of the mesoporous silicate (TLCT) sample (B) containing 2 % wt gold clusters

In Figure 4.18 not only are the channels and large clusters clearly visible but also smaller clusters are only observed upon enlarging these images; they are found inside the channels. The large clusters appear on the outside surface of the mesoporous silicate in a manner where their presence does not disturb the channel structures. These large clusters that begin as small clusters outside the surface, are not avoidable during the synthesis. Also they are not easily removed by filtration or washing. They also have a tendency to aggregate and grow after heat treatments.

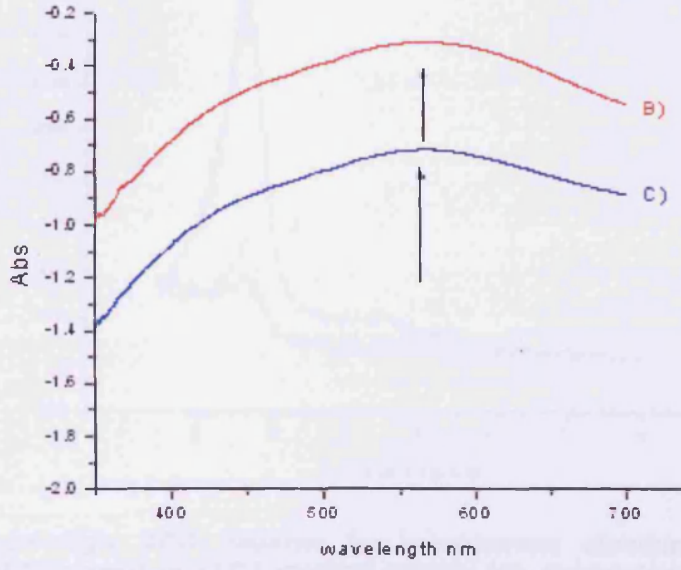

Figure 4.19 UV/VIS spectra for the mesoporous silicate (TLCT) containing 2 % wt gold clusters samples (B) and (C)

The UV/VIS spectra for the two samples (B, and C) were obtained as shown in figure 4.19. Both samples are red in colour and no significant difference can be observed between them by the UV/VIS spectra. And both samples have a maximum gold surface plasmon resonance peak at 570 nm as indicated by the arrows on figure 4.19. The difference in the absorbance is irrelevant because it is due the differences in the thickness of each sample. The broadness of the peaks indicates the existence of variety of cluster sizes in agreement with the HRTEM images.

4.1.2.3 Introducing Gold Clusters into Mesoporous Aluminosilicate

Here we adopted a similar strategy to examine gold clustering as was done in the previous section but this time, in an aluminosilicate host. Figure 4.20 presents the low-angle XRD patterns for three systems: 1) mesoporous aluminosilicate prepared employing **post** treatment of **TLCT** method (A), 2) 2 % wt/wt gold and calcined at 500 °C for one hour under H_2 and 4 hrs under ambient air (B), and 3) sample (B) calcined for additional 3 hours at 400 °C under ambient conditions (C).

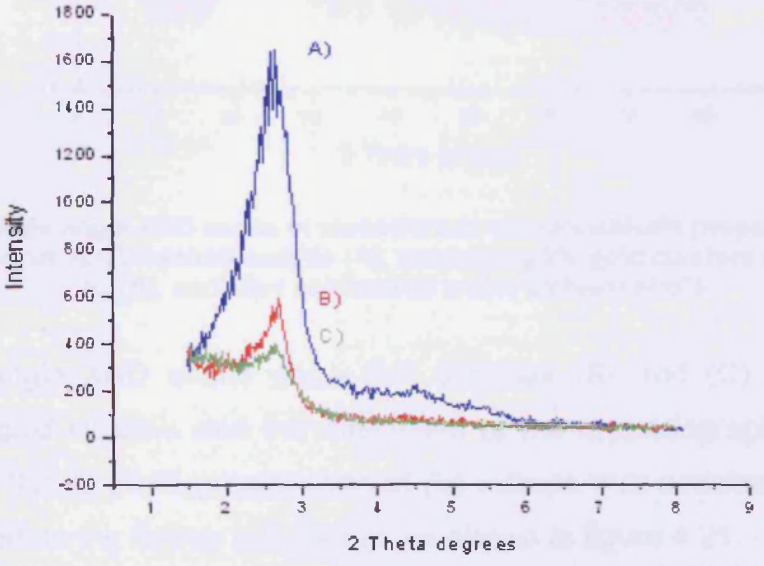

Figure 4.20 Low-angle XRD patterns for mesoporous aluminosilicate prepared employing post treatment of TLCT method sample (A), containing 2% gold clusters calcined under H_2 (B), and after calcination under ambient air (C)

Figure 4.20 shows that the XRD intensity of sample B drops by 60 % with respect to sample (A) and does not show any noticeable d spacing shift, indicating that gold clusters are occupying the pores of mesoporous aluminosilicate without causing deforming to the mesoporous structure. After further calcination of sample B, denoted C, an additional decrease in the peak intensity is observed. This is likely due to the nucleation of gold clusters inside the pores that eventually diffuse through the framework and grow to larger size, which destabilize the pores wall. The fact that no d spacing shift is observed for sample (B) and (C) indicates that they both share similar host framework morphology.

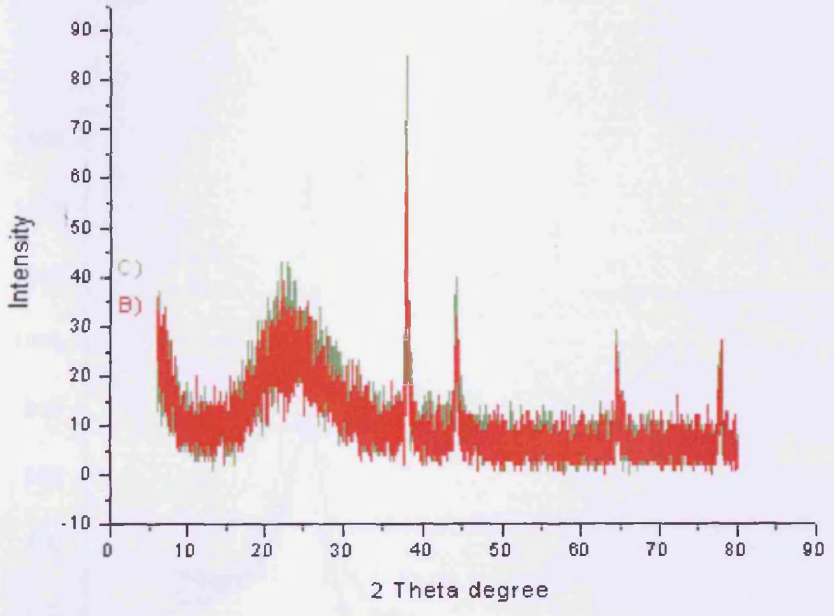

Figure 4.21 Wide-angle XRD scans of mesoporous aluminosilicate prepared employing post treatment of TLCT method sample (A), containing 2% gold clusters calcined under H_2 (B), and after calcination under ambient air(C)

The wide-angle XRD scans show that samples (B) and (C) both contain crystalline gold clusters and the intensities of the crystallographic planes of sample (C) that is 20 % greater than of (B) reflects that additional nucleation has occurred during further calcination, as shown in figure 4.21.

4.1.3 Introduction of Silver Clusters

4.1.3.1 Introducing Silver Clusters into Mesoporous Silicate

Here the impregnation of silver nano-particles into mesoporous silicate (TLCT) is examined using similar techniques to those stated previously. To compare the difference in the effects yielded from silver and gold nano-particle insertion into mesoporous silicate. A mesoporous silicate (TLCT), denoted (A) was divided into two portions: 1) 2 % wt/wt gold cluster were introduced to it, denoted (B) and 2) 2 % wt/wt silver clusters were introduced into it, called (C). These systems were examined by low-angle XRD techniques (see figure 4.22).

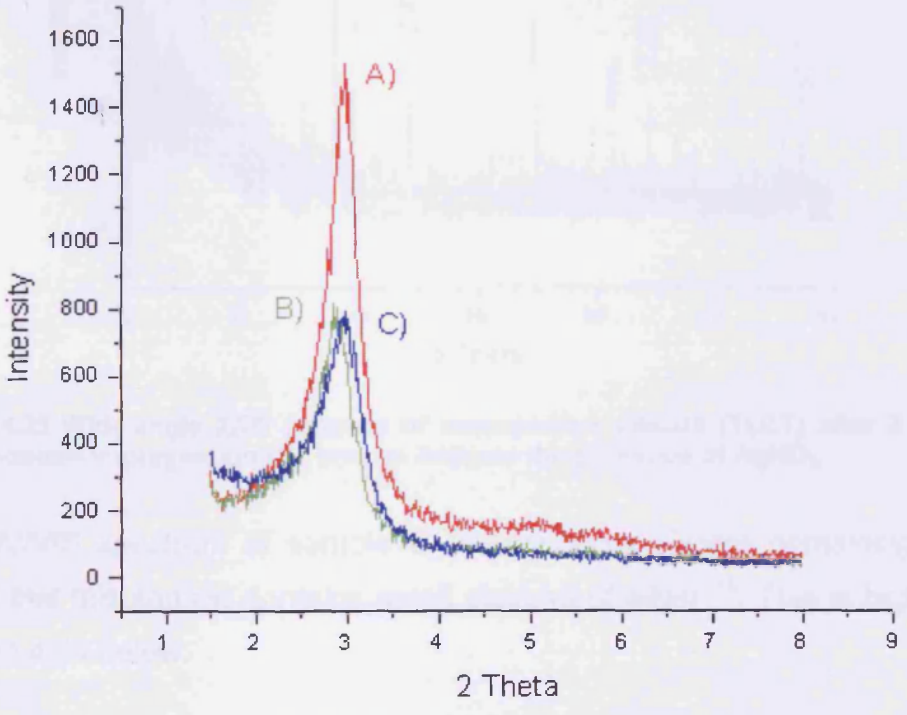

Figure 4.22 Low-angle XRD patterns of mesoporous silicate (TLCT) before impregnation (A); sample (A) after 2 % wt/wt gold clusters impregnation (B), and sample (A) after 2 % wt/wt silver clusters impregnation (C)

Figure 4.22 shows that the main peak intensity of mesoporous silicate containing silver clusters, is similar to that containing gold. Since no d spacing shift is observed, this provides reassurance that no structural deformation

occur upon silver or gold impregnation and that silver clusters occupy the host pores.

The wide-angle XRD patterns obtained confirm that clusters of crystalline silver are present as presented by the assigned planes, as well as to some residues of silver precursor[22] ($AgNO_3$) indicated by arrows in figure 4.23.

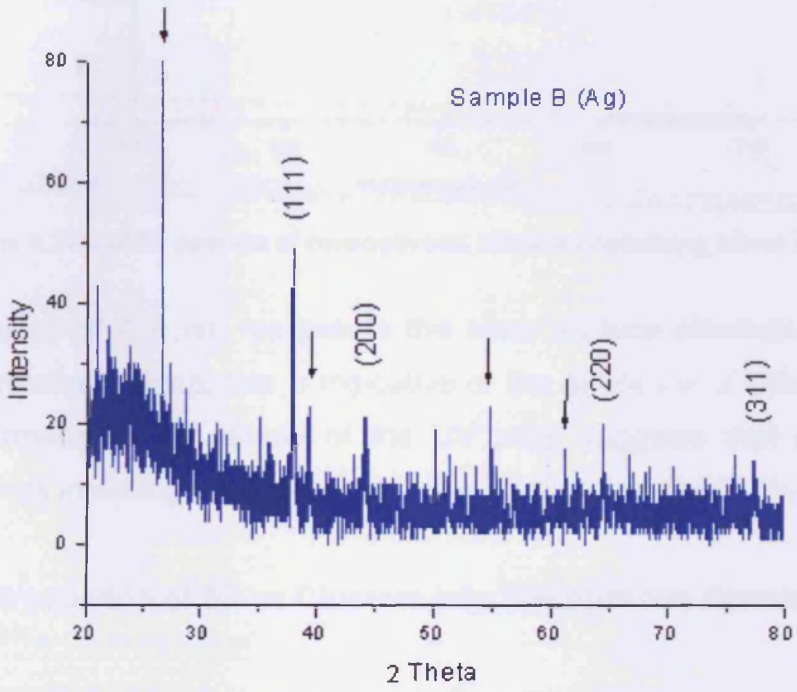

Figure 4.23 Wide-angle XRD patterns of mesoporous silicate (TLCT) after 2 % wt/wt silver clusters impregnation (C); arrows indicate the presence of $AgNO_3$

The UV/VIS spectrum of sample B (mesoporous silicate containing silver) shows that this sample contains small clusters of silver [23]. This is highlighted in figure 4.24 below.

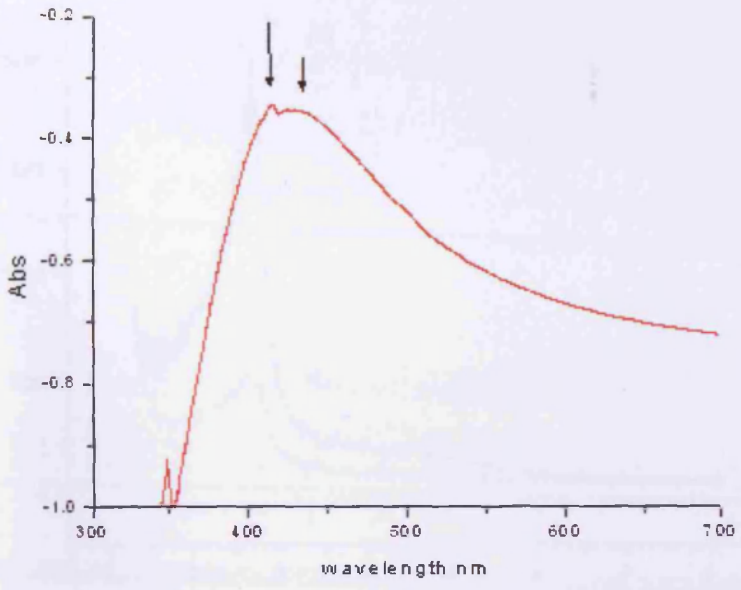

Figure 4.24 UV/VIS spectra of mesoporous silicate containing silver clusters

The UV peak at 400 nm represents the silver surface plasmon resonance, which is relatively sharp; this is indicative of the existence of different cluster sizes. Furthermore, the shape of the UV peak suggests that silver nano-particle sizes in mesoporous silicate have a narrow size distribution.

4.1.3.2 Introduction of Silver Clusters into Mesoporous Aluminosilicate

In a continuation of the incorporation of silver nano-particles into mesoporous aluminosilicate **post** treated **TLCT** method is examined. The techniques used here are analogous to those previously discussed. Figure 4.25 shows the low-angle XRD patterns of mesoporous aluminosilicate, sample (A) and after Ag clusters impregnation, sample (B).

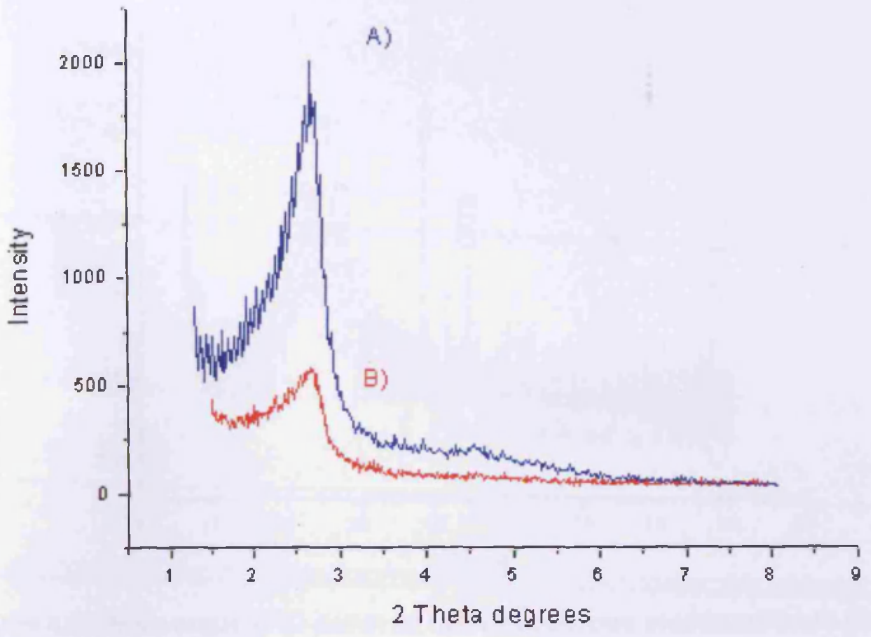

Figure 4.25 Low-angle XRD patterns of mesoporous aluminosilicate (TLCT), sample (A) and after Ag clusters impregnation into (sample A), called sample (B)

Figure 4.25 indicates clearly that the incorporation of silver particles reduces the intensity of the main peak, which indicates that the clusters are occupying the pores. Since there is no d spacing shift, this again, provides conclusive evidence that this method of metallic impregnation has no structural deformation.

The wide-angle XRD diffraction peaks of the crystalline planes, shown in figure 4.26, clearly indicate the distinct planes expected for crystalline silver. In addition no silver precursor peaks were observed.

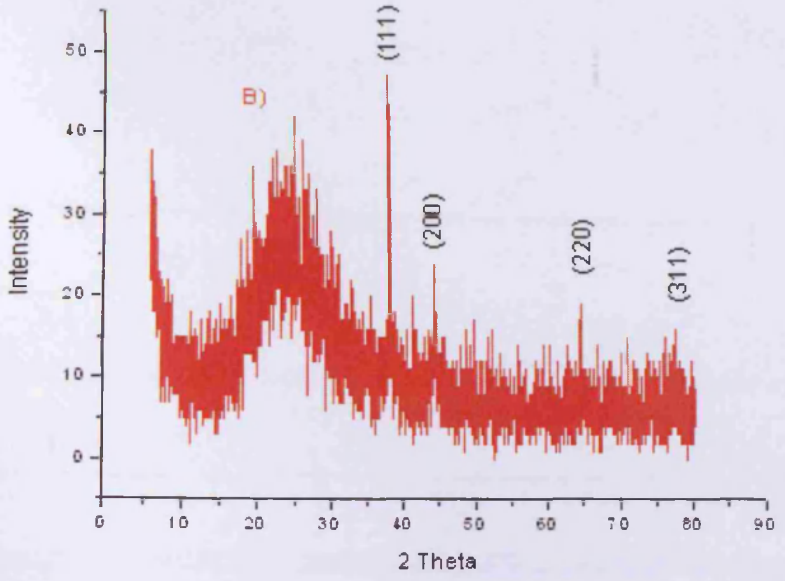

Figure 4.26 Wide-angle XRD patterns for mesoporous aluminosilicate (TLCT) containing 2% silver clusters, sample (B)

Low intensity TEM imaging also indicates the narrow size distribution of the silver clusters, in the range of approximately 3.3 nm; this supports the relatively sharp peak observed *via* the UV/VIS spectra. The TEM image is shown in figure 4.27 below.

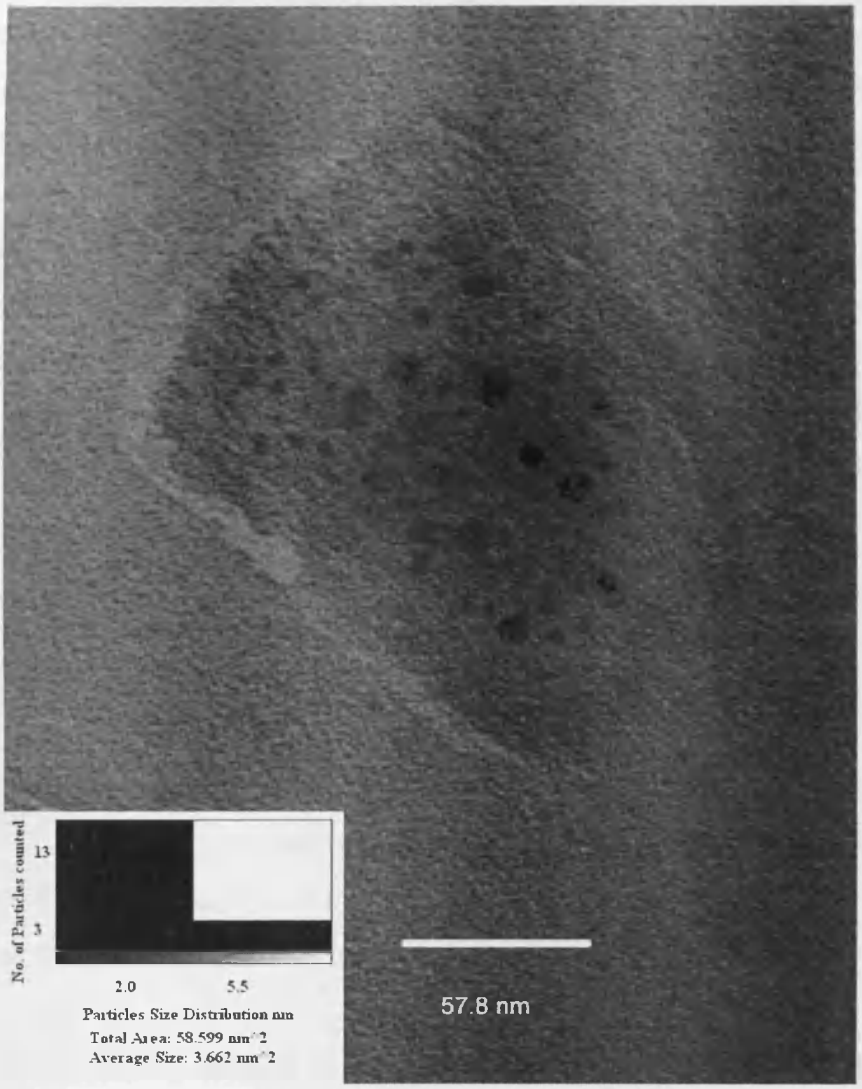

Figure 4.27 Low intensity TEM image of 2 % silver clusters in mesoporous aluminosilicate (TLCT) sample (B)

The low-resolution TEM image clearly indicates the good distribution of silver clusters in the host. Unfortunately however, it is not possible to determine whether the yielded clusters form within the pores from this image.

4.1.4 Optimising the Impregnation of Gold and Silver into Mesoporous Hosts

The work on gold and silver impregnation into mesoporous silicate and aluminosilicate has so far shown that using our novel methods it is possible to introduce gold and silver into their host's internal pores. The results presented

have shown that containing the clusters inside the pores restricts their growth during heat treatments *via* the "confinement effect". However unfortunately the work performed has also shown that some of the gold and silver cluster outside their host's pores. These clusters have been measured to have dimensions up to 170 Å and typically grow during the heat treatments. They are also hard to remove: filtration and washing have no detectable effects. In this part of the investigation, methods for minimizing the quantity of large clusters by lowering the concentration of gold and silver nanoparticles during the impregnation step, and by reducing the heat treatment temperatures, are described.

4.1.4.1 Optimising of Gold Impregnation into Mesoporous Hosts

Initially, gold clusters' incorporation into the pores of mesoporous materials were investigated for possible optimisation routes. The procedure adapted is similar to that described previously with the exception of the amount of gold 0.5 % wt/wt, of gold was used instead of 2.0 % and the calcining temperature was set at 300 °C for one hour under H_2 and three hours under static air.

The HRTEM imaging reveals that most of the gold clusters are formed inside the channels (pore packing). Their average sizes are below 20 Å, and the yielded clusters are well distributed in the sample, as shown in figure 4.28.

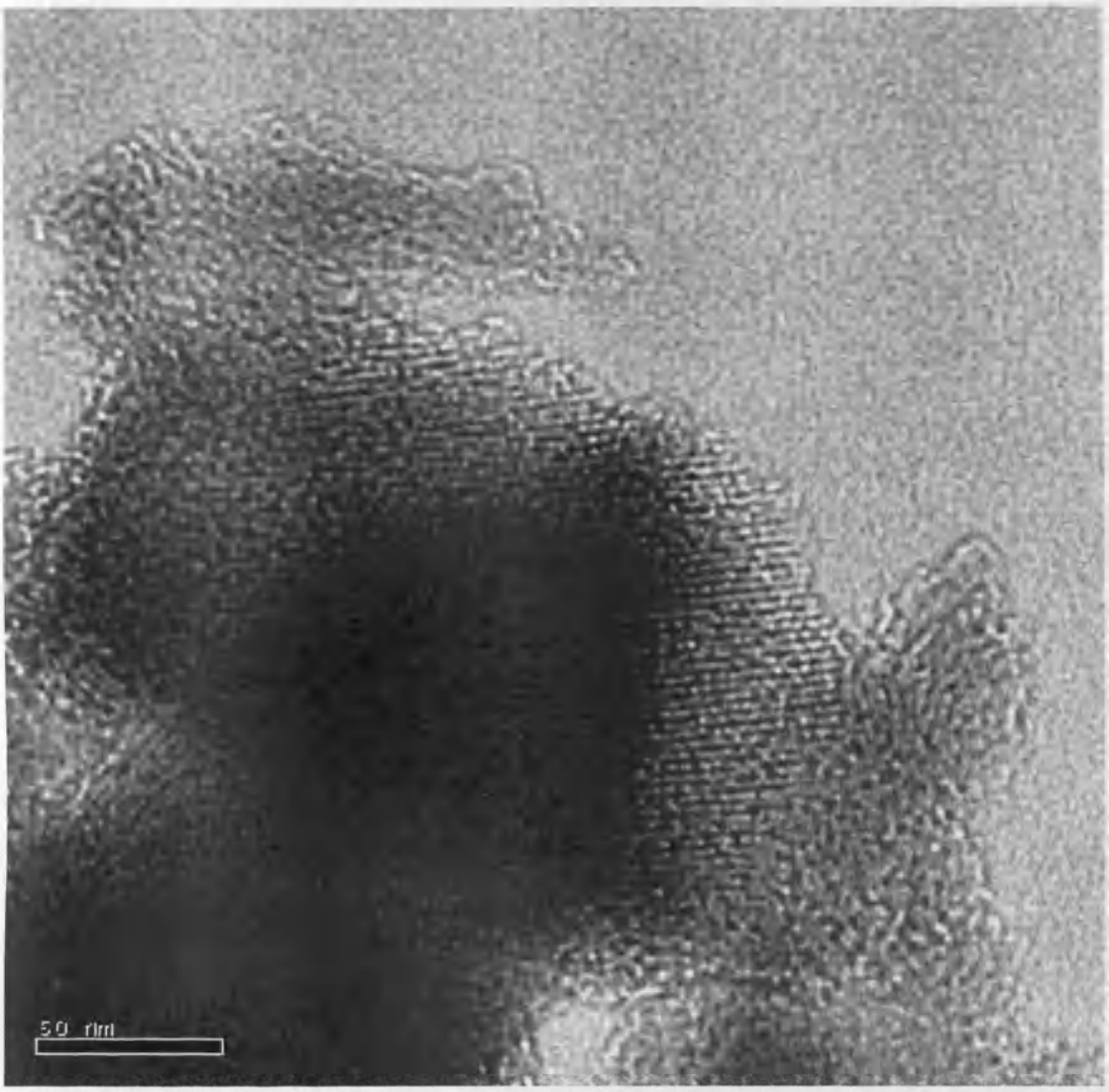

Figure 4.28 High-resolution TEM image showing gold clusters inside the channels of mesoporous silicate (TLCT) structure

The clusters's size distribution, which is shown in the inset in figure 4.29 below, shows that 50 % of the clusters have sizes of 6.0 Å, 40 % have sizes of 9.0 Å, 8 % have clusters sizes of 14 Å and only two clusters have sizes of 24 Å. In addition, since the channels are shown to extend across the sample (figure 4.28), as supported by the XRD analysis, the long-range order of the mesoporous host is therefore maintained after gold impregnation.

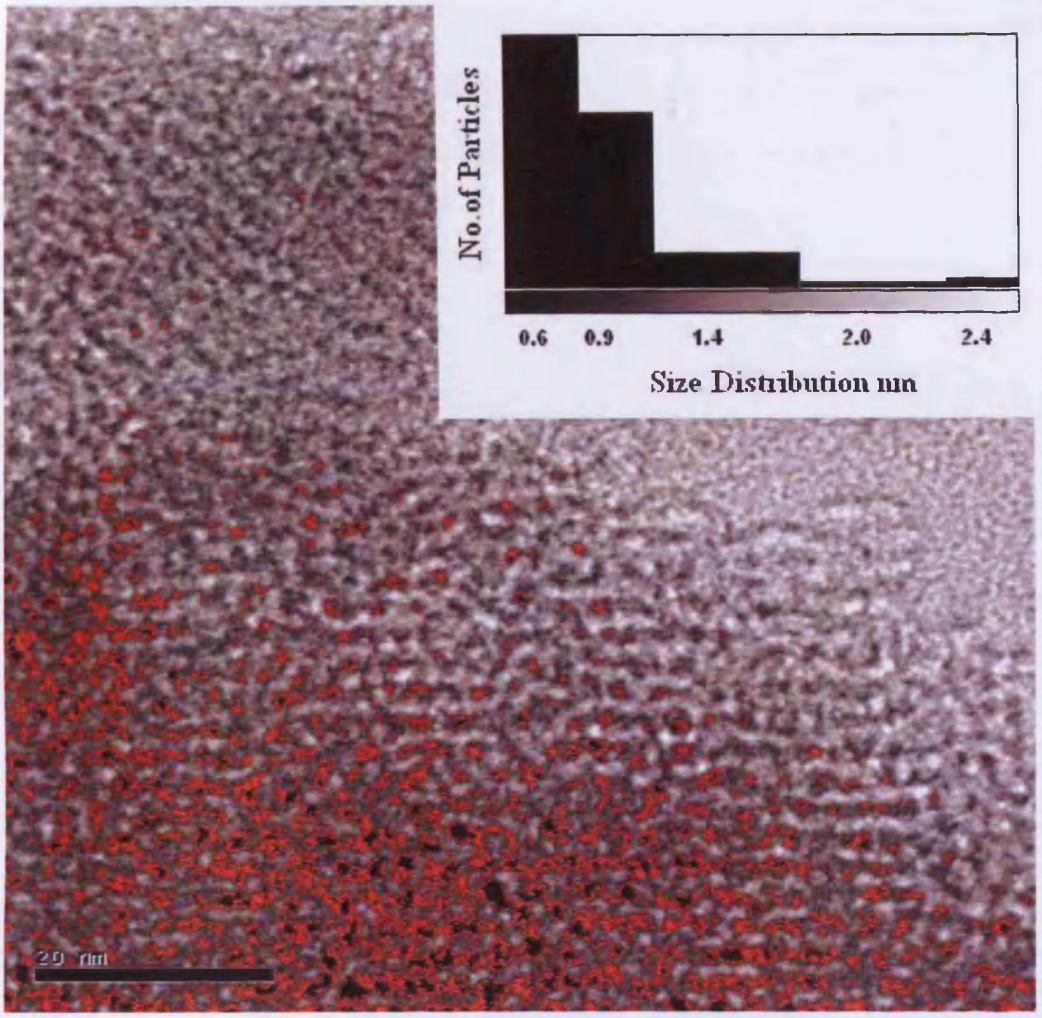

Figure 4.29 High-resolution TEM image of gold nano-particles inside mesoporous silicate host (TLCT). The red colour is an effect used by the ImageJ software to measure the particle sizes. The inset shows that there are only two clusters that are above 2 nm

The synthesised mesoporous silicate (TLCT) containing 0.5 % gold wt/wt adapted a magenta colour. To obtain more information, UV/VIS spectrum was performed. The UV/VIS spectrum, shown in figure 4.30, confirms that the size distribution of the gold particles at an impregnation level of 0.5 % wt/wt is narrow. Furthermore, the peak maximum shifts to 540 nm (Blue shift, rather than 570 nm discussed previously) this is indicative, and provides further evidence of the formation of smaller cluster sizes[24] at low gold incorporation levels.

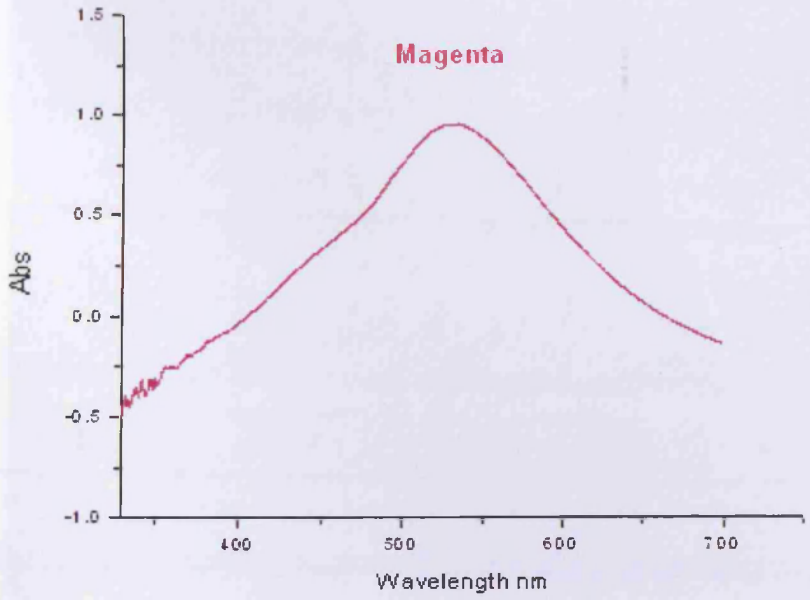

Figure 4.30 UV/VIS spectrum of mesoporous silicate (TLCT) impregnated with 0.5 %wt/wt gold particles

4.1.4.2 Optimising of Silver Impregnation into Mesoporous Hosts

In the next stage of the investigation, methods for maximising the impregnation of silver particles into mesoporous hosts, in particular mesoporous silicate was discussed. Initially the host material, including the silver precursor, were prepared in an analogous manner to that previously discussed; this time however, silver of 0.5 % wt/wt was introduced into the mesoporous host and the structure was calcined at 300 °C for one hour under H_2 and three hours under static air.

The high-resolution TEM image of mesoporous silicate (TLCT) containing 0.5 % wt/wt silver clusters is shown below in figure 4.31. The arrows highlight the silver clusters that exist within the pores channel system. Unfortunately it is not easy to show the clusters and the hexagonal pore packing of the channels in the same image as that shown in figure 4.28, because the channels require the electron beam to be out of focus whilst in order to observe the dense silver clusters, more precise focusing is required.

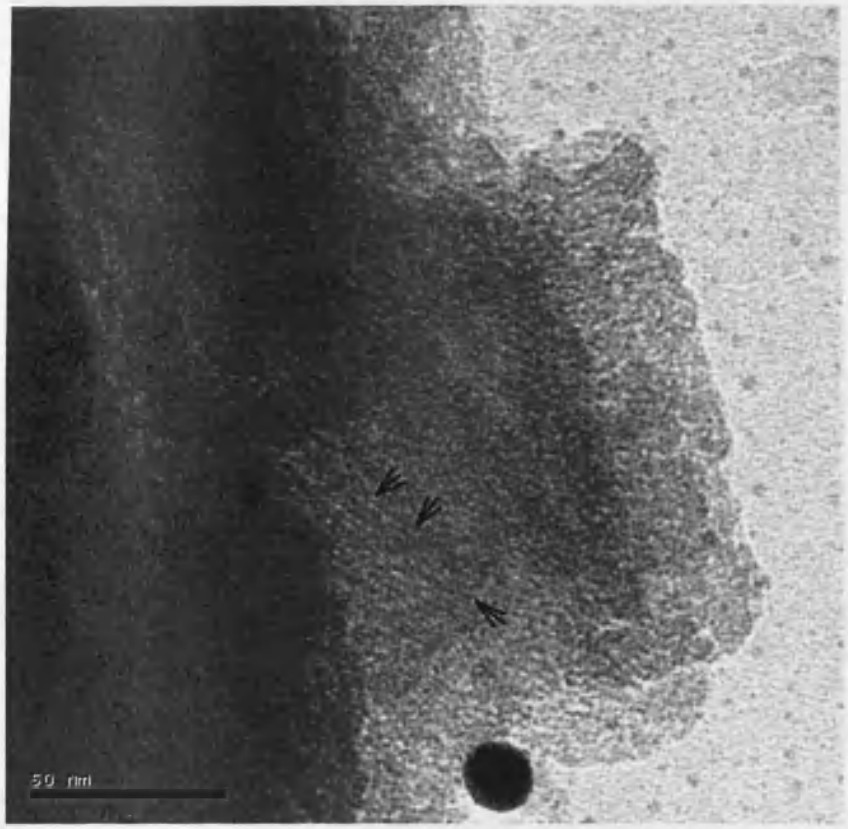

Figure 4.31 High-resolution TEM image of mesoporous silicate (TLCT) containing 0.5 % wt/wt silver clusters

The average sizes of the silver clusters in figure 4.31 are 10 Å, measured by the ImageJ software using the TEM scale bar. The sizes of the silver clusters are likely controlled due to the confinement effect of the pores of the mesoporous host. It should be noted however that, even at this low incorporation level of silver particles, a large cluster (with the dimensions of approximately 170 Å) is also detected. This cluster is however detached from the host's pores.

The sample showed a blue shift of the surface plasmon resonance of 400 nm to 340 nm (indicated by an arrow in figure 4.32), which indicates the formation of small silver clusters, as, has been confirmed by the TEM image shown above. In figure 4.32, the UV/VIS spectrum of the sample is shown, indicating a major peak at 340 nm that indexed to silver clusters ranging 0.6 - 0.8 nm and corresponding to Ag_8 - Ag_{20} respectively [23].

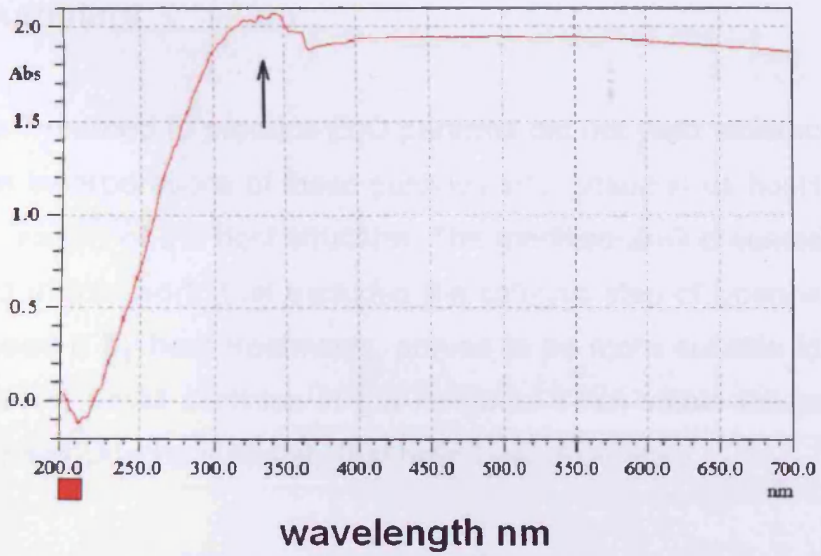

Figure 4.32 UV/VIS spectrum of mesoporous silicate (TLCT) containing 0.5 % wt/wt silver clusters highlighting the blue shift of silver surface plasmon resonance

4.2 In Summary

Spanhel's[18] method to produce ZnO particles did not yield satisfactory results during the incorporations of these particles into mesoporous hosts and led to a destabilisation of the host structure. The modified ZnO preparation method developed in this work, that excluded the catalytic step of Spanhel's method, and replaced it by heat treatments, proved to be more suitable for our work, and produced small particles in the range of 1 nm within the pores of the prepared mesoporous materials that have been examined.

A novel method was developed by us to introduce gold and silver clusters into mesoporous materials and is shown to be more economical since it decreases the impregnation time from three weeks to only 30 minutes and maintains the long-range order of the mesoporous structure, as confirmed by the HRTEM and XRD techniques. Furthermore impregnation was possible at a nano-scale level producing clusters with average sizes of 1 nm.

The final result obtained from this part of the work is the noticed relationship between the size of the gold particles incorporated within the mesoporous hosts and their colour. This work has shown that this phenomenon can be directly related to the characteristics of the heat treatment applied and the metal's concentration, which can shift the surface plasmon resonance peaks to the blue or red region.

4.3 References

1. N. S. Pesika, Z. Hu, K. J. Stebe, and P. C. Searson, *J. Phys. Chem. B*, 2002, **106**, 6985-6990.
2. Y. Usui, J. Noma, *J. Chem. Soc., Dalton Trans.*, 1999, 4397–4406.
3. E. O. Sako, H. Kondoh, *Chemical Physics Letters*, **413** (2005) 267–271.
4. D. V. Potapenko, J. M. Horn, Z. Song, M. G. White, *Surface Science*, **574** (2005) 244–258.
5. S. Xu, P. E. Laibinis, G. Liu, *J. Am. Chem. Soc.* 1998, *120,* 9356-9361.
6. D. M. Jaffey and R. J. Madix, *J. Am. Chem. SOC.* 1994,**116**, 3012-3019.
7. H. Wakita, Y. Tachibana, *Microporous and Mesoporous Materials*, **46**, 2001, 237-247.
8. K. Shimizu, N. Kobayashi, A. Satsuma, T. Kojima, and S. Satokawa, *J. Phys. Chem. B* 2006, **110**, 22570-22576.
9. E. Hosono, S. Fujihara, T. Kimura, and H. Imai, *Journal of Colloid and Interface Science*, 2004, **272**, 391-398.
10. Y. Li, W. Cai, G. Duan, B. Cao, F. Sun, F. Lu, *Journal of Colloid and Interface Science*, 2005, **287**, 634.639.
11. B. Cao, W. Cai, F. Sun, Y. Li, Y. Lei and L. Zhan, *Chem. Commun.*, 2004, 1604-5.
12. J. Hambrock, S. Rabe, K. Merz, A. Birkner, A. Wohlfart, R. A. Fischer, and M. Driess, *J. Mater. Chem.*, 2003, **13**, 1731–1736.
13. W. Zhang, J. Shi, L. Wang, and D. Yan, *Chem. Mater.*, 2000, **12**, 1408-1413.
14. H. Gies, S. Grabowski, M. Bandyopadhyay, W. Grunert, K.V. Klementiev, A. Birkner, *Microporous and Mesoporous Materials*, 2003, **60**, 31–42.
15. J. E. Readman, I. Gameson, J. A. Hriljac, P. P. Edwards and P. A. Anderson, *Chem. Commun.*, 2000, 595–596.
16. L. Khouchaf, M. H. Tuilier, M. Wark, *Micro. and Meso. Mater.*, 1998, **20**, 27-37.
17. S.E. Dapurkar, S.K. Badamali, P. Selvam., *Catalysis Today*, 2001, **68**, 63–68.
18. L. Spanhel, M.A. Anderson, *J. Am. Chem. Soc.*, 1991, **113**, 2826.
19. a) G. Ramakrishna and H. N. Ghosh, *Langmuir*, 2003, **19**, 3006-3012, and b) Noshir S. Pesika, Kathleen J. Stebe, and Peter C. Searson, *J. Phys. Chem. B* 2003, **107**, 10412-10415
20. C. Cao, X. Xiang, H. Zhu, *Journal of Crystal Growth*, **273** (2005) 375–380.
21. R. Glass, M. Moller, and J. P Spatz, *Nanotechnology*, **14** (2003) 1153–1160.
22. C. Weiping and Z. Lide, J. Phys., *Condens. Matter*, **9** (1997) 7257–7267.
23. V.S. Gurin, V.P. Petranovskii, M. A. Hernandez, N.E. Bogdanchikova, A. A. Alexeenko, *Materials Science and Engineering*, **A 391**, (2005) 71–76.
24. H. Shi, L. Zhang, W. Cai, *Materials Research Bulletin*, **35** (2000) 1689–1695.

Chapter 5

Sorption Reactions

This chapter starts by defining some of the accepted nomenclature used when discussing sorption before describing the procedures employed for sulphur-compound sorption analysis. The compounds included: thiophene, dibenzothiophene, dimethyl-dibenzothiophene, and dibenzosulfoxide. Furthermore we describe the methods used to characterise sulphur content and its fragments. We end this chapter with an overview of the success of porous frameworks to capture sulphur compounds.

Sorption Reactions

5.1 Definitions and Terminologies

5.1.1 Absorption

Absorption is the uptake of gas by a liquid or a solid, or a liquid by a solid in which the absorbed molecules permeate the substrate.

5.1.2 Adsorption

The adsorption process is the attachment of a particle to a surface, which is opposite to the desorption process. The substance that has been adsorbed on a surface is called an 'adsorbate' and the substrate that adsorbs it is called an 'adsorbent'. There are two types of adsorption processes: physisorption and chemisorption. [1]

'Physisorption', an abbreviation of physical adsorption, is when molecules or atoms can attach themselves to the surface by 'van der Waals' interaction; Van der Waals interactions are week attractions. The energy released during physisorption is in the same order of magnitude as the enthalpy of condensation, typically ranges *ca* 20 kJ mol^{-1}. The molecule will be bouncing across the surface until this small energy is lost in the form of vibration of the lattice or dissipated by thermal motion, then the molecule is adsorbed (accommodation). This small energy is insufficient to break the molecule's bonds. Therefore the molecule is intact but may be distorted by the surface species. [1]

'Chemisorption', an abbreviation of chemical adsorption, is when an atom sticks to the surface by forming a chemical bond, usually covalent and finds a site that maximizes its coordination number with the substrate. The enthalpy of chemisorption is much greater than physisorpton and typically ranges above 200 kJ mol^{-1}. The distance between the atom and the substrate is

shorter than in physiosorption. The adsorbed atom may be desorbed by the presence of other atoms on the surface or at the demand of the unsatisfied valences of the substrate atoms, this property is mostly used in catalytic reactions.[1]

5.1.3 Sorption

'Sorption' is a term used for adsorption and absorption processes because experimentally these two cannot be distinguished.[2]

5.2 Adsorption Procedure

We designed an adsorption reaction to remove specific sulphur compounds using the prepared mesoporous materials under controlled conditions. 50 mg of the prepared mesoporous materials were used as adsorbents. These adsorbents were soaked in 3.0 ml of prepared standard sulphur solution for at least 3 hours. Then three 0.2 µl is drawn from the standard solution above the soaked material and injected into the sulphur gas chromatography (GC) analyser. The result of each injection appears as integrated area under a peak, converted to concentration. Results are taken out of the average three injections and by subtracting the average result from the average results of the original reading of the standard sulphur solution, which was injected to the GC prior to each test at least for three times. The soaking test was performed at three different temperatures, 0, 25, and 40 °C, for most sorption reactions; samples were kept sealed as practically as possible to avoid evaporation.

5.3 Sorption Tests

5.3.1 Thiophene Results

A 40 ppm standard solution of thiophene was prepared in 50 % volume / volume of n-hexane, and n- dodecane. Table 5.1 represents the results of the sorption tests; empty cells mean the test was not performed, or results were

above the standard integration peak. PPT and TLCT mean that the mesoporous materials were prepared by precipitating or by the true liquid crystal templating method respectively.

Table 5.1 Adsorption Results of Removing 40 ppm Thiophene

Samples	Amount removed (ppm) at 0.0 °C	Amount removed (ppm) at 25.0 °C	Amount removed (ppm) at 40.0 °C
Ref. Thiophene 40ppm	0.0	0.0	0.0
2.2%Au-in 2.5%Al-SiO_2 (TLCT)*		12.0	9.9
2.2%Au-SiO_2 (TLCT)	9.5	9.0	21.0
Commercial ZnO		2.4	
Our Synthetic ZnO		4.5	
6%ZnO in SiO_2 (TLCT)	4.3	3.6	
5%ZnO in SiO_2 (TLCT)		8.4	
3% ZnO in 2%Al-SiO_2 (PPT)		5.0	
SiO_2 (TLCT)		3.0	
2.5% Al-SiO_2 (TLCT)		4.6	
2% Al-SiO_2 (PPT)		4.5	
2.7% Ag in SiO_2 (TLCT)	8.2	6.4	28.0
2.7% Ag in 2.5%Al-SiO_2 (TLCT)	6.3	9.5	30.0
0.5% Ag in 2.5%Al-SiO_2 (TLCT)		9.0	20.0

* Al-SiO_2 represents mesoporous aluminosilicate, SiO_2 mesoporous silicate

5.3.1.1 Adsorption Tests Performed at Room Temperature

5.3.1.1.1 Materials Containing ZnO particles

Adsorption at room temperature (25 °C), of commercially available ZnO powder gave the worst results, by removing only 2.4 ppm of the prepared standard thiophene solution, then mesoporous silicate (TLCT) removing 3.0 ppm. However, the ZnO powder that was prepared by our developed method, removed 4.5 ppm, and mesoporous silicate (TLCT) containing 5.0 % by weight (wt) ZnO aggregates removed 8.4 ppm. Mesoporous material (PPT) composing of 2.0 % wt aluminosilicate removed 4.5 ppm; however after introducing 3.0 % ZnO into its pores, removed 5 ppm.

5.3.1.1.2 Materials Containing Gold Clusters

Mesoporous silicate containing 2.2 % wt gold clusters within its pores removed 9.0 ppm from thiophene standard. Whereas mesoporous material that consists of 2.2 % wt aluminosilicate and 2.5 wt % gold clusters removed 12.0 ppm of the thiophene.

5.3.1.1.3 Materials Containing Silver Clusters

Mesoporous silicate containing 2.7 % wt silver clusters adsorbed 6.4 ppm of thiophene, whereas the mesoporous structure consisting of 2.5 % wt aluminosilicate that contains 0.5 % wt silver clusters adsorbed 9.0 ppm, and mesoporous material consisting of 2.5 % wt aluminosilicate that contains 2.7 % wt silver clusters adsorbed 9.5 ppm.

Studying all the results presented previously, the mesoporous adsorbent consisting of 2.5 % wt aluminosilicate in the framework and containing 2.2 % wt gold clusters adsorbed the maximum amount of thiophene 12.0 ppm, which represents 30 % removal of the sulphur standard at room temperature.

5.3.1.2 Adsorption Performed at 0 °C

Mesoporous silicate that contains 6.0 % wt ZnO removed 4.3 ppm at 0 °C instead of 3.6 ppm at room temperature, and mesoporous silicate containing 2.2 % wt gold clusters removed 9.5 ppm instead of 9.0 ppm at room temperature. Similar trends were observed for mesoporous silicate containing 2.7 % wt silver clusters, which removed 8.2 ppm at 0 °C instead of 6.4 ppm at room temperature.

Thus, so far, mesoporous materials containing gold clusters adsorbed the most thiophene compound by removing 9.5 ppm, which represents 24 % removal of thiophene at 0 °C.

5.3.1.3 Adsorption Performed at 40 °C

Heating to 40 °C improved adsorption for most samples, mesoporous aluminosilicate containing 2.7 % wt silver clusters adsorbed the most amount of thiophene reaching 30 ppm, which represents 75 % removal of the standard thiophene solution, see table 5.1.

5.3.2 Dibenzothiophene Sorption Results

56 ppm of dibenzothiophene standard solution was prepared using 50 ml benzene, 25 ml n-dodecane, and 25 ml n-hexane. Table 5.2 shows the results of the adsorption tests; empty cells mean the test was not performed or results were above the standard integration peak.

Sorption tests were also performed on regenerated samples. The regeneration of the samples was performed by filtering under reduced pressure for the soaked sample then washed three times with fresh n-heptane, dried over night at 100 °C, then at 150 °C for an additional three hours.

Table 5.2 Dibenzothiophene Removal Results

Samples	Amount removed (ppm) at 0.0 °C	Amount removed (ppm) at 25.0 °C	Amount removed (ppm) at 40.0 °C
Ref. Dibenzothiophene (56 ppm)	0.0	0.0	0.0
2.2%Au-in 2.5%Al-SiO_2 (TLCT)*		10.6	
2.2% Au in SiO_2 (TLCT)		14.8	
0.5%Au-SiO_2 (TLCT)		6.5	
0.5%Au-SiO_2 (TLCT)		7.4	
SiO_2 (TLCT)		20.8	
5.4%ZnO in SiO_2 (TLCT)		6.8	
5.4%ZnO in2.5%Al-SiO_2 (TLCT)		16.6	
2.7% Ag in SiO_2 (TLCT)	16.0	13.1	15.0
0.5% Ag in 2.5%Al-SiO_2 (TLCT)		6.3	
0.5% Ag in SiO_2 (TLCT)		10.5	
Regenerated Samples			
0.5% Ag in 2.5%Al-SiO_2 (TLCT)		8.0	
2.7% Ag in SiO_2 (TLCT)		12.0	
5.4%ZnO in2.5%Al-SiO_2 (TLCT)		11.0	
5.4%ZnO in SiO_2 (TLCT)		4.0	
2.2% Au in SiO_2 (TLCT)		4.0	

* Al-SiO_2 represents mesoporous aluminosilicate, SiO_2 mesoporous silicate

5.3.2.1 Adsorption Tests Performed at Room Temperature

5.3.2.1.1 Mesoporous Material Containing ZnO Particles

Adsorption test results (table 5.2) show that mesoporous silicate containing 5.4 % wt ZnO particles adsorbed 6.8 ppm, however, the mesoporous material composed of 2.5 % wt aluminosilicate containing 5.4 % wt ZnO particles, removed 16.6 ppm, which is almost double the amount. The maximum amount of sulphur adsorption by these materials was 16.6 ppm, which represents 30 % sulphur removal of the original standard dibenzothiophene solution (56 ppm).

After regeneration of the sample that adsorbed 6.4 ppm of dibenzothiophene, its adsorption dropped to 4.0 ppm; that is a drop of 37 %. The regeneration of

the sample that adsorbed 16.6 ppm, caused its adsorption to decrease to 12.0 ppm, which represents a drop of 28 % of its original adsorption ability.

5.3.2.1.2 Mesoporous Material Containing Gold Clusters

Mesoporous silicate containing 0.5 % wt gold clusters adsorbed 7.0 ppm, whereas on increasing the gold percentage to 2.2 % wt, adsorption increased to 14.8 ppm. On the other hand mesoporous material composed of 2.5 % wt aluminosilicate containing 2.2 % wt gold clusters, removed 10.6 ppm. 14.8 ppm was the maximum removal of sulphur compound by mesoporous materials containing gold clusters, which is 26 % of the standard sulphur solution.

A solid state EDXS test was performed, to confirm adsorption of 14.8 ppm of dibenzothiophene reference (56 ppm) compound, on the mesoporous silicate that contained 2.2 % wt gold. It revealed that an average (of the three EDXS scans table 5.3 column 3) of 0.33 sulphur / silicate percentage was present in the sample, which is ten times larger than the calculated result from the adsorption tests (ppm converted to %wt). That could be interpreted as an instrument error (it cannot measure any element correctly if its contents are below 1 % wt) see table 5.3.

Table 5.3 EDXS Results of The Mesoporous Silicate Containing 2.2 % wt Gold Cluster That adsorbed 14.8 ppm of dibenzothiophene, then filtrated under reduced pressure

Element	Weight%	Atomic%
1st scan		
O K	58.02	70.86
Si K	41.10	28.60
S K	0.88	0.54
Totals	100.00	
2nd Scan		
O K	55.77	68.90
Si K	43.90	30.90
S K	0.33	0.20
Totals	100.00	
3rd Scan		
O K	56.31	69.38
Si K	43.28	30.37
S K	0.41	0.25

Figure 5.1 shows SEM images, of selected areas that had been analysed by the EDX beam and their corresponding peaks. Note that the EDX was performed to cover maximum areas, by zooming out as far as possible from the sample to get the total sulphur contents (the sulphur amount is too low to detect by selecting a small area). Furthermore, gold particles were not detected because the electron beam was far from the surface, and gold should be analysed directly at flat grains (surfaces) in short distances at higher magnifications (TEM images proved gold clusters existence in this sample, see chapter 4).

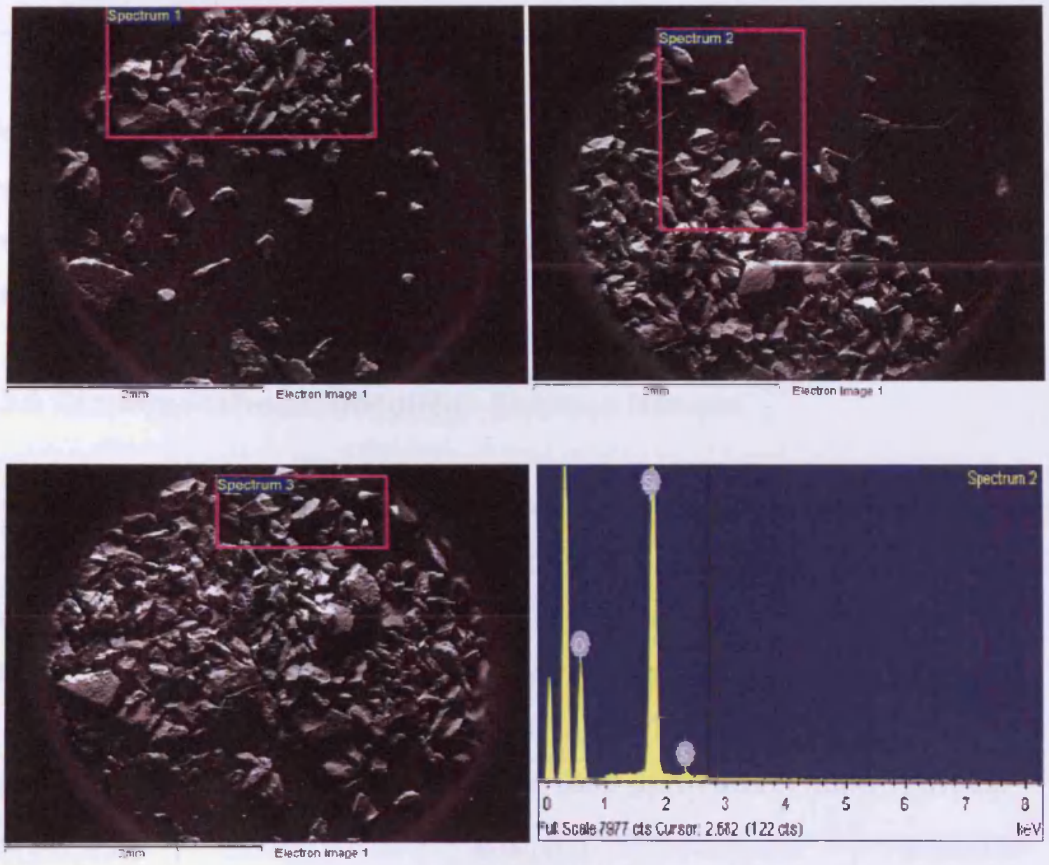

Figure 5.1 SEM images, of selected areas to detect sulphur atoms, and the corresponding EDX peaks

5.3.2.1.3 Mesoporous Material Containing Silver Clusters

Mesoporous material composed of 2.5 % wt aluminosilicate containing 0.5 % wt silver clusters adsorbed 6.3 ppm, and mesoporous silicate having a similar amount of silver removed 10.5 ppm. However, increasing the amount of silver to 2.7 % wt in mesoporous silicate increased adsorption to13.1 ppm that is 2.0 ppm above expectation. This sample was tested at 0 °C, where it adsorbed 16 ppm out of the dibenzothiophene standard and also tested at 40 °C, adsorbing 15 ppm. However after the regeneration of this sample it adsorbed 12 ppm. This result is very close to the results of the fresh sample, which removed 13 ppm (that indicate that regeneration decreased the ability of this sample to adsorb sulphur compound by *ca* 8 %). The maximum removal of sulphur compound by these materials was 16 ppm at 0 °C, which represents 28.5 % removal of the original sulphur concentration.

5.3.2.1.4 Mesoporous silicate

Mesoporous silicate adsorbed 20.8 ppm at room temperature, which represents 37 % removal out of total sulphur compound and surprisingly this sample proved to be the best sample to remove the dibenzothiophene compound.

5.3.3 Dimethyl-dibenzothiophene Sorption Results

A 300 ppm standard solution of 4,6-dimethyldibenzothiophene was prepared in 10 % volume n-dodecane and 90 % volume n-cyclohexane. Different preprepared mesoporous materials were soaked in this solution to study their adsorption-sorption properties; table 5.4 represents the sorption results.

Table 5.4 Dimethyl-dibenzothiophene (300 ppm) adsorption removal Results

Samples	Amount of sulphur removed (ppm) at 0.0 °C	Amount of sulphur removed (ppm) at 25.0 °C	Amount of sulphur removed (ppm) at 40.0 °C
4,6-dimethyl dibenzothiophene 300 (ppm) reference solution	0.0	0.0	0.0
2.2%Au-in 2.5%Al-SiO_2 (TLCT)*			148
0.5%Au-SiO_2 (TLCT)	161		
Fumed silicate		80.3	
SiO_2 (TLCT)	158.0	91.0	169.5
5.4%ZnO in SiO_2 (TLCT)	137		120
5.0%ZnO in SiO_2 (TLCT)	169		170
3.0%ZnO in2.0%Al-SiO_2 (ppt)	170	29	150
2.7% Ag in 2.5%Al-SiO_2 (TLCT)	156	28	139
0.5% Ag in SiO_2 (TLCT)		63	40
2.0% Al-SiO_2 (ppt)	145	58	123
Regenerated Samples			
0.5% Ag in 2.5%Al-SiO_2 (TLCT)		68	
0.5% Au in SiO_2 (TLCT)			151
2.2% Au in 2.5%Al-SiO_2 (TLCT)			159

- Al-SiO_2 represents mesoporous aluminosilicate, SiO_2 mesoporous silicate

5.3.3.1 Mesoporous Silicate and Aluminosilicate

Adsorption performed at room temperature showed that fumed silicate adsorbed 80.3 ppm whereas mesoporous silicate prepared by our modified TLCT method removed 91 ppm. However, at 0 °C this mesoporous silicate adsorbed 158 ppm and at 40 °C removed 169.5 ppm. Mesoporous material that composed of 2.0 % wt aluminosilicate adsorbed 58 ppm at room temperature but removed 123 ppm at 40 °C and 145 ppm at 0 °C. Maximum adsorption observed was 57 % of total sulphur compound *via* mesoporous silicate prepared by modified TLCT method.

An EDXS test was performed, to confirm the adsorption of 169 ppm out of the 4,6-dimethyl-dibenzothiophene (300 ppm reference solution), on the mesoporous silicate sample. It revealed that an average of three EDXS scans (0.17, 0.17, 0.30) which is 0.21 atomic percent were present in the sample, which is ten times larger than the calculated result of the adsorption tests. That could be interpreted as an instrument error (the SEM/EDX instrument cannot measure the amount of any element correctly if it below 1 % wt) see table 5.5.

Table 5.5 EDXS results of The Mesoporous Silicate That adsorbed 169 ppm out of the 4,6-dimethyl-dibenzothiophene (300 ppm reference solution)

Element	Weight%	Atomic%
1st Scan		
O K	57.07	70.02
Si K	42.65	29.81
S K	0.27	0.17
2nd Scan		
O K	58.12	70.93
Si K	41.38	28.77
S K	0.49	0.30
3rd Scan		
O K	57.43	70.61
Si K	41.72	29.22
S L	0.85	0.17

Figure 5.2 shows the SEM images, of selected areas tested by the EDXS and their corresponding peaks. Note that the EDXS was performed at maximum area as far as possible from the sample to get the total sulphur present in that sample.

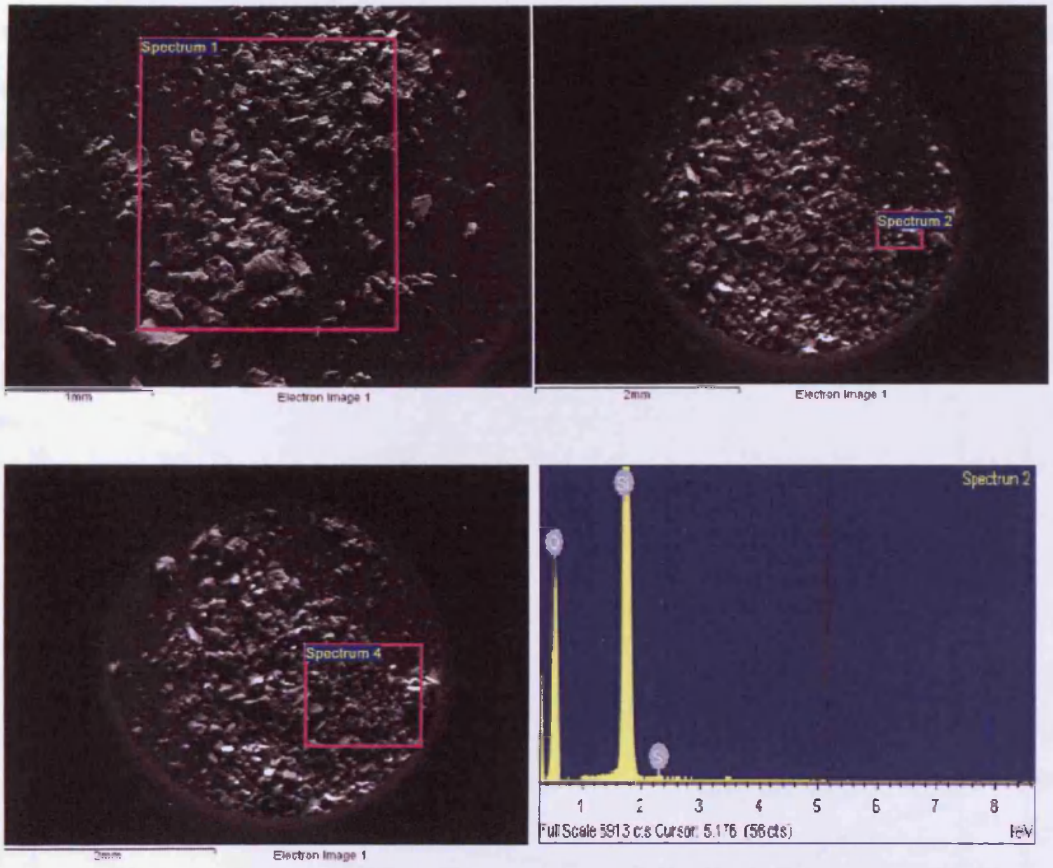

Figure 5.2 SEM images, of selected areas to detect sulphur, and the corresponding EDX peaks

5.3.3.2 Mesoporous Materials Containing ZnO Clusters

A TLCT mesoporous silicate containing 5 % wt ZnO clusters removed 170 ppm at 40 °C and 169 ppm at 0 °C out of the 4,6-dimethyl-dibenzothiophene (300 ppm reference solution). Whereas mesoporous material composed of 2.0 % wt aluminosilicate containing 3.0 % wt ZnO particles, prepared by precipitating method (PPT) adsorbed 150 ppm at 40 °C and 170 ppm at 0 °C. The maximum adsorption of sulphur compound was 170 ppm, which represents 57 % removal of total sulphur of the 4,6-dimethyl-dibenzothiophene 300 ppm reference solution.

5.3.3.2.1 TGA-MS Results

Mesoporous silicate that contains 5 % wt ZnO clusters prepared by the modified TLCT method that removed 169 ppm out of the 4,6-dimethyl-dibenzothiophene (300 ppm reference solution), was filtered under reduced pressure and dried at room temperature after finishing the adsorption test, then TGA/MS test was carried out on this sample, starting from room temperature to 300 °C at a heating rate of 10 °C min^{-1}. The TGA curve shows that this sample lost 40.2% of its mass at 124 °C (see figure 5.3) and continued to lose its mass gradually as a function of temperature.

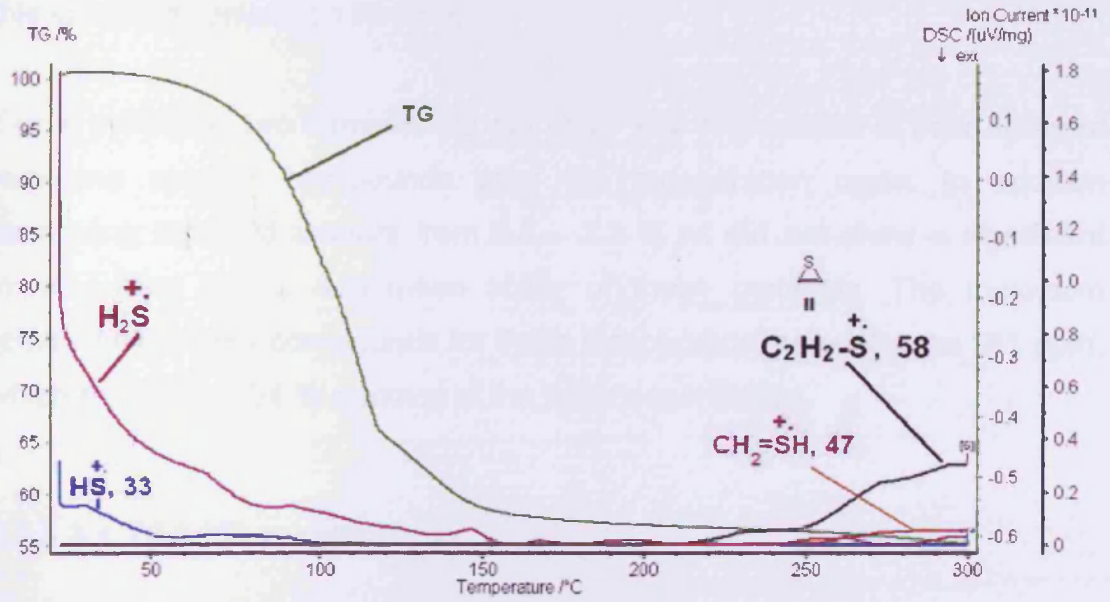

Figure 5.3 TGA-MS test on TLCT mesoporous silicate containing 5 % ZnO clusters that removed 169 ppm out of the 4,6-dimethyl-dibenzothiophene (300 ppm reference solution), and corresponding sulphur fragments of the adsorbate as a function of temperature

The sample was releasing H_2S, and HS positive radicals of charged masses of 34 and 33 respectively, during the heating cycle, at temperatures 30 °C – 150 °C. At this temperature range there was a substantial loss of these fragments; then they were produced at a constant rate at temperature range of 150 - 300 °C. On the other hand, fragments of charged mass 47 that represent CH_2 = SH positive radical started to appear at a temperature range of 250 °C – 300 °C and their production was increasing as a function of

temperature. Whereas fragment of charged mass equal to 58 units, representing a cyclic structure of C_2H_2S, started to appear at 200 °C and was increasing as a function of temperature.

5.3.3.3 Mesoporous Materials Containing Gold Clusters

A TLCT mesoporous silicate containing 0.5 % gold clusters adsorbed 161 ppm of the 300 ppm standard solution of 4,6-dimethylbenzothiophene at 0 °C, and after the regeneration cycle it removed 151 ppm at 40 °C. However, TLCT mesoporous material composed of 2.5 % wt aluminosilicate containing 2.2 % wt gold clusters removed 148 ppm at 40 °C, and after a regeneration cycle of this sample it removed 159 ppm.

These particular two samples did not show any degradation in their ability of removing sulphur compounds after the regeneration cycle. In addition increasing the gold amount from 0.5 – 2.2 % wt did not show a significant improvement in the adsorption ability of these materials. The maximum removal of sulphur compounds for these mesoporous materials was 161 ppm, which represents 54 % removal of the total concentration.

5.3.3.3.1 TGA/MS results

Mesoporous silicate, which contains 0.5 % gold clusters adsorbed 161 ppm out of the 4,6-dimethyl-dibenzothiophene (300 ppm reference solution) was filtered under reduced pressure and dried at room temperature. Then TGA/MS test was carried out on this sample starting from room temperature to 300 °C at a heating rate of 10 °C min^{-1}. This sample lost 43.6 % of it mass at 124 °C (see figure 5.4) and continued to lose its mass gradually as a function of temperature.

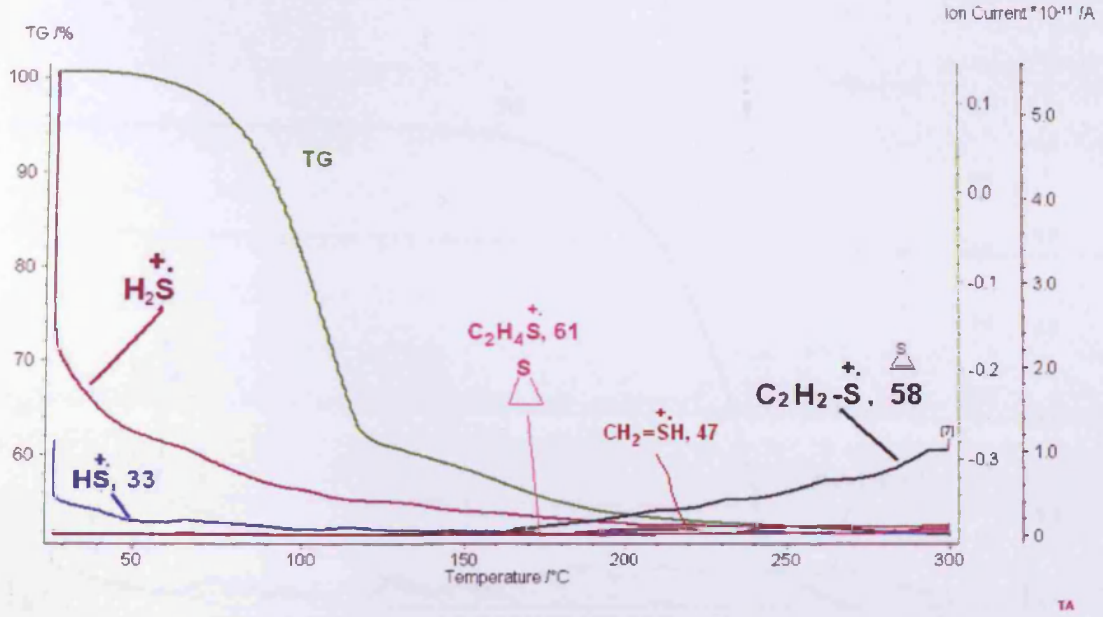

Figure 5.4 TGA/MS test on mesoporous silicate containing 0.5 % gold clusters that adsorbed 161 ppm out of the 4,6-dimethyl-dibenzothiophene (300 ppm reference solution), and the corresponding sulphur fragments as a function of temperature

This sample was releasing H_2S, and HS positive radicals fragments of masses 34 and 33 respectively during the heating step of the mesoporous sample. At temperatures 30 °C – 150 °C there was a substantial loss of these fragments, then they were produced at a constant rate at temperature range of 150 - 300 °C. However, a fragment of charged mass 47 that represents CH_2=SH was observed at a temperature range of 180 °C – 300 °C. Whereas a fragment of charged mass equal to 58 units, representing a C_2H_2S cyclic structure, started to appear at 150 °C and was increasing as a function of temperature. Moreover, a new fragment appeared in this sample possessing a charged mass of 61, representing a cyclic C_2H_4S compound. It's intensity was very small, which reflects its quantity, it was produced in a constant rate from the starting test temperature of 30 °C to the end at 300 °C.

A TGA/MS test was also performed under identical conditions for dry 4,6-dimethyl-dibenzothiophene solid compound (figure 5.5) to be used as a reference material to observe its behaviour under the test conditions. It reveals that the compound lost 93 % of its total mass at 247 °C and 100 % at 270 °C. Fewer sulphur fragments were observed such as HS, H_2S, and CH_2S that had similar behaviour of that desorbed from mesoporous material.

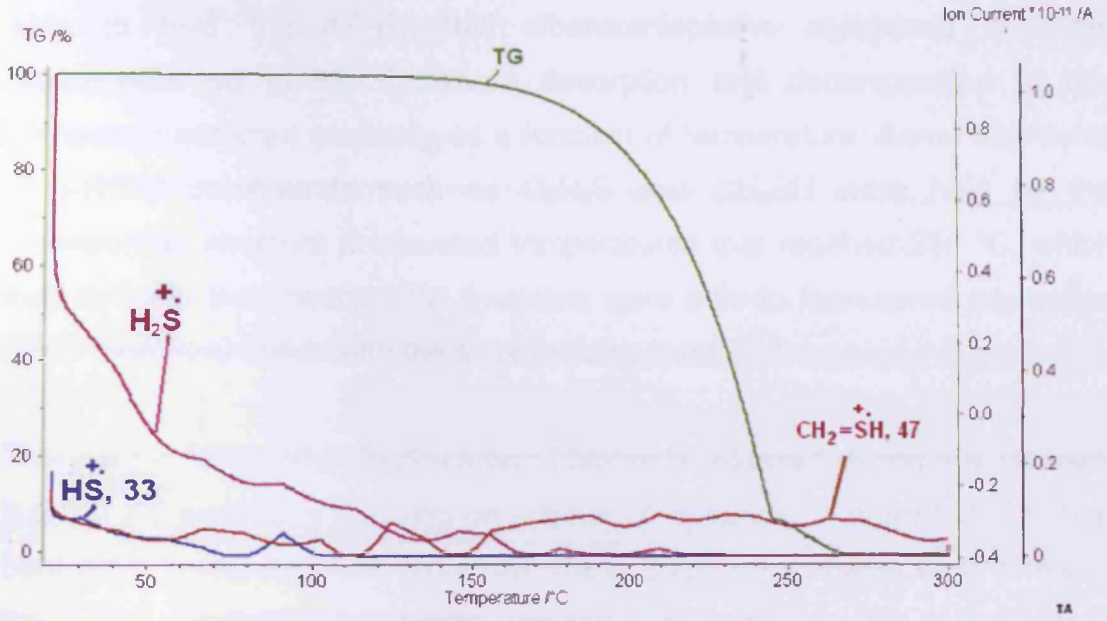

Figure 5.5 TGA/MS test for the dry reference (4,6-dimethyl-dibenzothiophene) compound, and its corresponding sulphur fragments as a function of temperature

A DSC curve, omitted from all TGA graphs for clarity purposes, showed that this compound had an endothermic process represented in a sharp peak (figure 5.6) at 155 °C, which could reflect expansion caused by melting or evaporation of this compound associated with fast mass loss. Another less intense peak appeared at 250 °C, which represents the second endothermic process before the second decrease of the compound's mass percentage.

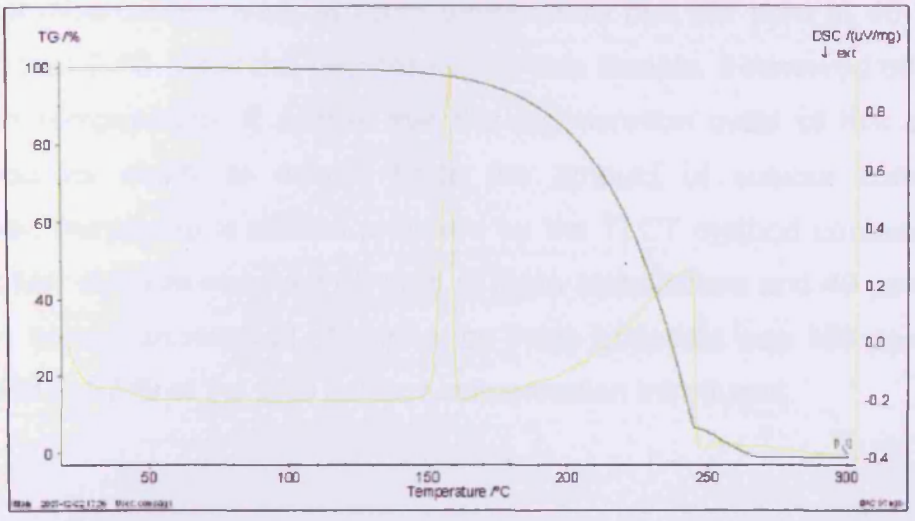

Figure 5.6 DAC/TGA curves for 4,6-dimethyl dibenzothiophene solid compound

After analysing TGA/MS results we found that mesoporous materials were able to hold the 4,6-dimethyl dibenzothiophene compound at room temperature up to 85 °C, where desorption and decomposition of this compound occurred gradually as a function of temperature. Some fragments of sulphur compounds such as C_2H_2S and CH_2SH were held by the mesoporous structure at elevated temperatures that reached 250 °C, which may indicate that mesoporous materials were able to form some interaction (chemisorption) bonds with the sulphur compound.

There were many other hydrocarbon fragments released during the TGA/MS test but we were only focusing on sulphur compounds, in order to track their behaviour during this test. Moreover, these sulphur fragments were a few of the most probable fragments predicted by us for the 4,6-dimethyl-dibenzothiophene adsorbate, some of the predicted sulphur fragments were not observed during the TGA-MS test such as methyl-benzothiophene and dimethyl-benzothiophene having charged masses of 124 and 136 respectively.

5.3.3.4 Mesoporous Materials Containing Silver Clusters

The TLCT prepared mesoporous material composed of 2.5 % wt aluminosilicate containing 2.7 % wt silver clusters adsorbed 28 ppm of 4,6-dimethyl dibenzothiophene at room temperature but 139 ppm at 40 °C and 156 ppm at 0 °C. After the regeneration of this sample, it removed 68.3 ppm at room temperature. It seems that the regeneration cycle of this sample; improved its ability to adsorb twice the amount of sulphur compound. However, mesoporous silicate prepared by the TLCT method containing 0.5 % wt silver clusters removed 63 ppm at room temperature and 40 ppm at 40 °C. The maximum removal of sulphur by these materials was 156 ppm at 40 °C, which is 52 % of the total sulphur concentration introduced.

5.3.4 Dibenzosulfoxide

A concentration of 2100 ppm of dibenzosulfoxide solution was prepared, using 50 % volume (v / v) isopropanol and acetonitrile to be employed as adsorbate medium and by soaking various mesoporous materials in it at room temperature. Table 5.6 shows the sorption results.

Table 5.6 Dibenzosulfoxide Sorption Results

Samples	Amount of sulphur compound removed (ppm) at 25 °C
Dibenzosulfoxide 2100 ppm reference solution	0
2.2%Au-in SiO_2 (TLCT)*	1867
SiO_2 (TLCT)	1841
5.4%ZnO in SiO_2 (TLCT)	1891
5.4%ZnOin 2.5%Al-SiO_2 (TLCT)	1725
3.0%ZnO in2.0%Al-SiO_2 (ppt)	1793
0.5% Ag in SiO_2 (TLCT)	1870
2.0% Al-SiO_2 (ppt)	1911

*** Al-SiO_2 represents mesoporous aluminosilicate, SiO_2 mesoporous silicate**

5.3.4.1 Sorption Test Results

5.3.4.1.1 Mesoporous Silicate and Aluminosilicate

Mesoporous silicate prepared by the TLCT method adsorbed 1841 ppm of dibenzosulfoxide whereas mesoporous material that composed of 2 % wt aluminosilicate prepared by the PPT method adsorbed 1911 ppm, which represents 91 % of total sulphur compound introduced.

5.3.4.1.2 Mesoporous Silicate and Aluminosilicate Containing ZnO Particles

Mesoporous silicate prepared by the TLCT method containing 5.4 % wt ZnO adsorbed 1891 ppm, and mesoporous material (TLCT) composed of 2.5% wt aluminosilicate that contained 5.4 % wt ZnO removed 1725 ppm. Mesoporous

2 % wt aluminosilicate (PPT) containing 3% wt ZnO adsorbed 1793 ppm. The maximum adsorption of sulphur compounds for these materials was equivalent to 90 % of the total sulphur introduced.

5.3.4.1.3 Mesoporous Silicate Containing Gold or Silver Clusters

Mesoporous silicate (TLCT) that contained 2.2 % wt gold clusters adsorbed 1867 ppm that represents 89 %, a similar percentage to that containing 0.5 % wt silver clusters, which removed 1870 ppm of sulphur compound.

An EDXS test was performed, to confirm adsorption of 1867 ppm of the 2100 ppm dibenzosulfoxide reference solution, by the mesoporous silicate (TLCT) that contained 2.2 % gold clusters. It revealed that an average of 1.5 atomic percent (table 5.7) was present in this sample, which was greater by one order of magnitude than the calculated result, out of adsorption tests, that could be related to the instrument limits (it cannot measure any element correctly below 1% wt) as shown in table 5.7. Figure 5.7 shows the SEM images, of the selected areas tested by the EDX and the corresponding peaks. Note that the EDX was performed as far as possible from the sample, to maximize the scanned area in order to detect the total sulphur (sulphur amount was too low to detect by scanning small areas). Furthermore, gold particles were not detected because the electron beam was far and gold clusters should be analysed directly at flat grains in short distances at higher magnifications (TEM images that reveal gold clusters of this sample are presented in chapter 4).

Table 5.7 EDXS results of 2.2 % gold sample that adsorbed 1867 ppm of dibenzosulfoxide reference solution

Element	Weight%	Atomic%
1st Scan		
O K	67.60	78.75
Si K	29.42	19.52
S K	2.98	1.73
2nd Scan		
O K	67.70	78.79
Si K	29.84	19.78
S K	2.46	1.43
3rd Scan		
O K	73.81	83.35
Si K	23.82	15.32
S K	2.37	1.33

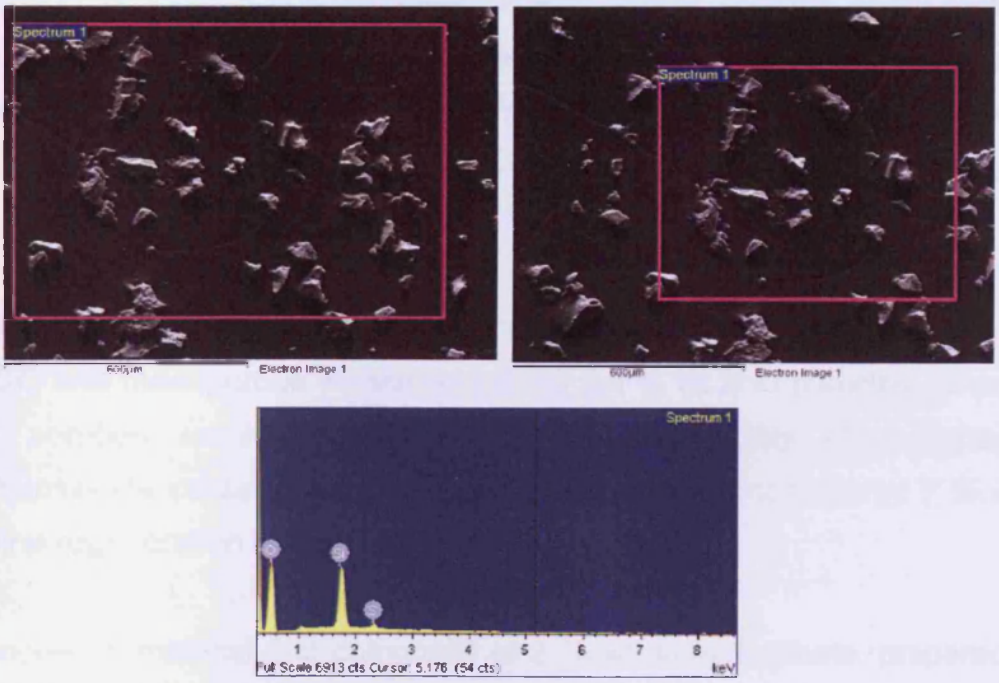

Figure 5.7 SEM images, of the selected areas to detect sulphur element, and the corresponding EDX peaks

5.4 Summary

5.4.1 Sorption Ability

ZnO that had been prepared by our developed method showed a better removing ability towards thiophene than commercially available ZnO powder. At room temperature and at 0 °C, mesoporous (TLCT) containing 2.2 % wt gold clusters gave the best thiophene removing ability. But at 40 °C, mesoporous aluminosilicate (TLCT) containing 2.7 % wt silver clusters had the best removing ability, which was 75 % removal of thiophene.

In addition, mesoporous silicate (TLCT) had the best removal ability of dibenzothiophene at room temperature, which was 37 %. Mesoporous silicate (TLCT) containing 2.7 % wt silver showed similar sorption ability towards dibenzothiophene compound to a fresh sample after the first regeneration cycle, whereas, the sorption ability of mesoporous aluminosilicate containing 0.5 % wt silver clusters had improved after the first regeneration cycle by 20 %.

Sorption results for 4,6-dimethyldibenzothiophene, mesoporous silicate (TLCT) and mesoporous silicate containing 5.0 % wt ZnO particles, gave the best sorption results of 57 %. The sorption ability of mesoporous aluminosilicate containing 2.2 % wt gold clusters had improved by 7 % after the first regeneration cycle.

Mesoporous material that composed of 2 % wt aluminosilicate, prepared by the PPT method showed the best ability to remove the dibenzosulfoxide compound as it removed 91 % of the total dibenzosulfoxide compound introduced, whereas the rest of the prepared mesoporous materials sorption results varied by removing 88 - 90 %, which indicates that these types of materials are excellent sulphur molecular sieves.

The TGA/MS test was performed under identical conditions as for the dry 4,6-dimethyl dibenzothiophene solid compound (figure 5.5) to be used as a reference material and to observe its behaviour under the test conditions. It revealed that this compound lost 93 % of its total mass at 247 °C and 100 % at 270 °C. Fewer sulphur fragments were observed such as HS, H_2S, and CH_2S that followed the same trends of that desorbed from the mesoporous material. The DSC curve showed that this compound had endothermic processes represented in a sharp peak (figure 5.6) at 155 °C, which could reflect expansion caused by melting or evaporation of this compound associated with fast mass loss. Another less intense broader peak appeared at 250 °C, representing the second endothermic process before the second decrease of the compound's mass percentage.

After analysing the TGA/MS results we found that mesoporous materials were able to hold 4,6-dimethyl dibenzothiophene adsorbate at room temperature up to 85 °C, where desorption and decomposition of this compound occurred gradually as a function of temperature. Some fragments of sulphur such as C_2H_2S and CH_2SH were held by the mesoporous structure at elevated temperatures of 250 °C, which may indicate that the mesoporous materials were able to form some interaction (chemisorption) bonds with the sulphur compound.

There were many other hydrocarbon fragments released during the TGA/MS tests but we were only focused on sulphur compounds, for the interest of this project, to track their behaviour during this test. Moreover, these sulphur fragments were few of the most probable fragments predicted by us for the 4,6-dimethyl-dibenzothiophene adsorbate. Some of the predicted sulphur fragments were not observed during the TGA/MS test such as methyl-benzothiophene and dimethyl-benzothiophene having charged masses of 124 and 136 respectively.

5.5 References

1. P. W. Atkins, *Physical Chemistry*, Oxford University Press, Sixth edition, 1998, 855-868.
2. D. J Show, *Introduction to Colloid and Surface Chemistry*, Butterworth Heinemann, Fourth Edition, 2000, 115 - 136.

Chapter 6

Conclusion

6.1 Conclusion

6.1.1 Mesoporous Preparation Method (Chapter 3)

The effect of the heating rate depends on the morphology of the prepared structure and depends upon the synthesis route used, for example a fast heating rate at or above 4 °C min^{-1} could decrease the long-range order or completely destroy the cubic mesoporous structure. We found that a heating rate of 3 °C min^{-1} deforms the structure of a cubic mesoporous structure prepared by the precipitating method (ppt), however 2 °C min^{-1} was proven to be the best heating rate for this method, and a heating rate of 3 °C min^{-1} was the best rate for the same structure prepared by the solvothermal method. 3 - 4 °C min^{-1} was a suitable rate for a hexagonal mesoporous silicate prepared by the TLCT method, whereas, the calcination temperatures of 550 - 600 °C showed an improvement in the long-range for both structures: hexagonal and cubic mesoporous.

Aging of the as-synthesized mesoporous materials plays an important role in the overall long-range order by enhancing the condensation step and strengthening the framework by forming more metal oxygen bonds. We found that increasing the temperature at the aging step, to be slightly less than the temperature of mesophase formation, provided an improvement to the stability of the mesoporous framework. It is equally important to point out that the aging time is strongly dependent on the synthesis procedure employed.

We found that the average aging time for the as-synthesized samples prepared using the TLCT technique should be held between two to four days in order to produce the best long-range order for the mesoporous structure and to enhance the overall stability. On the other hand, elongated aging times will transform the mesophase or deform the morphology of interests and could participate in the weakening of the framework rather than strengthening it, for the solvothermal preparation methods. One day aging is proven to produce

the best cubic mesoporous silicate morphology for both solvothermal and precipitating methods.

6.1.2 Mesoporous Stability (chapter 3)

Hydrolysis, thermal and hydrothermal tests are essential to determine the stability of the mesoporous materials. The products of the standard method of synthesizing mesoporous silicate failed the stability tests designed for this project. Monitoring and controlling individual preparation steps helped us to produce better mesoporous material. Only modified samples showed acceptable stability to fit the purpose of this project. Moreover, mesoporous materials prepared by various methods behave differently under given conditions. Observing the structural and morphological changes of these materials upon exposing them to different conditions will provide a better understanding of their behaviour during doping and sorption reactions. We found that the modified TLCT and precipitating methods are more suitable to be employed for this project.

The structural stability of mesoporous materials is tuneable by modifying their preparation methods or by post treatments. Two types of pore packing were produced and tested, hexagonal and cubic mesoporous materials. We were able to produce relatively stable mesoporous materials, against hydrolyses and thermal tests that fit the criteria and the conditions of this project. For example, mesoporous silicate and aluminosilicate that could withstand hydrolyses for one hour at 100 °C, hydrothermal treatments for one hour under humid conditions at 280 °C, and multiple calcination cycles at 570 °C for 102 hours total time.

6.1.3 Impregnation Methods (Chapter 4)

Spanhel's method to produce ZnO particles did not yield satisfactory results during the incorporations of these particles into mesoporous hosts and led to a destabilisation of the host structure. The modified ZnO preparation method developed in this work, that excluded the catalytic step of Spanhel's method, and replaced it by heat treatments, proved to be more suitable for our work, and produced small clusters in the range of 1 nm within the pores of the prepared mesoporous materials that been examined.

A novel method was developed by us to introduce gold and silver clusters into mesoporous materials. It is shown to be more economical since it decreases the impregnation time from three weeks to only 30 minutes and maintains the long-range order of the mesoporous structure, as confirmed by the HRTEM and XRD techniques. Furthermore impregnation was possible at a small nano-scale level producing clusters with average sizes of 1 nm.

Moreover, introducing silver and gold clusters to mesoporous materials restricts their growth and their leaching by the confinement effect and was found very practical to produce nanoclusters. The percentages of silver and gold did not exceed 2 % weight/weight of mesoporous material that decrease the over all price of these materials, rather than using pure crystals of gold or silver, which would be more expensive.

The final result obtained from this part of the work is the noticed relationship between the size of the gold particles incorporated within the mesoporous hosts and their colour. This work has shown that this phenomenon can be directly related to the characteristics of the heat treatment applied and impregnated metals concentrations, which can shift the surface plasmon resonance peaks to the blue or red region.

6.1.4 Sorption Ability (chapter 5)

Many researches had focused on removing sulphur during the process stages that employed harsh conditions such as high pressure, temperatures and steam (as reviewed in chapter 1). However, we chose to explore the adsorption route because it is safer and involves milder conditions, which can be performed at any stage of petroleum production; to remove sulphur from feeds, intermediates, or final products. This method has proven to be satisfactory and has a high number of potential applications. The following paragraphs will summarise these findings.

ZnO that been prepared by our developed method showed a better removing ability towards thiophene than commercially available ZnO powder. At room temperature and at 0 °C, mesoporous (modified TLCT method) containing 2.2 % wt gold clusters gave the best thiophene removing ability, but at 40 °C, mesoporous aluminosilicate (modified TLCT method) containing 2.7 % wt silver clusters had the best adsorption ability, which was 75 % removal of total thiophene.

In addition, mesoporous silicate (modified TLCT method) had the best removal ability of dibenzothiophene at room temperature, which was 37 %. Mesoporous silicate (modified TLCT method) containing 2.7 % wt silver showed similar sorption ability towards dibenzothiophene compound to a fresh sample after the first regeneration cycle, whereas the sorption ability of mesoporous aluminosilicate containing 0.5 % wt silver clusters had improved after the first regeneration cycle by 20 %.

Sorption results for 4,6-dimethyldibenzothiophene, mesoporous silicate (modified TLCT method) and mesoporous silicate containing 5.0 % wt ZnO particles, gave the best sorption results of 57 %. The sorption ability of mesoporous aluminosilicate containing 2.2 % wt gold clusters had improved by 7 % after the first regeneration cycle.

Mesoporous material that composed of 2 % wt aluminosilicate, prepared by the modified PPT method showed the best ability to remove the dibenzosulfoxide compound (it removed 91 % of the total dibenzosulfoxide compound introduced), whereas the rest of the prepared mesoporous materials sorption results varied by removing 88 - 90 %, which indicates that these types of materials are excellent sulphur molecular sieves.

After analysing the TGA/MS results we found that mesoporous materials were able to hold 4,6-dimethyl dibenzothiophene adsorbate at room temperature up to 85 °C, where desorption and decomposition of this compound occurred gradually as a function of temperature. Some fragments of sulphur such as C_2H_2S and CH_2SH were held by the mesoporous structure at elevated temperatures up to 250 °C, which may indicate that the mesoporous materials were able to form some interaction (chemisorption) bonds with the sulphur compound.

There were many other hydrocarbon fragments released during the TGA/MS tests but we were only focused on sulphur compounds, for the interest of this project, to track their behaviour during this test. Moreover, these sulphur fragments were few of the most probable fragments predicted by us for the 4,6-dimethyldibenzothiophene adsorbate. Some of the predicted sulphur fragments were not observed during the TGA/MS test such as methyl-benzothiophene and dimethyl-benzothiophene having charged masses of 124 and 136 respectively.

The TGA/MS test was performed under identical conditions for dry 4,6-dimethyl-dibenzothiophene solid compound, to be used as a reference material, and to observe its behaviour under the test conditions. It revealed that this compound lost 93 % of its total mass at 247 °C and 100 % at 270 °C. Fewer sulphur fragments were observed such as HS, H_2S, and CH_2S that followed the same trends of that desorbed from mesoporous material. The DSC curve showed that this compound had endothermic processes represented in a sharp peak at 155 °C, which could reflect expansion caused by melting or evaporation of this compound associated with fast mass loss.

Another less intense peak appeared at 250 °C representing the second endothermic process before the second decrease of the compound's mass percentage.

6.2 Future work

In general this type of work is very interesting and has more probabilities of mixing metals and mesoporous materials before optimising the composition of the final products and their usage. For example, testing the adsorption ability of these materials after multiple regeneration cycles and against other types of sulphur compounds, that not been tackled in this project, or mixing more than one type of sulphur compound in one solution and testing the affinity of these mesoporous materials to adsorb certain sulphur compounds at different temperatures and concentrations. In addition we could introduce different metals or metal oxides that may enhance the adsorption ability of these materials.